

Universität
Rostock



Traditio et Innovatio

Preparation and investigation of the photocatalytic properties of Brookite

Dissertation

zur

Erlangung des akademischen Grades

doctor rerum naturalium (Dr. rer. nat.)

der Mathematisch-Naturwissenschaftlichen Fakultät

der Universität Rostock

vorgelegt von Huyen Thuong Thi Tran, geb. am 19.04.1983 in Bacninh, Vietnam

Rostock, 27.01.2016

Die vorliegende Arbeit wurde in der Zeit von April 2014 bis Januar 2016 am Institut für Chemie der Universität Rostock am Lehrstuhl für Anorganische Chemie in der Arbeitsgruppe von Prof. Dr. Axel Schulz angefertigt.

1. Gutachter: Prof. Dr. Axel Schulz
2. Gutachter:

ERKLÄRUNG

Ich versichere hiermit an Eides statt, dass ich die vorliegende Arbeit selbstständig angefertigt und ohne fremde Hilfe verfasst habe. Dazu habe ich keine außer den von mir angegebenen Hilfsmitteln und Quellen verwendet und die den benutzten Werken inhaltlich und wörtlich entnommenen Stellen habe ich als solche kenntlich gemacht.

Rostock, 27.01.2016

.....
Huyen Thuong Thi Tran

Acknowledgements

First of all, I would like to gratefully and sincerely thank Prof. Dr. Axel Schulz (Department of Inorganic Chemistry, Institute of Chemistry, University of Rostock) who provided me the opportunity to join his AK Schulz research group. I am grateful to Prof. Dr. Nguyen Quang Liem (Institute of Materials Sciences, Vietnam Academy of Sciences and Technology) who gave me a great chance to study and complete my PhD thesis at University of Rostock and supported me with many advices. Without their precious support and the cooperation between University of Rostock and Institute of Materials Science (IMS), Vietnam Academy of Science and Technology (VAST), Hanoi, Vietnam, I would not have been able to conduct this interesting research topic. I would also like to express my deepest and sincere gratitude to my supervisor Dr. Hendrik Kosslick for the continuous support of my PhD study and related research, for his patience and motivation. Beside my supervisor, I would also like to thank Dr. Muhammad Farooq Ibad for sharing his experience and assistance in N₂ adsorption and X-ray measurements from the beginning to help me doing well. I would also like to say special thanks for their supports: Dr. Alexander Villinger for X-ray diffraction, MSc. Katharina Sievert for TG-DSC analysis, Mrs. Petra Duncker for TOC measurements (University of Rostock); Dr. Christine Fischer for ESI-TOF-MS analysis; MSc. Vuong Thanh Huyen for UV-vis diffuse reflectance measurements (Prof. Dr. Angelika Brückner, Dr. Ursula Bentrup, LIKAT); and Dr. Ung Thi Dieu Thuy for SEM analysis (Institute of Materials Science (IMS), Vietnam Academy of Science and Technology (VAST), Hanoi, Vietnam). Also I thank to all my Vietnamese PhD friends in Rostock and my colleagues in AK Schulz group for all their encouragement, friendship and support during my work in the laboratory. Last not the least I would like to thank my family: my parents and parents-in-law, my husband and my little daughter for supporting me spiritually throughout doing this thesis and my life in general. Again, sincere thanks to all my teachers, colleagues, friends and family who have given me love and support throughout my life.

This work has been supported by the European Union in the frame of the FP7 program (EU-project PCATDES) which is gratefully acknowledged.

Zusammenfassung

In dieser Arbeit wurden Brookit-, Anatas-, und Rutil-Nanokristalle mittels hydrothormaler Behandlung eines amorphen Titandioxids als Vorstufe bei erhöhter Temperatur (175-200 °C) unter sauren Bedingungen (Zusatz von Salzsäure bzw. Essigsäure) hergestellt. Die amorphe Vorstufe wurde durch Hydrolyse von Tetraisopropyltitanat erhalten. Die drei Titandioxid-Polymorphe wurden mittels XRD, Raman-Mikroskopie, REM, TG-DSC, UV-vis, und Stickstoff-Sorptionsmessungen charakterisiert. Die photokatalytischen Abbauexperimente wurden an niedrig konzentrierten wässrigen Lösungen (10 ppm, Katalysator zu Substrat-Verhältnis = 4) unter Bestrahlung mit einer 60 W UV-vis Solariumlampe durchgeführt. Der photokatalytische Abbau wurde mittels UV-vis-Spektroskopie und Messungen des Kohlenstoff-Gesamtgehaltes (TOC) verfolgt. Als Modellsubstrate wurden Zimtsäure, Ibuprofen, Phenol, Amidotrizoesäure sowie die Farbstoffe Rhodamin B und Bengalrosa verwendet. Die Bildung von Zwischenprodukten beim photokatalytischen Abbau wurde mittels ESI-TOF-MS-Messungen untersucht. Die Anwesenheit von aktiven Spezies wie von Valenzbandlöchern (h^+), Hydroxyl-Radikalen ($\bullet OH$), und Superoxid-Radikalanionen ($O_2^{\bullet -}$) oder Hydroperoxid-Radikalen ($\bullet OOH$) wurden mittels Lösungs-Versuchen (Quenching) unter Zusatz selektiver Radikalfänger geprüft. Reiner Anatas wurde in essigsauen Reaktionsmischungen erhalten, während Brookit ausschließlich in salzsauen Mischungen zusammen mit Rutil kristallisierte. Phasenreiner Brookit wurde mittels Peptisation mit Wasser aus den Mischungen mit einer optimierten Aufarbeitungsprozedur abgetrennt. Brookit und Anatas kristallisierten als sphärisch geformte agglomerierte Nanopartikel. Rutil kristallisierte in Form stabförmiger großer Nanopartikel. Die direkte (3,44 eV) und die indirekte Bandlücke (3,25 eV) von Brookit liegen zwischen den Bandlücken von Anatas und Rutil. Brookit zeigte eine hohe photokatalytische Aktivität, ähnlich der von Anatas und dem kommerziellen Photokatalysator P25 Degussa/Evonik. Die Aktivität sinkt in der Reihe: Anatas \geq Brookit > Rutil, und mit wachsender Rekalzitranz (Stabilität des aromatischen Ringes) der Substratmoleküle. Die Unterschiede in der Aktivität sind bei der Mineralisation deutlich ausgeprägter. Die Experimente mit den Radikalfängern machen deutlich, dass beim Anatas und Brookit die Löcher des Valenzbandes und die Superoxid-Radikalanionen die hauptsächlich aktiven Spezies sind, beim Rutil dagegen die Hydroxyl-Radikale und Superoxid-Radikalanionen, was die geringere Aktivität des Rutils erklärt. Die Kopplung von unterschiedlichen Titandioxidphasen, führt nicht zu einer Erhöhung der Aktivität. Eine komplementäre Nutzung von UV-vis-Spektroskopie und der TOC-Messung erforderlich führt eine wirklichkeitsnahe Bewertung der Leistungsfähigkeit der Titandioxid-Katalysatoren.

Summary

In this study, Brookite, Anatase, and Rutile nanocrystals were synthesized via hydrothermal treatment of an amorphous titania as starting material at elevated temperatures between *ca.* 175 to 200 °C using titanium(IV) *i*-propoxide as the titanium source with hydrochloric acid or acetic acid. The three polymorphs were characterized by XRD, Raman spectroscopy, SEM, TG-DSC, UV-vis, and nitrogen adsorption measurements. The photocatalytic degradation experiments were performed with low concentrated solution (10 ppm, catalyst to substrate ratio of 4) using a 60W UV-vis solarium lamp irradiation. The photocatalytic degradation was monitored by UV-vis absorption spectroscopy and TOC measurements of treated solutions using cinnamic acid, ibuprofen, phenol, diatrizoic acid and the dyes rhodamine B and rose bengal as model pollutants. The formation of reaction intermediates was studied by ESI-TOF-MS measurements. The presence of active species, valence band holes (h^+), hydroxyl radicals ($\bullet OH$), and superoxide radical anions ($O_2^{\bullet -}$) or hydroperoxyl ($\bullet OOH$) radicals was checked by quenching the activity by addition of scavenger.

The use of acetic acid yielded phase-pure Anatase, while Brookite always crystallized in the mixture with Rutile by using hydrochloric acid. Phase-pure Brookite could be obtained by peptization with water using an improved work up procedure. Brookite and Anatase crystallized in form of agglomerated spherical-shaped nanoparticles, Rutile formed rod-like large nanocrystals. Both the direct band gap (3.44 eV) and the indirect band gap (3.25 eV) of Brookite were between those of Anatase and Rutile. Brookite showed high photocatalytic activity, close to Anatase and commercial photocatalyst titania P25 Degussa (Evonik). The activity decreased in the order: Anatase \geq Brookite $>$ Rutile, and with growing recalcitrance (stability of the aromatic ring) of the substrate molecules. The differences in the degradation activity are more pronounced in the mineralization behaviour. Scavenger experiments revealed that valence band holes and superoxide radicals were the major active species with Anatase and Brookite. Hydroxyl ($\bullet OH$) radicals and superoxide ($O_2^{\bullet -}$) radicals were the main active species with Rutile, which explains the lower photocatalytic activity of Rutile. The coupling of the titania polymorphs with each other did not enhance the activity. The complementary use of UV-vis absorption spectra and TOC measurements was required to obtain a comprehensive realistic assessment on the performance of the titania polymorphs in the photocatalytic degradation of organic contaminants.

Table of contents

List of abbreviations	IX
Unit conversion	IX
1 Objectives.....	1
2 Introduction	2
3 Results and discussion.....	21
3.1 Phase-pure TiO ₂ preparation: Brookite, Anatase, and Rutile	21
3.2 Characterization of materials.....	25
3.2.1 XRD analysis	25
3.2.2 Raman spectroscopy	26
3.2.3 Thermal Analysis (TG-DSC).....	27
3.2.4 Scanning electron microscopy (SEM)	30
3.2.5 UV-vis diffuse reflectance	33
3.2.6 Nitrogen adsorption-desorption	34
3.3 Photocatalytic performance of Brookite (B), Anatase (A), and Rutile (R)	38
3.3.1 Brookite	38
3.3.2 Anatase.....	49
3.3.3 Rutile.....	54
3.4 Comparison of the photocatalytic activity of titania polymorphs with different organic compounds	60
3.4.1 The photocatalytic degradation of cinnamic acid (CA).....	60
3.4.2 The photocatalytic degradation of ibuprofen (IBP)	61
3.4.3 The photocatalytic degradation of phenol (Ph).....	62
3.4.4 The photocatalytic degradation of diatrizoic acid (DA)	63
3.4.5 The photocatalytic degradation of rose bengal (RB)	64
3.4.6 The photocatalytic degradation of rhodamine B (RhB).....	65
3.5 Comparison of the impact of hole/radical scavenger on the photocatalytic abatement of IBP over the titania polymorphs Brookite, Anatase, and Rutile.....	69
3.5.1 Impact of the hole scavenger on the photocatalytic abatement of ibuprofen.....	69
3.5.2 Impact of the •OH radical scavenger on the photocatalytic abatement of ibuprofen.....	70
3.5.3 Impact of the O ₂ ^{•-} radical scavenger on the photocatalytic abatement of ibuprofen	72
3.6 Origin of different activity of Rutile compared to Anatase and Brookite	74
3.7 The photocatalytic activity of mixed-phase TiO ₂ composites	77
Anatase/Brookite	78
Anatase/Rutile.....	80
Brookite/Rutile.....	80

4	Final conclusion	84
5	Appendix	85
5.1	Material preparation	85
5.1.1	Amorphous sol-gel preparation.....	85
5.1.2	Hydrothermal treatment	86
5.1.3	Separation of phase-pure Brookite particles by peptization	87
5.2	Characterization methods	90
5.2.1	Photocatalyst powder characterization	90
5.2.2	Analysis of photocatalytic treated solution characterization	91
5.3	Photocatalytic activity test.....	92
5.4	List of chemicals used	94
6	References.....	95

List of abbreviations

AOPs	<i>Advanced oxidation processes</i>	Ph	Phenol
A	Anatase	p/p₀	Relative pressure
A_m	Amorphous titania	ppm	Parts per million
Ads.	Adsorption	SEM	<i>Scanning electron microscopy</i>
B	Brookite	SHE	<i>Standard hydrogen electrode</i>
BET	<i>Brunauer–Emmett–Teller</i>	SSA	<i>Specific surface area</i>
BJH	<i>Barrett, Joyner, Halenda</i>	R	Rutile
BQ	Benzoquinone	RB	Rose bengal
CA	Cinnamic acid	Ref.	Reference
ca.	Approximately	RhB	Rhodamine B
CB	<i>Conduction band</i>	ROS	<i>Reactive oxygen species</i>
conc.	Concentration	RT	<i>Room temperature</i>
DA	Diatrizoic acid	T	Temperature
DSC	<i>Differential Scanning Calorimetry</i>	TG	Thermogravimetry
e_{CB}⁻	Conduction band electron	TOC	<i>Total organic carbon</i>
EDTA	Ethylenediaminetetraacetic acid	TTIP	Titanium(IV) isopropoxide
e.g.	For example	TOF-MS	<i>Time-of-flight mass spectrometry</i>
Eq.	Equation	UV	Ultraviolet
ESI	<i>Electrospray ionization</i>	UVC	Ultraviolet C
FWHM	<i>Full width at half maximum</i>	UV-vis	Ultraviolet–visible
h_{VB}⁺	Valence band hole	V	Volume
IBP	Ibuprofen	VB	<i>Valence band</i>
ICM	<i>Iodinated X-ray contrast media</i>	vol.%	Volume percent
m/z	mass to charge ratio	vs.	versus
NHE	<i>Normal hydrogen electrode</i>	XRD	<i>X-ray diffraction</i>
NPOC	<i>Non-purgeable organic carbon</i>	wt%	Weight percent

Unit conversion

Quantity	Symbol	Name	Conversion
Length	Å	Angstrom	1 Å = 10 ⁻¹⁰ m
	µm	micrometer	1 µm = 10 ⁻⁶ m
	nm	nanometer	1 nm = 10 ⁻⁹ m
Power	mW	milliwatt	1 mW = 10 ⁻³ kg·m ² ·s ⁻³
Temperature	°C	degree Celsius	x °C = (x + 273.15) K
Volume	ml	milliliter	1 ml = 1 cm ³ = 10 ⁻⁶ m ³
Wavenumber	cm ⁻¹	reciprocal centimeter	1 cm ⁻¹ = 100 m ⁻¹
Wavelength	nm	nanometer	1 nm = 10 ⁻⁹ m
Time	h	hour	1 h = 3600 s
	min	Minute	1 min = 60 s
Pressure	Bar	bar	1 bar = 100000 Pa
	hPa	hectopascal	1 hPa = 100 Pa
Energy	eV	Electron volt	1 eV = 1.6 x 10 ⁻¹⁹ J

1 Objectives

This study focuses on the preparation and characterization of the least known titania polymorph Brookite and the detailed investigation of its photocatalytic performance in the ultraviolet-visible (UV-vis) light driven degradation of recalcitrant organic contaminants. The main objectives are:

- Synthesis, characterization, and photocatalytic testing of nano-sized Brookite compared to Anatase, Rutile, and commercial photocatalyst Titania P25 Degussa (Evonik).
- Investigation of photocatalytic degradation of different reactive organic and pharmaceutical contaminants (cinnamic acid, ibuprofen, phenol, diatrizoic acid, rhodamine B, and rose bengal) and formation of reaction intermediates/by-products.
- The contribution of active species (valence band holes (h^+), hydroxyl ($\bullet OH$) and superoxide ($O_2^{\bullet -}$)/hydroperoxyl ($\bullet OOH$) radicals) to the photocatalytic degradation of contaminants has been studied by the addition of the scavengers EDTA (h^+), *t*-BuOH ($\bullet OH$), and 1,4-BQ ($O_2^{\bullet -}$ or $\bullet OOH$).
- Study of the effect of coupling of synthesized titania polymorphs by physical mixing (Anatase/Brookite, Anatase/Rutile, and Brookite/Rutile composites) on the photocatalytic degradation performance.

2 Introduction

Water is of major importance to all living things. In some organisms, up to 90% of their body weight comes from water. Up to 60% of the human adult body is water. In recent years, the growth of population and industry has increased the demand for water. As a result, the water pollution is mostly caused and raised by increasing industrialization and human activities. An estimated 90% of all wastewater in developing countries is discharged untreated directly into rivers, lakes or the oceans (Figure 1).^[1] Therefore, there has been overwhelming concern about water treatment and reuse requiring the strictest standards, recently.

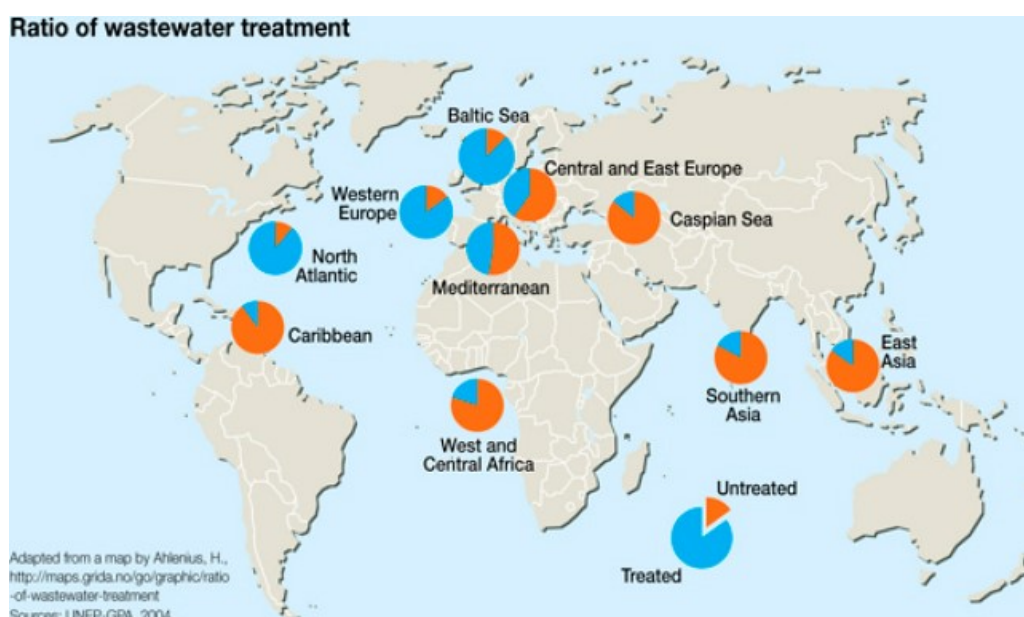


Figure 1. The ratio of treated to untreated wastewater reaching water bodies from 10 regions across the globe (taken from Ref. [1]).

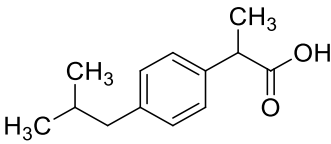
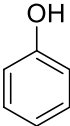
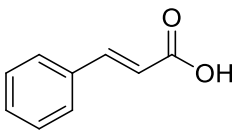
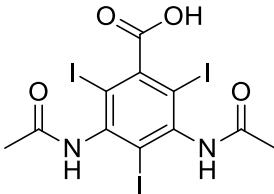
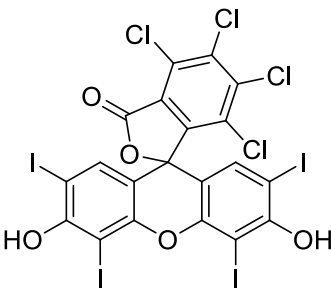
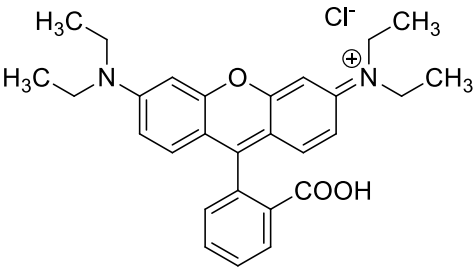
There is a wide range of pollutants that affect water resources, each of which is hazardous in different concentrations and originates from diverse activities as given in Table 1. Among various pollutants, organic compounds like pharmaceuticals, dyes containing aromatic hydrocarbons (aromatic rings) have impacted seriously on natural ecosystems and public health.^[2–4] They not only easily decompose in water but also consume dissolved oxygen.^[2] However, much attention is focused on pharmaceuticals because they can display a biological response at very low concentrations.^[5] More important point is that water is a critical raw material in pharmaceutical and chemical manufacturing operations.^[1] A number of studies have been reported about the widespread occurrence of pharmaceuticals.^[5–13] The pharmaceutical contaminants vary not only in composition but also in quantity depending on the raw materials and the processes used in the manufacturing of various pharmaceuticals.^[1]

Table 1: Main contaminants affecting water quality and their main sources.

Contaminants		Industry	Agriculture	Hospital	Human settlements	Ref.
Pharmaceuticals	Antibiotics	+		+	+	[5–13]
	Analgesics and antipyretics					
	Non-steroidal anti-inflammatory drugs					
	Beta blocker					
	Anticholestric					
Dyes		+			+	[2–4,14,15]
Phenolic compounds		+				[4,16–18]
Toxic organic compounds (chemicals, pesticides, herbicides)		+	+			[19,20]
Drugs		+	+	+	+	[19]
Nuclear waste		+				[19,20]

The presence of pharmaceuticals detected in domestic wastewater, natural aquatic systems and groundwater is raising public health concerns. As a result, there is a growing interest in the development of innovative technologies to efficiently transform these compounds to non-toxic and pharmaceutically inactive by-products. Table 2 summarizes the molecular formula, chemical structure, and molecular weight of pharmaceuticals and dyes used as model pollutants in this study. Among pharmaceutically active compounds, ibuprofen (IBP) is one of the original non-steroidal anti-inflammatory drugs (NSAIDs) for treatment of pain and fever relieve.^[7,10] A survey conducted between 2006 and 2010 confirmed the presence of IBP over a wide range of concentrations from 65 to 7100 ng/L in sewage treatment plants and raw sewage effluents, up to 360 ng/L in freshwater.^[7,12] A series of new technologies have been applied in order to more effectively reduce the presence of IBP in the environment.^[10,11,13] The reported efficiency of IBP removed by biological treatment is *ca.* 70%, but the remaining IBP content can cause environmental problems.^[6] Studies of IBP degradation using TiO₂/UV system have received increasing attention in recent years.^[8,11,12] However, the reports about the photocatalytic decomposition of IBP in low IBP concentration as well as the detailed investigations about the contribution of active species and formation of intermediates (by-products) during the photocatalytic reaction are very limited so far.^[9–11]

Table 2: Molecular formula, chemical structure, and molecular weight of studied organic compounds.

Compound	Chemical structure	Molecular weight (g/mol)
Ibuprofen (IBP) $C_{13}H_{18}O_2$		206.29
Phenol (Ph) C_6H_6O		94.11
Cinnamic acid (CA) $C_9H_8O_2$		148.486
Diatrizoic acid (DA) $C_{11}H_9I_3N_2O_4$		613.91
Rose bengal (RB) $C_{20}H_4Cl_4I_4O_5$		973.67
Rhodamine B (RhB) $C_{28}H_{31}ClN_2O_3$		479.02

Beside the pharmaceutical compounds, the presence of phenol (Ph) and their derivatives in wastewater of many industries including resins, petrochemical, paint, textile, oil refineries, food, photographic chemicals, antioxidants and flavouring agents is another problem attracting global concern.^[4,17] Phenol is typical of phenolic compound and it is considered to be an intermediate product in the oxidation reactions of higher molecular weight aromatic compounds.^[16] European Union (EU) has classified several phenols as priority contaminants

and the 80/778/EC directive states a maximum concentration of 0.5 µg/L for total phenols in drinking water. Individual concentration should be under 0.1 µg/L.^[4] Due to their toxic and endocrine disrupting properties, many studies have focused on removing phenolic compounds from drinking water and wastewater as well.^[16,21,22]

Cinnamic acid (CA) is an organic compound existed as both a *cis* and a *trans*-isomer, the latter is more common. Cinnamic acid is used in flavours, especially used as an important pharmaceutical for preventing high blood pressure or possessing antitumor activity.^[23] *Trans*-cinnamic acid can be found in many cosmetic products. Literature reported that the human skin is exposed frequently to *trans*-cinnamic acid but unclear about its toxicity.^[24]

Diatrizoic acid (DA) (or its anionic form, diatrizoate) is an ionic ICM (iodinated X-ray contrast media), which is one of the most widely used chemical compounds for intravascular administration.^[25] DA can be detected in hospital effluents, sewage treatment plants, surface water, and ground water.^[26] The traditional wastewater treatment processes have not effectively removed ICMs. Their concentration at the µg.L⁻¹ level in effluents of wastewater treatment plants, surface water, and ground water has been detected. In drinking water treatment, ICMs were only partially removed by ozonation at 35–55% of non-ionic ICMs and below 20% of ionic ICMs.^[27,28]

Dyes, known as containing the chromophore (colour-bearing) group and auxochrome (colour helpers) group, are used for imparting colour to a substrate such as cloth, paper, plastic, or leather. It has been estimated that approximately 15% of the total world production of dyes is lost during the dyeing process and then released to the environment through textile effluents.^[2,22] Consequently, removal of colour from wastes is considered to be more essential than the other organic substances. The presence of small amounts of dyes (below 1 ppm) is clearly visible and influences the water environment significantly.^[2] For that reason, dyes have been received much attention in studies on the removal of synthetic dyes in the last few decades. Some studies reported that dyes are higher toxic and heavier coloured after dyeing process.^[4,29] Unlike most organic compounds, dyes possess colour because they: (i) absorb light in the visible spectrum (400-700 nm); (ii) have at least one chromophore (colour-bearing group); (iii) have a conjugated system containing the alternating double and single bonds; and (iv) exhibit resonance of electrons, which is a stabilizing force in organic compounds.^[14] Many dyes are difficult to decolorize due to their synthetic origin and complex structure. One of the

most common xanthene dyes for textile industry is rhodamine B (RhB). This dye has a high stability at different pH values. It is currently used as dye laser material, and also used as biological stain.^[30] Rhodamine B is highly soluble in water and organic solvent, and its colour is fluorescent bluish-red. This compound is now banned in foods and cosmetics because it has been found to be potentially toxic and carcinogenic.^[31] Therefore, the photocatalytic degradation of RhB is essential regarding the purification of dye effluents.

Beside the RhB, the other xanthene dyes namely rose bengal (RB) is extensively used in the printing, insecticides and in dyeing industries.^[32] It is considered one of new emerging pollutants in surface and probably drinking water. Rose bengal contains three aromatic rings in a linear arrangement and an oxygen atom in the center of the ring. It can be used in (1) treatment of particular cancer and skin conditions as eczema and psoriasis or (2) medical and biological diagnostics as a contrast agent.^[33]

General problem of depollution – water cleaning, contaminated aqueous solutions require the advanced oxidation processes for treatment from low concentrated pollution. Since the late 1990s, the scientific and engineering interest in the photocatalytic materials and processes in order to find and develop the water treatment technologies with enhanced efficiency and applicability has grown exponentially.^[34] The traditional technologies based on a combination of physical, biological, and chemical processes not only are non-destructive but also transform pollutants from one phase to another phase which further requires treatment to avoid secondary pollution.^[3,16,35] To purify the polluted water sources with powerful ability and to reduce the degree of pollution in energy-saving and environmentally-benign manners, the Advanced Oxidation Processes (AOPs) have been chosen as an alternate method.^[34,36,37] The AOPs involve two main stages of oxidation: (i) the formation of highly active species, and (ii) the redox reactions of active species with organic contaminants.^[34] The AOPs can be driven by external energy sources such as electric power, ultraviolet radiation (UV) or solar light. In addition, the AOPs also use strong oxidizing agents like hydrogen peroxide (H₂O₂), ozone (O₃), catalysts (iron ions, electrodes, or metal oxides), and radiation sources (UV light, solar light, ultrasounds).^[38] The AOPs driven by solar light seems to be the most popular technology for wastewater treatment due to the abundance of solar light, low cost, and high efficiency.^[39] Compared to conventional techniques, one of the AOPs's advantages is the possibility to totally degrade and mineralize the organic compounds into environmental friendly species such as CO₂, H₂O and harmless inorganic.^[40–42]

Among available AOPs, heterogeneous photocatalysis is an attractive candidate for drinking water, wastewater treatment applications.^[21,43] Heterogeneous photocatalysis has been widely studied in the last decades, which uses solid catalysts activated by light (UV or visible light) with the corresponding wavelength in order to degrade pollutants in liquid-phase.^[18,38,44] The non-selective photocatalytic performance takes place by means of parallel and series reduction/oxidation reactions. Furthermore, the heterogeneous photocatalysis has been evidenced that numerous organic contaminants are fully decomposed, even totally mineralized owing to its efficiency in production of holes (h^+) formed upon irradiation on catalyst sites and radical species such as hydroxyl ($\cdot OH$), superoxide ($O_2^{\cdot -}$), and hydroperoxyl ($\cdot OOH$) radicals produced by reduction/oxidation of photogenerated electrons/holes.^[40,45] Besides, catalyst in solid form is of potential because it is easily separated from the solution. This suggested that catalyst can be reused and the cost can be further cut off to run the process as well.^[9,15,32]

In general, a photocatalytic mechanism consists of three steps: (i) photo-excitation generates electrons and holes, (ii) the electrons and holes migrate to the surface of catalyst, and (iii) the electrons and holes react with adsorbed electron acceptors and donors (oxidizing agents), respectively, to complete the photocatalytic reaction.^[46–48]

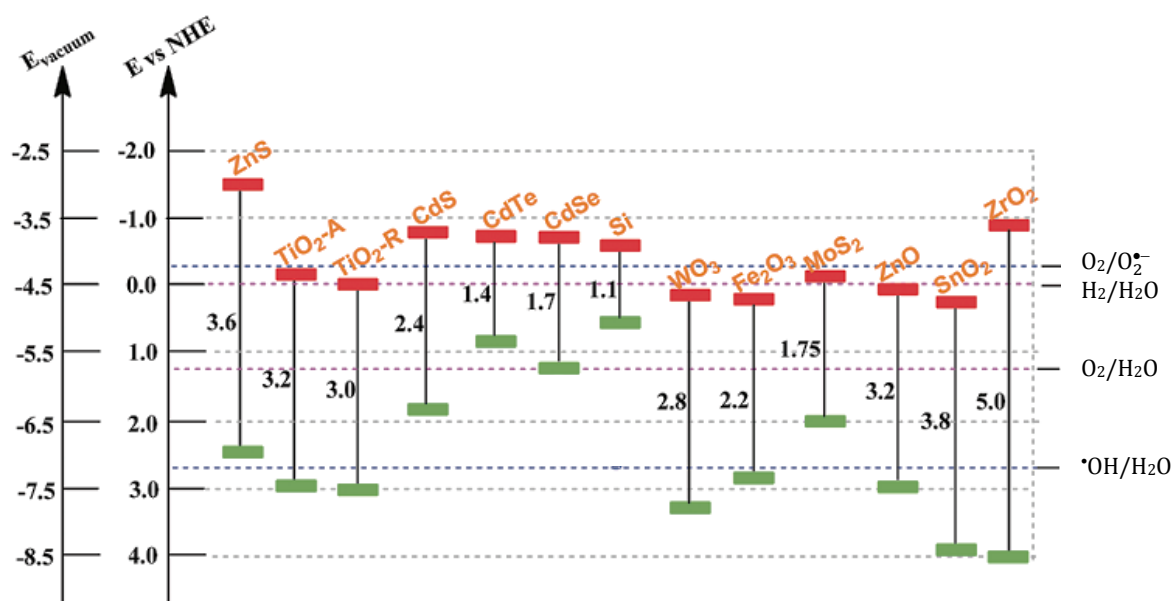


Figure 2. Band gaps and band edge positions of some semiconductor photocatalysts on a potential scale (V) versus the normal hydrogen electrode (NHE) at pH 0 (taken from Ref. [49]).

To achieve photocatalytic degradation of organic compounds, the valence band (VB) and conduction band (CB) edge positions of semiconductors should be located in such a way that the redox potential of oxidizing agents (Table 3) lie well within the band gap of semiconductors (Figure 2).^[49] This special band structure plays an important role in determining not only the light absorption properties but also the redox capability of the

semiconductor.^[47] For that reason, semiconductor material has been used as a photocatalyst in most studies for photocatalytic applications including water and wastewater treatment.

Table 3: Oxidation potential (E_{ox}) of various oxidizing agents at pH 0 (taken from Ref. [50-52]).

Oxidizing agent	E_{ox}/V vs. NHE
Hydroxyl radical ($\bullet OH$)	2.80
Ozone (O_3)	2.07
Hydrogen peroxide (H_2O_2)	1.77
Chlorine (Cl_2)	1.36
Chlorine dioxide (ClO_2)	1.27
Oxygen (O_2)	1.23

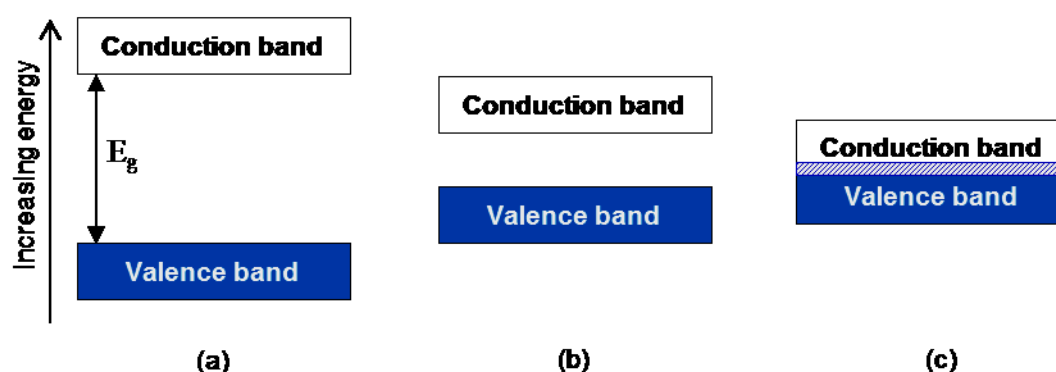


Figure 3. Band gap diagram of (a) an insulator, (b) a semiconductor, and (c) a conductor.

The difference in the band structure between semiconductor, insulator, and metal is shown in Figure 3 and is explained as follows:^[53–55]

- With typical conductors such as metals, the valence band (VB) and the conduction band (CB) overlap in energy each other or they are partly filled by the valence electrons.

The VB is formed by the interaction of the highest occupied molecular orbital (HOMO), while the CB is formed by the interaction of the lowest unoccupied molecular orbital (LUMO).^[47] The energy difference between the lowest point of CB (CB edge) and the highest point of VB (VB edge) is called forbidden band gap (also called energy gap or band gap, denoted as E_g) in solid-state physics, and HOMO/LUMO gap in chemistry.

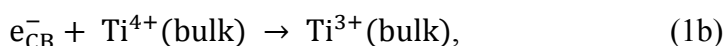
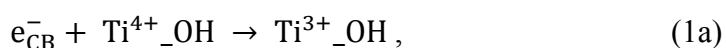
- If the valence electrons exactly fill one or more bands, leaving others empty, the crystal will be an insulator at 0K and can be an insulator or a semiconductor at other temperatures, depending on the value of the minimum energy gap between the filled and the empty band.^[56]

A material with a band gap of greater than 3 eV will commonly be regarded as an insulator. An external electric field will not cause current flow in an insulator.

- In comparison, the semiconductors have the same band structure as insulators but smaller band gap ($E_g < 3$ eV). Under normal conditions without photo-excitation, the semiconductor is at the ground state where electrons are localized in the VB. However, upon photo-excitation, electrons get sufficient energy to overcome the band gap barrier and move to CB.^[55]

The fundamental mechanism of photocatalysis is reported as an oxidation process of organic compounds in the presence of catalyst under the ultraviolet or visible light irradiation by means of highly active species that feature the advanced oxidation process.^[36] As a result, organics are converted to carbon dioxide, water, and harmless inorganic. Taking TiO_2 as an example, the detailed photocatalytic mechanism is described and shown in Figure 5. In addition, Figure 6 shows an overview of the possible photo-induced events inside and on the surface of TiO_2 photocatalyst in the time scale region from femtoseconds (fs) to microseconds (μs).^[57,58] When TiO_2 is irradiated by UV-vis light whose excitation energy is greater than its band gap energy ($h\nu > 3.2$ eV) or wavelength is less than 385 nm ($\lambda < 385$ nm), electrons (e_{CB}^-) are excited from the VB to the CB leaving positive holes (h_{VB}^+) in the valence band. This exciting occurs in the fs timescale.^[59] The photogenerated electrons and holes rapidly migrate to the surface of TiO_2 catalyst. The tendency of these charge carriers may take different pathways.^[55,60]

➤ Firstly, they can be trapped by defect sites in the crystal lattice, either in shallow traps or in deep traps. Tamaki's group suggested that they transfer randomly and are trapped at catalyst surface in the sub-ps timescale.^[61] Some other reports proposed that the CB electrons are trapped at two different Ti^{3+} sites.^[43,60,62–65]



where $\text{Ti}^{3+}\text{-OH}$ is a surface-trapped electron and $\text{Ti}^{3+}(\text{bulk})$ denotes an electron trapped in the bulk. The dynamic equilibrium of Eq. (1a) represents a reversible trapping of a CB electron in a shallow trap. Eq. (1b) represents the irreversible trapping of an electron in a deep trap. In contrast, the trapping sites in TiO_2 for VB holes remain unclear. Murai's group suggested that the holes are trapped at the TiO_2 surface in adsorbed OH^- groups yielding weakly adsorbed hydroxyl radicals $\text{Ti}^{4+}\text{-}\cdot\text{OH}$.^[66]

➤ Secondly, they can recombine, non-radiatively or radiatively, with an undesired release of thermal energy.^[63] The recombination of electrons and holes is an important electronic process in semiconductors. The recombination rate also plays a critical role in practical photocatalytic reaction systems.^[62,67]

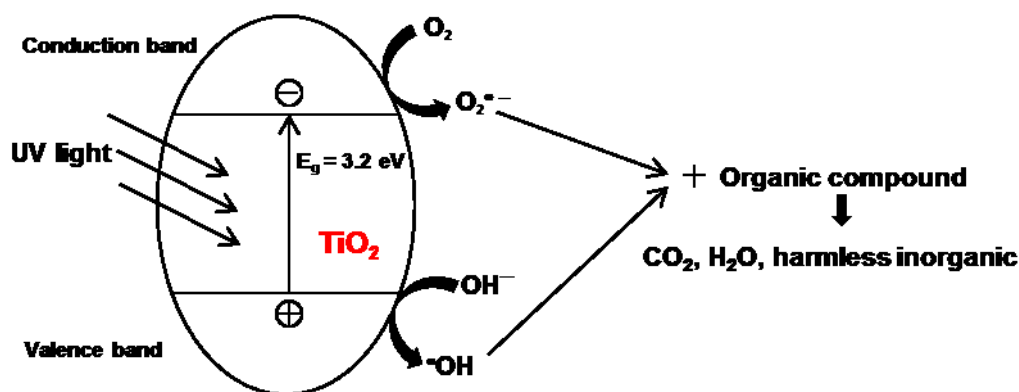


Figure 4. Mechanism of TiO₂ semiconductor photocatalysis.

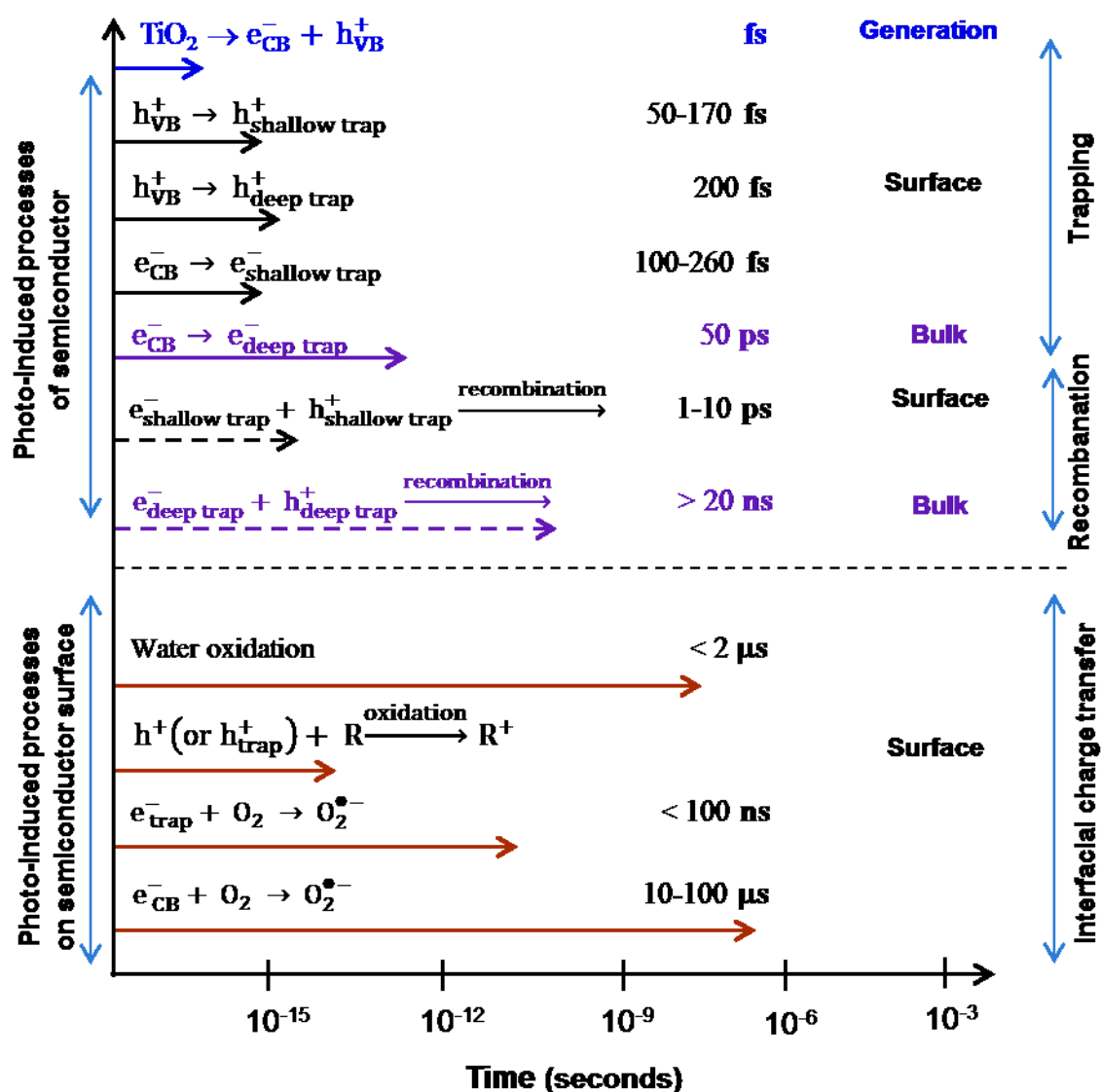
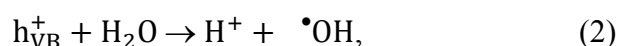


Figure 5. Photo-induced reactions on TiO₂ photocatalyst and the corresponding time scales (taken from Ref. [58]).

According to this mechanism, in the picosecond to nanosecond time domain the overall quantum efficiency for interfacial charge transfer is limited by two competitive procedures: recombination and trapping of charge carriers. However, the charge carrier trapping is dominated by another competition between trapped carrier recombination and interfacial charge transfer in the range of millisecond to microsecond.^[44,59] The quantum efficiency is expected for the photocatalytic reaction by extending the lifetime of photogenerated electron-hole pairs and facilitating the rate of the interfacial charge transfer process as well.^[68,69]

➤ Finally, they can react with donor or acceptor molecules which adsorbed on the catalyst surface to form active species.^[34,42,70]

- The photogenerated holes (VB holes) either (i) directly oxidize the adsorbed organic pollutant or (ii) indirectly via reaction pathway with the surface-bound hydroxyl group (OH^-) and/or the adsorbed water molecules to produce hydroxyl radicals ($\cdot\text{OH}$).



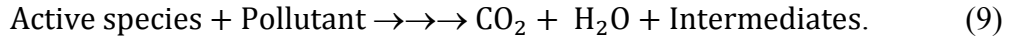
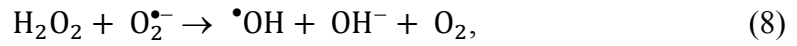
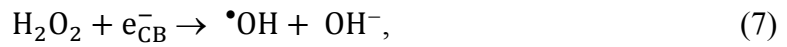
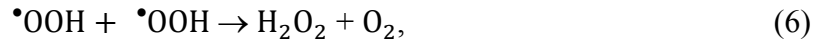
In general, the highly active $\cdot\text{OH}$ radicals are known to work as the principal reactive species capable of destructing a variety of organic pollutants.^[38,45] Furthermore, the formation of $\cdot\text{OH}$ radicals also might be achieved by a multistep reduction of molecular oxygen.^[2,71,72]

In the photocatalytic degradation reaction, one of the main uncertainty is whether oxidation proceeds via a direct electron transfer between organic compounds and photogenerated holes or an $\cdot\text{OH}$ radical-mediated pathway.^[10,73] Basically, both the direct oxidation of organic compounds and the formation of $\cdot\text{OH}$ radicals are proceeded by these holes which have strong oxidation potential (+1.0 to +3.5 V vs. NHE depending on the semiconductor and pH^[44]). Most studies favor the $\cdot\text{OH}$ radical mechanism, while holes oxidation has been suggested for compounds lacking abstractable hydrogen and for some aromatic compounds.^[38,45,51,73,74] Yates's group reported that $\cdot\text{OH}$ radicals did not play any important role in photo-induced oxidation of trichloroethylene on commercial photocatalyst titania P25 in gas-phase. Besides, using means of a fluorescence probe method to measure the quantum yield of the formation of $\cdot\text{OH}$ radicals, Hashimoto's group also suggested that the formation of $\cdot\text{OH}$ radicals was not the major process on irradiated TiO_2 in aqueous solutions. Using time-resolved spectroscopy, a few systematic studies demonstrated for the one-electron oxidation processes, in which the primary one-electron oxidation should be initiated by free or trapped holes.^[70,75-77]

- The photogenerated electrons (CB electrons) which have a reduction potential of +0.5 to -1.5 V vs. NHE^[44] react with adsorbed molecular oxygen (O_2) on the catalyst surface to form superoxide radicals ($\text{O}_2^{\cdot-}$). The $\text{O}_2^{\cdot-}$ radicals can react with H^+ to generate hydroperoxyl

radicals ($\bullet\text{OOH}$) (Eq. (5)). $\bullet\text{OOH}$ radicals also have electron scavenging properties similar to oxygen, thus prolonging the lifetime of VB holes.^[70,71]

The role of molecular oxygen during photocatalytic degradation processes has been long debated. Oxygen is normally not desired as it competes with the pollutant molecules for the CB electrons which are responsible for initiating photo-reduction reactions (Eq. (4)).^[78] On the other hand, oxygen is also considered very important since it acts as a predominant reactant to produce reactive oxygen species.^[2,63]



All of active species including VB holes, CB electrons, $\bullet\text{OH}$ radicals, $\text{O}_2^{\bullet-}$ (or $\bullet\text{OOH}$) radicals, H_2O_2 and O_2 molecules may play an important role in the photocatalytic degradation reactions.^[22] The contribution of active species to the photocatalytic reaction can be detected by selective trapping experiments. Ethanol, citric acid, glycerol, or ethylenediaminetetraacetic acid (EDTA) acts as an effective sink for holes (hole scavenger) diminishing the recombination of electron-hole pairs at the surface of photocatalyst.^[79–82] Also AgNO_3 has been used as electron scavengers in water oxidation under UV light irradiation since AgNO_3 itself decomposed under irradiation alone to generate O_2 .^[83] The oxygen radical scavengers are commonly used such as *tert*-Butanol (*t*-BuOH) or *i*-Propanol acts as a hydroxyl ($\bullet\text{OH}$) radical scavenger,^[10,74,80,84,85] benzoquinone acts as a superoxide ($\text{O}_2^{\bullet-}$)/hydroperoxyl ($\bullet\text{OOH}$) radical scavenger.^[85,86] Electron spin resonance (ESR) or electron paramagnetic resonance (EPR) and photoluminescence spectroscopy have been used to detect free radicals.^[87,88]

A large number of studies have investigated the photocatalytic pollutant degradation over different photocatalysts. However, the elementary steps involved in the complex degradation process are not fully understood so far. Proposed reaction mechanisms, e.g. for ibuprofen (IBP) degradation, are based on formed reaction intermediates (by-products) determined by gas chromatography–mass spectrometry (GC-MS) and electrospray ionization time-of-flight mass spectrometry (ESI-TOF-MS)^[9,11,13,89] (Figure 6). Namely, when titania-based catalysts excited by UV light, the active species (h^+ , $\bullet\text{OH}$, $\bullet\text{OOH}$, or $\text{O}_2^{\bullet-}$) are formed.^[22] The photocatalytic degradation of IBP proceeds via formation of (1) different side chain partial

oxidation products, (2) deeper oxidized aromatic ring intermediates, and (3) ring-opening products, followed by the total oxidation (mineralization) of ring-opening products to carbon dioxide and water. Taking phenol (Ph) as an example of IBP intermediate, the pathway of aromatic ring opening is described and shown in Figure 6.^[90,91] E.g., the highly active species, hydroxyl $\cdot\text{OH}$ radicals attack phenol molecules leading to the formation of dihydroxybenzene (3a). Further photocatalytic degradation proceeds through the cleavage of dihydroxybenzene. Two possible ways for aromatic ring opening with the prolonged UV irradiation time: (i) the formation of Pent-2-enedioic acid (3b) and formaldehyde (3c) and (ii) the formation of maleic acid (3d) and benzoquinone (3e). The aromatic ring opening of benzoquinone (3e) and the decarboxylation (“photo-Kolbe” reaction)^[92] of maleic acid (3d) result in the formation of oxalic acid (3f). Decarboxylation of oxalic acid further leads to the formation of carbon dioxide and water molecules (mineralization step). The reaction can proceed in parallel because the photocatalytic oxidation is not selective.

Many semiconductors are based on metal oxides or sulphides such as TiO_2 , ZnO , ZrO_2 , SnO_2 , WO_3 , CeO_2 , Fe_2O_3 , Al_2O_3 , ZnS and CdS .^[44] They are characterized by the difference in band gap energy (E_g), potential energy of valence band and conduction band (Figure 2). Among them, titanium dioxide (TiO_2) is an especially attractive photocatalyst for non-selectivity oxidation of pollutants.^[93,94] TiO_2 -based photocatalytic water treatment processes which make it superior to other photocatalysts have interesting advantages:^[41,46,95]

- Chemical stability in aqueous media and in large range of pH ($0 \leq \text{pH} \leq 14$)
- Low cost of titania
- Cheap chemicals in use
- No additives required (only oxygen from the air)
- System applicable at low concentrations
- Great deposition capacity for noble metal recovery
- Absence of inhibition or low inhibition by ions generally present in water
- Total mineralization achieved for many organic pollutants
- Highly photocatalytic efficiency with halogenated compounds
- Possible combination with other decontamination methods (in particular biological).

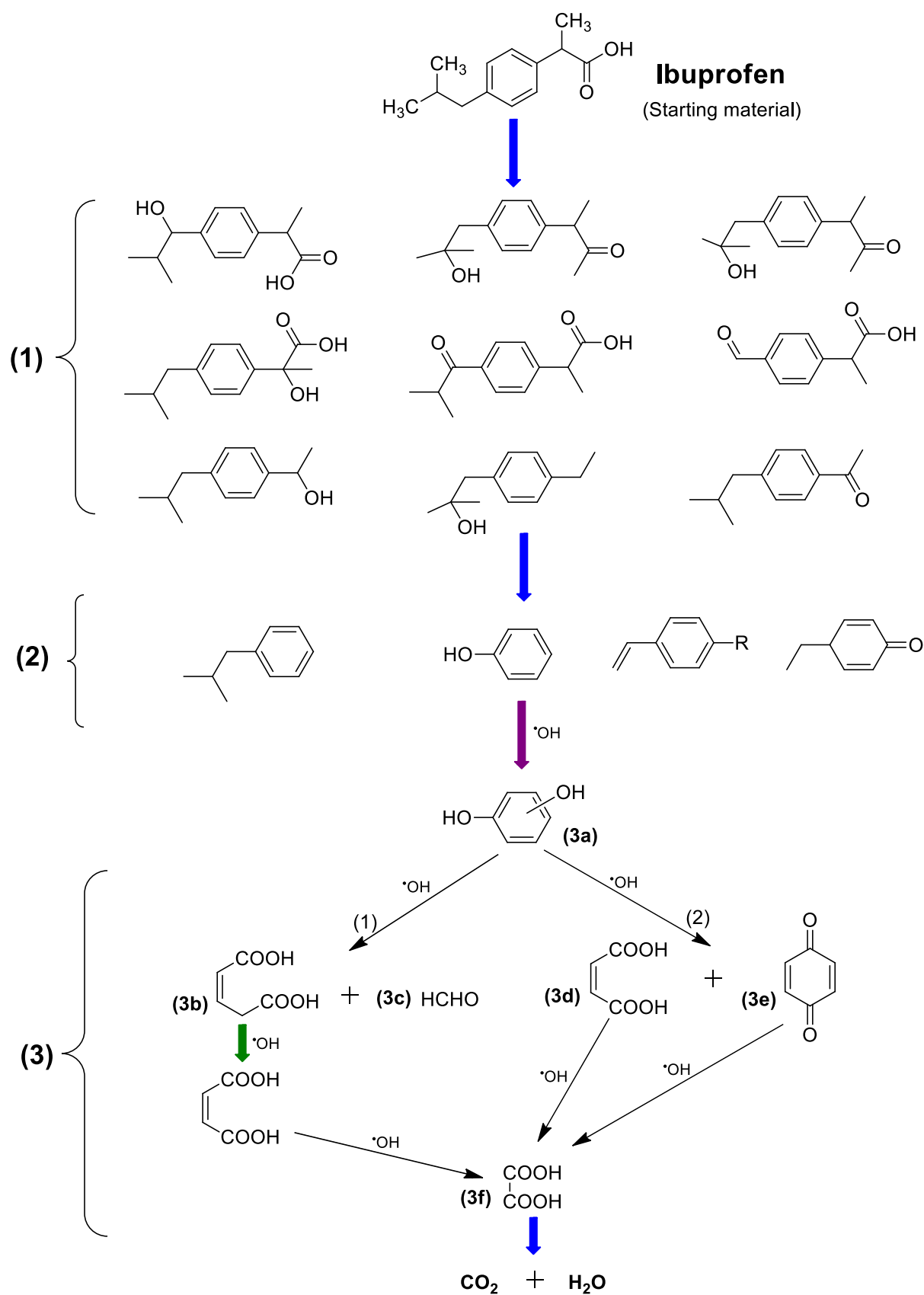


Figure 6. Formation of (1) side chain products and (2) deep oxidation products, (3) aromatic ring opening of phenol as intermediate during the photocatalytic degradation of ibuprofen (taken from Ref. [9,90]).

In 1972, Fujishima and Honda discovered the photocatalytic splitting of water on TiO_2 electrodes.^[96,97] This event marked the beginning of a new era in heterogeneous photocatalysis. Although TiO_2 absorbs only 5% of the solar light reaching the surface of the earth, it shows high efficiency in the photocatalytic degradation (depollution). In recent years, the TiO_2 -based photocatalytic degradation of organics has been employed to solve the important problems of environmental interest such as waste and drinking water treatment and air purification as well.^[34,36,43,46,98]

The TiO_2 occurs in three main polymorphs Anatase, Brookite, and Rutile.^[98,99] With bulk material, the band gap energy of Anatase phase is 3.2 eV and of Rutile phase is 3.0 eV.^[95,100] Brookite is the least studied titania phase and the experimental band gap energies in the range of 3.1 to 3.4 eV are reported.^[101] In the structure of TiO_2 , O 2p orbitals contribute to the filled valence band, while Ti 3d, 4s, 4p orbitals contribute to the unoccupied conduction band (CB). The lower position of CB is dominated by Ti 3d orbitals.^[102] Among the three polymorphs, Rutile is most thermodynamically stable, whereas Anatase and Brookite are metastable and can be transformed to Rutile by thermal treatment at elevated temperatures.^[51,98,103]

According to the previous reports, the photocatalytic activity of TiO_2 is dependent on the surface and structural properties such as surface area,^[104,105] crystal composition,^[106] particle size distribution, porosity, band gap and surface hydroxyl density.^[65,107,108] In general, the smaller the catalyst particle size, the larger the surface area.^[51] Thus, it can increase the number of active surface sites, and adsorb more target molecules (higher organic loading) leading to enhance the photocatalytic efficiency significantly. At nanoscale range, physical and chemical properties of semiconductor catalysts are easily modified and optimized by changing their diameters. Nanoparticles usually not only offer desired crystalline structure but also come with a large surface area (high adsorption capacity).^[2,109]

Generally, Anatase has been found to be most active for various types of photocatalytic reactions.^[110,111] In contrast, Rutile usually show lower activity, which might be related to (i) higher temperature needed for Rutile preparation leading to increase in particle size, (ii) higher electron-hole recombination rate in Rutile, (iii) different extents of surface hydroxylation (hydrophilicity), and (iv) lower reduction potential of CB electrons.^[112] However, a suitably high active mixed-phase photocatalyst titania P25 Degussa (Evonik) is known. This catalyst consists of 80% Anatase and 20% Rutile manufactured by the high-temperature combustion of titanium(IV) chloride (TiCl_4).^[113,114] However, the reasons for high activity have not been elucidated in detail.

The differences between titania polymorphs Anatase, Brookite, and Rutile are following:

❖ The difference in crystalline structure as given in Figure 7: Both Anatase and Rutile have a tetragonal crystal structure but unit cell of Anatase has larger volume than that of Rutile. This is due to the Ti-Ti distances in Anatase structure which is greater than in Rutile, whereas Ti-O distances are shorter. Brookite has an orthorhombic crystalline structure. However, all of them consist of deformed TiO_6 octahedra (Ti^{4+} ions bordered by six O^{2-} ions).^[115] The difference between the three crystal structures are the various degrees of distortion and 3-D assembly of the TiO_6 octahedra. Rutile's crystal structure is built up from octahedral units that are connected by their edges. In contrast, each octahedron shares corners in Anatase's crystal structure. In Brookite's crystal structure, both corners and edges are connected.^[98,116] Obviously, the different arrangement leads to the distinct densities and band structures which reflect the difference in optical/electrical properties between titania polymorphs.^[100]

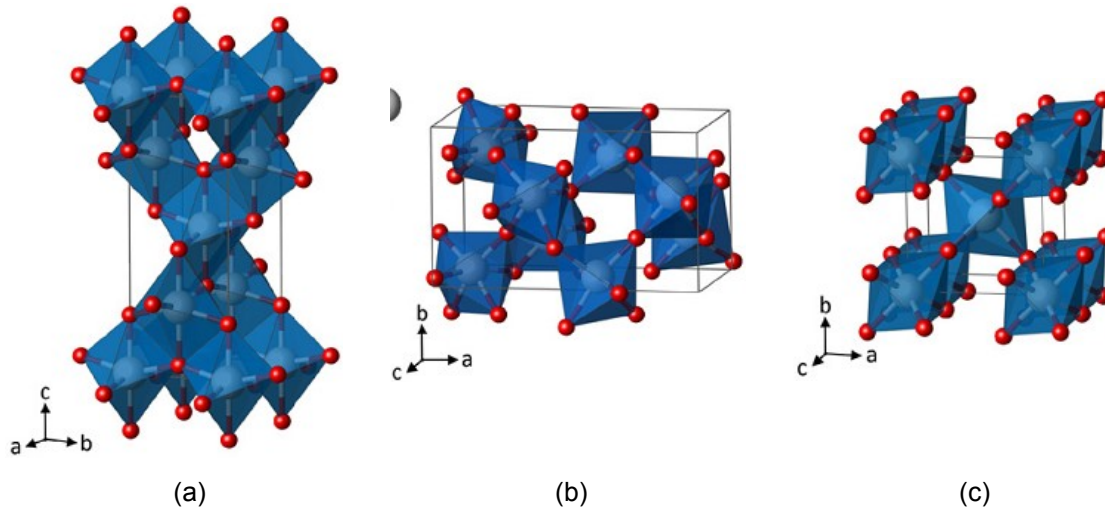


Figure 7. TiO_6 polyhedra for the TiO_2 phases (a) Anatase, (b) Brookite and (c) Rutile (Ti^{4+} (white), O^{2-} (red), and gray lines represent the unit cell) (taken from Ref. [117]).

❖ The difference in band structure (including the band gap energy and the positions of VB and CB with reference to the water redox potential): Both Anatase and Brookite have greater band gap energy than Rutile.^[98,118] Additionally, both Anatase and Brookite have indirect band gaps, while Rutile has a direct band gap.^[101,119-121] A longer lifetime of charge carriers originating from the nature of the indirect band gap compared to the direct band gap would make it more likely for charge carriers to participate in surface reactions.^[53,54,56,120,122] Comparison of recombination processes of photogenerated electron-hole pairs within direct and indirect band gap semiconductors is shown in Figure 8. The minimum CB and the maximum VB locate at the same momentum values for the direct band gap semiconductor and at different momentum values for the indirect band gap semiconductor.^[54,56,108,119]

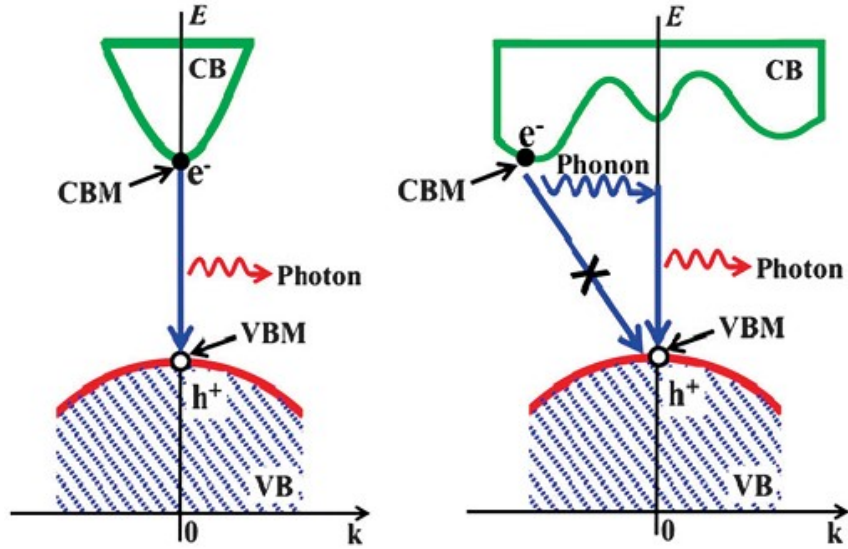


Figure 8. The difference in recombination pathways of photogenerated electron-hole pairs in (left) direct and (right) indirect band gap semiconductors (taken from Ref. [108]).

When the excited electrons come back from CB to VB due to the recombination of electron-hole pairs, these electrons must be followed by the transition selection rule of momentum conservation.^[108] For the direct band gap semiconductor, an electron only emits a photon for the recombination. In contrast, the recombination of electron-hole pair is assisted by a phonon for indirect band gap semiconductor. The nature of phonon relates to the vibration energy of atoms within crystal lattice (thermal energy).^[54] Thus, the CB electrons cannot recombine directly with VB holes leading to the extending of electron-hole lifetime with indirect band gap semiconductor compare to that of direct band gap semiconductor.

A search using the Web of ScienceDirect database of articles published from 1995 to 2016 was carried out as shown in Figure 9. The search keywords were “TiO₂ and photocatalytic activity” and “Brookite and photocatalytic activity”. The obtained search identified 2648 articles for “TiO₂ and photocatalytic activity” and only 218 articles reported to “Brookite and photocatalytic activity” in 2015. It can be seen that a great deal of research has been conducted on the photocatalytic performance of titania-based materials, while the studies on Brookite polymorph have been restrained. The reason is probably that purification (obtaining in a phase-pure form) is difficult because the formation of Brookite is always accompanied by secondary phases as Anatase or Rutile.^[98,123] Recently, the interest in Brookite has increased, although most of the researches fully concern the preparation of Brookite. As a photocatalyst, Brookite is still a promising candidate in order to improve the activity of titania-based catalysts working in ultraviolet region for photocatalytic applications.^[124]

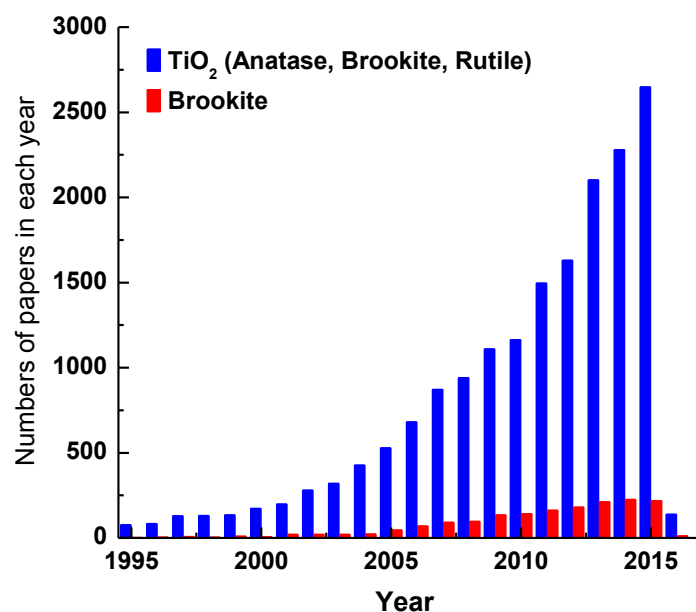


Figure 9. Relative numbers of research articles focused on photocatalysis per year: search results in the period of 1995–2016 with the “Web of ScienceDirect” by the keyword “TiO₂ and photocatalytic activity” (blue bars) and by the keyword “Brookite and photocatalytic activity” (red bars).

Many synthetic techniques have been utilized in the preparation of phase-pure Brookite as well as titania-based materials such as sol-gel method,^[95,114,125-127] hydrothermal method,^[101,128,129] thermolysis method,^[130,131] or peptization in acid/base media.^[132,133] Among these methods, sol-gel method, hydrothermal method or a combination of sol-gel and hydrothermal methods are more commonly used.

In sol-gel method: the hydrolysis reaction between the Ti precursor derived from alkoxide complexes and water/alcohol leads to the formation of original nuclei or basic units of titanium dioxide, whereas the parallel condensation reaction in which the Ti-O-Ti network is formed, conducts to the formation of a gel. The obtained gel which is dried at ambient temperature is amorphous. The final powders are mostly annealed at elevated temperatures to release organic residuals from the TiO₂ matrix.^[114,134]

Beside the sol-gel method, the hydrothermal treatment has been attracted much attention considering that it directly produces highly crystalline titania nanoparticles in a wide range of compositions within a short period of reaction time.^[135] In hydrothermal method: chemical reactions occur in aqueous or organo-aqueous media at raised temperatures and pressures.^[136,137] Noticeably, significant variations to the sol-gel method have been adopted to prepare titania-based materials, such as the replacement of the calcination step by hydrothermal treatment.^[137]

With alkoxides or tetrachloride as the titanium source, previous work showed that selective crystallization of Anatase and Rutile is readily achievable,^[111,131,138,139] and the phase selection is significantly influenced by chemical modification of the acid or base agents, the reaction

solution pH, the reactant concentration.^[134,136,137] On the other hand, it is difficult to obtain Brookite nanoparticles which crystallize in a phase-pure form and are stable to against recrystallization. Some studies reported that Brookite is classically obtained from aqueous or organic media via hydrothermal treatment (Table 4).

Table 4: Summary of studies of preparation and photocatalytic degradation of pollutants in water using phase-pure Brookite as photocatalyst.

Synthesis method	Photocatalytic testing conditions					Conversion (%)	Ref.
	Target	Lamp	Ratio of cat./sub	Light source	Irradiation time		
Hydrothermal	Methylene blue (MB)	Xe lamp 300W	20	UV	120 min	86	[140]
Hydrothermal	Methyl orange (MO)	Hg lamp 150W	33	UV	-	-	[130]
Sol-gel Hydrothermal	Alprazolam	Hg lamp 125W	108	UV	30 min	98	[141]
Thermohydrolysis	4-nitrophenol	Hg lamp 125W	0.03	UV	-	-	[142]
Hydrothermal	Bisphenol A (BPA)	Hg lamp 150W	12.5	UV	60 min	10	[106]
Hydrothermal	Methyl orange (MO)	Xe lamp 300W	100	UV	60 min	100	[143]
Hydrothermal	Orange II dye (0.02M)	Fluorescent lamp, 13W	-	UVA	180 min	100	[144]
Hydrothermal	Methylene-blue (MB)	-	12.5	UV	10h	50	[145]
Hydrothermal	Rhodamine B (20ppm)	Hg lamp 250W	-	UV	-	35	[146]
Hydrothermal	Rhodamine B (20ppm)	Hg lamp 300W	50	UV	100 min	73	[147]
Hydrothermal	Methyl orange (20μM)	Hg lamp 200W	-	UV	-	-	[135]
Hydrothermal	Rhodamine B	Halogen lamp, 200W	-	UV	-	-	[149]
Hydrothermal	Methylene-blue (MB)	20 W	12.5	UVA	90 min	20	[150]
Hydrothermal	Methyl orange 10ppm	-	-	UV	120 min	100	[151]

Table 4 also lists the reported investigations about the photocatalytic activity of phase-pure Brookite. However, the photocatalytic performances mostly carried out by using traditional UV irradiation source such as mercury vapour high or low pressure lamp. The major drawback of vapour lamp is known that: (1) power instability during long time operation, (2) low photonic efficiency, (3) high voltage at initial stage, (4) cooling, (5) sufficient vapour pressure, (6) less lifetime, (7) emit broader spectral wavelength, (8) use of hazardous metal.^[35] The mercury (Hg) vapour lamps, widely used in UV water treatment, produce UVC radiation of 254 nm. In principle, UVC which is the highest energy UV light is very damaging to cells. UVC does not

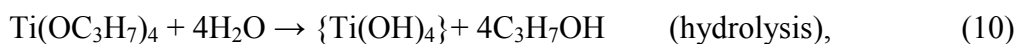
normally reach the Earth's surface because it is absorbed by the ozone layer.^[148] Therefore, the efficient use of solar light based photocatalytic reaction is clear and sustainable to environment. Besides, the high ratio of catalyst to substrate instead of high organic loading is considered to apply for the photocatalytic reaction. Furthermore, dyes (such as azo dye MB, MO, RhB) are commonly used as model pollutants and the photocatalytic degradation mostly reflect the decolourization behaviour, rarely report the abatement of aromatic rings presented in corresponding dye molecules. For that reason, the synthesis and investigation of photocatalytic behaviour of Brookite need to be studied in more detail and comparison with Anatase, Rutile, and P25 Degussa. This study would contribute an alternative photocatalyst, Brookite polymorph, and give further information about the difference in the photocatalytic activity of different crystalline types of TiO_2 and in the chemical reactivity of pharmaceutical compounds and dyes as well. For that reason, the photocatalytic performance of Brookite in the degradation of organic pollutants needs to be studied in more detail and compared with Anatase, Rutile, and titania P25 Degussa. More reliable photocatalytic conditions as sunlight equivalent low power UV-vis solarium lamps, lower catalyst concentration combined with enhanced pollutant loading, different reactive pollutants including highly recalcitrant X-ray contrast agent should be studied. The latter belong to new emerging pollutants. This also includes the role of different active species as well as the formation of reaction intermediates.

The aim of this study is a comprehensive investigation of the photocatalytic performance of the less known titania polymorph Brookite compared to Anatase, Rutile, and the commercial photocatalyst titania P25 Degussa as well as of the behaviour of mixed-phase titania. For this purpose, Brookite, Anatase, and Rutile will be hydrothermally synthesized and characterized regarding structure, textural properties and band gap energies.

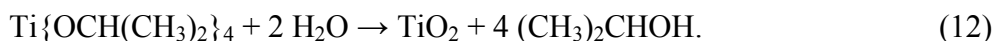
3 Results and discussion

3.1 Phase-pure TiO₂ preparation: Brookite, Anatase, and Rutile

Precursor: In this study, the nano-sized TiO₂ polymorphs Brookite, Anatase, and Rutile have been prepared by hydrothermal treatment of an amorphous titania precursor at elevated temperatures between *ca.* 175 to 200 °C under acidic conditions, using acetic and hydrochloric acid, respectively. The amorphous titania precursor has been obtained by combined hydrolysis and condensation processes of titanium(IV) *i*-propoxide (TTIP) and formed hydrolysed species in isopropanol (*i*-Propanol). The hydrolysis in *i*-Propanol, containing only small amount of water, proceeds slowly allowing parallel condensation of intermediately formed monomeric or low condensed hydrolysis products. These reactions can be schematically represented as follows.^[127]



or can be written:^[134]

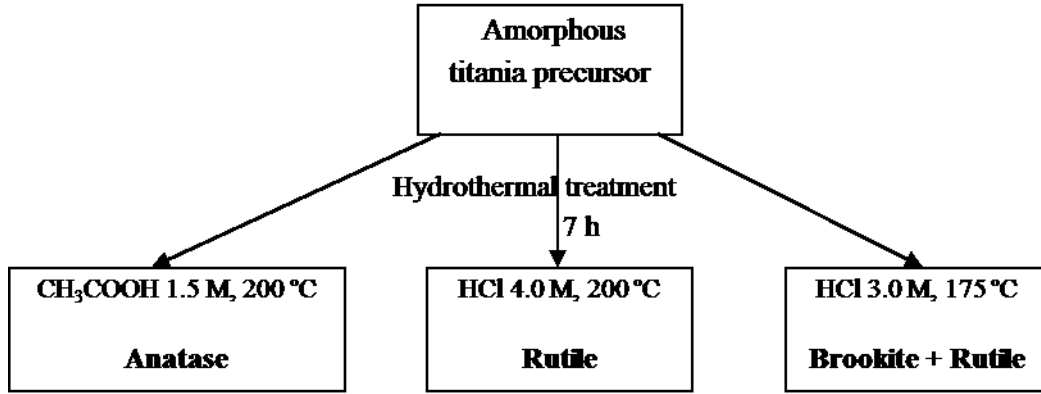


The titanium hydroxide is not stable and forms titanium oxyhydroxide of different composition formal written: TiO(OH)₂ or TiO₂xH₂O. This material is used as amorphous precursor for the hydrothermal synthesis of the titania polymorphs. The hydrolysis/condensation process can be influenced by the titanium and water content of the starting solution. In this case, the synthesis yield of the amorphous precursor has been optimized by changing the titanium content, water content as well as the work up procedure (compare Appendix). The vacuum dried amorphous titania has been used as precursor for the hydrothermal synthesis of Anatase, Brookite/Rutile mixture and Rutile.

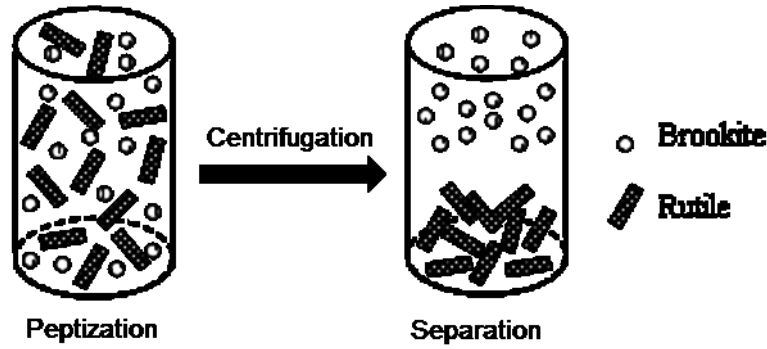
Titania polymorphs: The titania polymorphs Anatase, Brookite and Rutile have been prepared by hydrothermal treatment of the amorphous titania precursor using acetic and hydrochloric acid, respectively (Scheme 1). The advantage of this synthetic approach is that all polymorphs are obtained from the same precursor under similar reaction conditions with one process type. Therefore, the impact of synthesis procedure on the photocatalytic properties is diminished allowing a reasonable comparison of the different crystal phase structures. Whereas Anatase and Rutile have been obtained as pure materials, Brookite is crystallized always in mixture with Rutile. If acetic acid is used, phase-pure Anatase is obtained after hydrothermal heating for 7 h at 200 °C. The use of 4.0 M HCl yields phase-pure Rutile at 200 °C. When HCl concentration is changed to 3.0 M and the temperature is set at 175 °C for 7 h, a mixture of

Brookite and Rutile is formed. However, pure Brookite could be effectively separated from the mixture by peptization. The peptization was carried out using water or nitric acid solution as shown in Scheme 2.

Scheme 1. Synthesis of phase-pure titania.



Scheme 2. Separation of Brookite from the mixture by peptization.



The phase composition of the synthesized mixture of Brookite/Rutile as well as of Brookite-rich and Rutile-rich materials after peptization with HNO_3 (Figure 10) or double distilled water (Figure 11) has been determined based on the intensities of selected XRD reflections of the contained phases. The comparison of the experimental XRD pattern with the calculated pattern of Brookite and Rutile shows that the as-prepared titania contains only Brookite and Rutile. No trace of Anatase is detected as indicated by the absence of the characteristic reflection of Anatase at $2\theta = 62.57^\circ$.^[98] This reflection does not overlap with a diffraction peak of Brookite. The phase content of mixed TiO_2 was estimated based on the integrated intensities of Brookite (121) and Rutile (110). The weight fraction W of TiO_2 polymorphs can be derived by the following equation.^[152,153]

$$W_A = \frac{k_A \cdot A_A}{k_A \cdot A_A + k_B \cdot A_B + A_R}, \quad W_B = \frac{k_B \cdot A_B}{k_A \cdot A_A + k_B \cdot A_B + A_R}, \quad \text{and} \quad W_R = \frac{A_R}{k_A \cdot A_A + k_B \cdot A_B + A_R}, \quad (13)$$

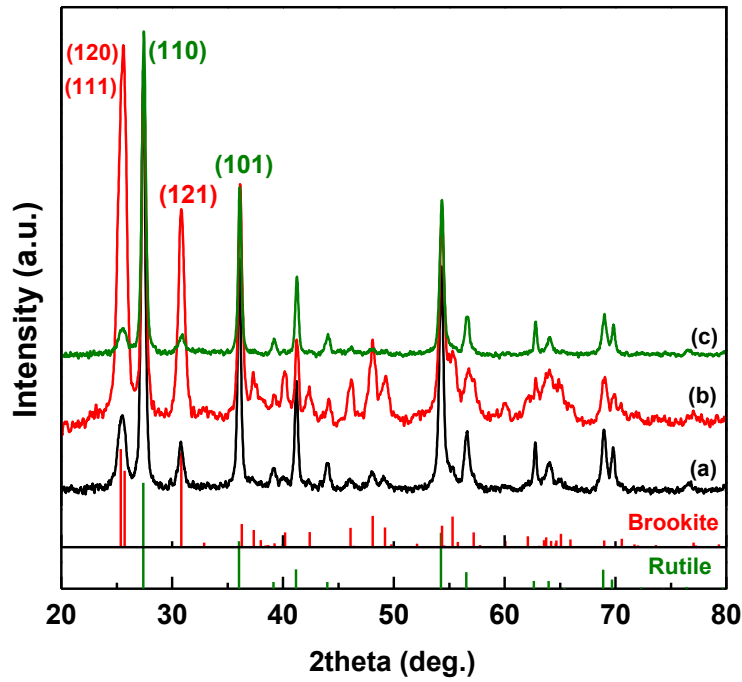


Figure 10. XRD patterns of titania materials obtained by peptization of Brookite/Rutile mixture with HNO_3 : (a) Brookite/Rutile mixture, (b) Brookite-rich phase, (c) Rutile-rich phase, and theoretical diffraction patterns with corresponding lines of Brookite and Rutile.

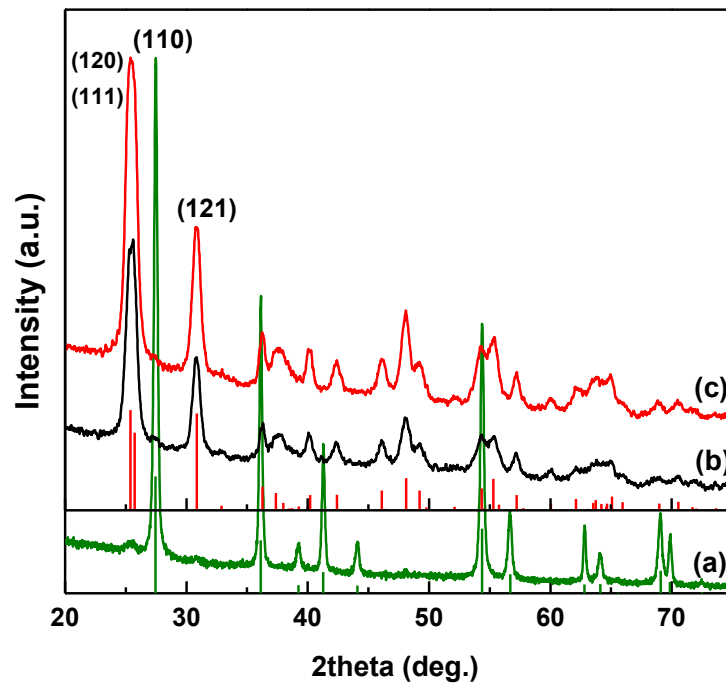


Figure 11. XRD patterns of titania materials obtained by peptization of Brookite/Rutile mixture with water: (a) Rutile, Brookite after the (b) first and (c) second peptization. Pattern (a) and (b) include the calculated diffraction lines from the corresponding JCPDS database (a) 96-900-9084 and (b) 96-900-9088.

where W_A , W_B and W_R refer to the weight fraction of Anatase (A), Brookite (B), and Rutile (R) respectively. A_A , A_B and A_R represent the integrated intensities of Anatase (101), Brookite (121) and Rutile (110), respectively and k_A , k_B are two coefficients which were optimized ($k_A = 0.886$ and $k_B = 2.721$).

The calculations show that the Brookite/Rutile mixture contained *ca.* 23% Brookite and *ca.* 77% Rutile. The Brookite-rich phase obtained by peptization with nitric acid contained *ca.* 63% Brookite and the Rutile-rich phase contained *ca.* 87% Rutile (Table 5). The phase separation by peptization in water is more effective. Phase-pure Brookite and Rutile have been obtained. The corresponding XRD patterns are shown in Figure 11.

Table 5: Compositions and weight fraction of the as-prepared titania powders.

Sample		Weight fraction of Brookite (%)	Weight fraction of Rutile (%)
Hydrothermal		23	77
Peptization with HNO ₃	Brookite-rich	63	37
	Rutile-rich	13	87
Peptization with H ₂ O	Brookite ¹	100	0
	Brookite ²	100	0
	Rutile	0	100
1: Brookite obtained after the first peptization with H ₂ O			
2: Brookite obtained after the second peptization with H ₂ O			

3.2 Characterization of materials

The morphology, crystallinity, structure and size of synthesized titania particles have been investigated using powder X-ray diffractometry (XRD), Raman spectroscopy and scanning electron microscopy (SEM). The samples have been additionally characterized by combined thermogravimetric (TG) and differential scanning calorimetric analysis (DSC) in order to check the thermal stability and the presence of amorphous by-products.

3.2.1 XRD analysis

Figure 12 shows the XRD patterns of the different TiO_2 polymorphs Anatase, Brookite and Rutile obtained by hydrothermal treatment of the amorphous titania precursor. The starting titania material obtained by hydrolysis/condensation processes of titanium(IV) *i*-propoxide in 2-Propanol is amorphous and shows no diffraction pattern. After hydrothermal treatment under different conditions, highly crystalline polymorphs Anatase and Rutile have been obtained as indicated by the characteristic and well resolved XRD patterns (Figure 12b and d). Intensity and diffraction angle of reflections agree with the theoretical diffraction pattern from the JCPDS databases. No additional peaks corresponding to impurities were detected.

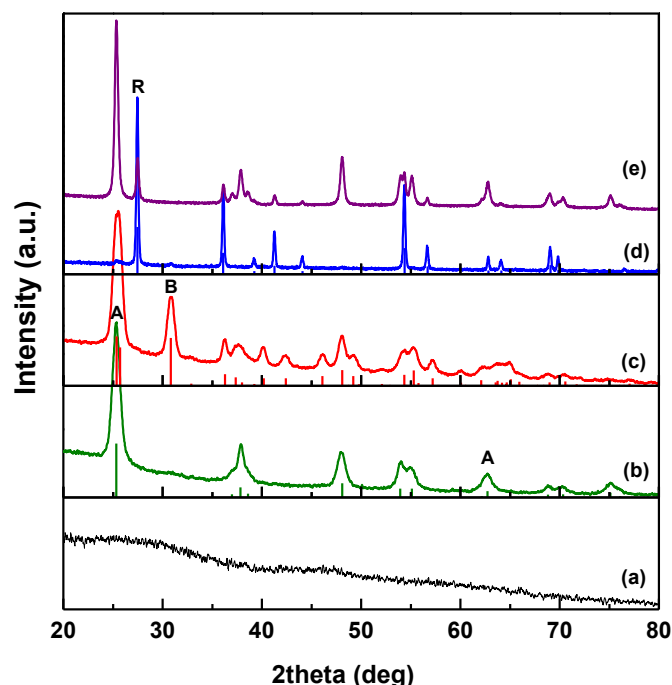


Figure 12. XRD patterns of (a) amorphous titania, (b) Anatase, (c) Brookite, (d) Rutile, and (e) titania P25 for comparison. Pattern (b), (c) and (d) include the calculated diffraction lines from the corresponding JCPDS database (b) 96-900-9087, (c) 96-900-9088 and (d) 96-900-9084. A, B, and R represent Anatase, Brookite, and Rutile phase, respectively.

In both XRD patterns of Anatase and Brookite (Figure 12b and c), the width of diffraction reflections are broad which indicating that the crystallite size is very small as confirmed by

SEM. Besides, the intensity of these reflections showed the high degree of crystallinity of Anatase and Brookite. For comparison, the commercial titania P25 (Degussa) representing an Anatase/Rutile mixture (*ca.* 80/20) has been included. With titania P25 and the synthesized Rutile, the diffraction reflections are narrower (Figure 12d and e) than that of the synthesized Anatase and Brookite indicating higher degree of crystallinity and larger crystallite size (Table 6). It has to be noted that titania P25 is synthesized in the industrial high temperature combustion process of TiCl_4 . The average crystallite size, meaning the range of 3-dimensional perfect periodicity of lattice planes, was calculated by Scherrer equation.^[133]

$$D = \frac{k\lambda}{\beta \cdot \cos\theta}, \quad (14)$$

where D is the crystallite size, k is shape factor that varies from 0.89 for spherical to 0.94 for cubic particles. Usually, this is set to 0.9 for particles of unknown shape. λ is the wavelength of the X-rays ($\lambda = 0.15406$ nm for CuK_α radiation), β is the width of the reflection at half height, and θ is the diffraction angle of the reflection.

Indeed, Anatase and Brookite hydrothermal synthesized from amorphous titania showed small crystallite sizes of *ca.* 10 nm, pointing to the formation of nanoparticles, whereas the Rutile particles showed larger crystallite sizes (Table 6).

Table 6: The crystallite size of the as-prepared Anatase, Brookite, Rutile, and titania P25.

Sample		Crystallite size D (nm)
Anatase		10
Brookite		12
Rutile		98
Titania P25	Anatase	21
	Rutile	67

3.2.2 Raman spectroscopy

Raman spectroscopy is useful to investigate TiO_2 samples, because they show structure dependent characteristic Raman bands which allow identifying the crystal phase and composition of mixtures especially regarding the titania phases Anatase, Brookite and Rutile. Raman spectra give complementary information for XRD analysis. The Raman spectra of synthesized titania samples are in agreement with that of Anatase, Brookite and Rutile confirming the XRD results. The Raman spectrum of titania P25 Degussa containing Raman bands of Anatase and Rutile is studied for comparison (Figure 13b).

The lattice of Brookite has the D_{2h}^{15} symmetry (space group: $Pbca$). According to group theory, there are 69 optical modes ($9A_{1g} + 9B_{1g} + 9B_{2g} + 9B_{3g} + 9A_{1u} + 8B_{1u} + 8B_{2u} + 8B_{3u}$), among which, only A_{1g} , B_{1g} , B_{2g} , and B_{3g} are Raman active.^[123,154] With the synthesized Brookite (Figure 13d), beside the strong band at 155 cm^{-1} (A_{1g}), the weaker Raman bands are observed in the range $200\text{--}700\text{ cm}^{-1}$. They can be assigned to the vibration modes A_{1g} (249, 411, 545 and 637 cm^{-1}), B_{1g} (213 cm^{-1}), B_{3g} (324 and 501 cm^{-1}), B_{2g} (366 , 460 and 584 cm^{-1}), respectively.^[146,155,156] Importantly, the absence of the characteristic Raman bands of Rutile at 442 cm^{-1} ^[157] and of Anatase at 516 cm^{-1} ^[98,156] further confirm the formation of phase-pure Brookite.

In case of Anatase (Figure 13c), four Raman bands appear at 147 , 398 , 516 , and 638 cm^{-1} , which can be assigned to the corresponding E_g , B_{1g} , A_{1g} , and E_g modes, respectively.^[156,158,159] With Rutile as shown in Figure 13e, three typical Raman bands at 245 , 442 , and 607 cm^{-1} are observed, respectively.^[154,157]

The Raman spectroscopic investigations confirm that all samples synthesized in present study, Anatase, Brookite and Rutile, are of high quality and of phase-pure.

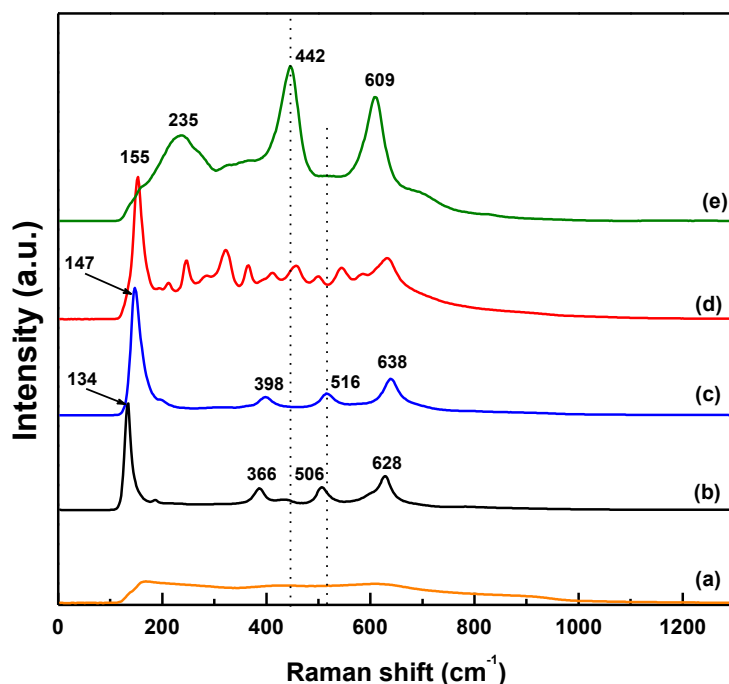


Figure 13. Raman spectra of (a) amorphous titania, (b) titania P25, and the synthesized titania polymorphs (c) Anatase, (d) Brookite, (e) Rutile, respectively.

3.2.3 Thermal Analysis (TG-DSC)

Even XRD patterns and Raman spectra give no further information about the nature of amorphous titania. Some information can be derived from TG-DSC curves as shown in Figure 14. In the DSC curve of the starting amorphous titania material (Figure 14, left), we observed

well resolved peak arising at 120 °C (endothermic) due to the release of more strongly adsorbed water. It is extended to 200 °C indicating starting dehydroxylation process. This assignment is in line with the marked weight loss of *ca.* 23 wt% in this temperature range. The weight loss is extended with further heating to 400 °C, but with *ca.* 5 wt% much lower. At the same time, two exothermic peaks appear at *ca.* 272 and 375 °C in the DSC curve. Both findings point to the occurrence of a combined dehydroxylation/condensation (endothermic/exothermic) process in the amorphous titania. The appearance of such TG-DSC curve can be used to identify the presence of amorphous by-products in synthesized crystalline titania. Figure 14 (right) presents an example of the synthesized Brookite/Rutile mixture showing the additional DSC peaks pointing to the presence of amorphous titania species. Indeed, this sample shows distinctly lower activity in the photocatalytic degradation of Ibuprofen compared to other Brookite/Rutile mixtures obtained by physical mixing. It has been assigned to blocking of the surface of Rutile or Brookite by amorphous deposits.

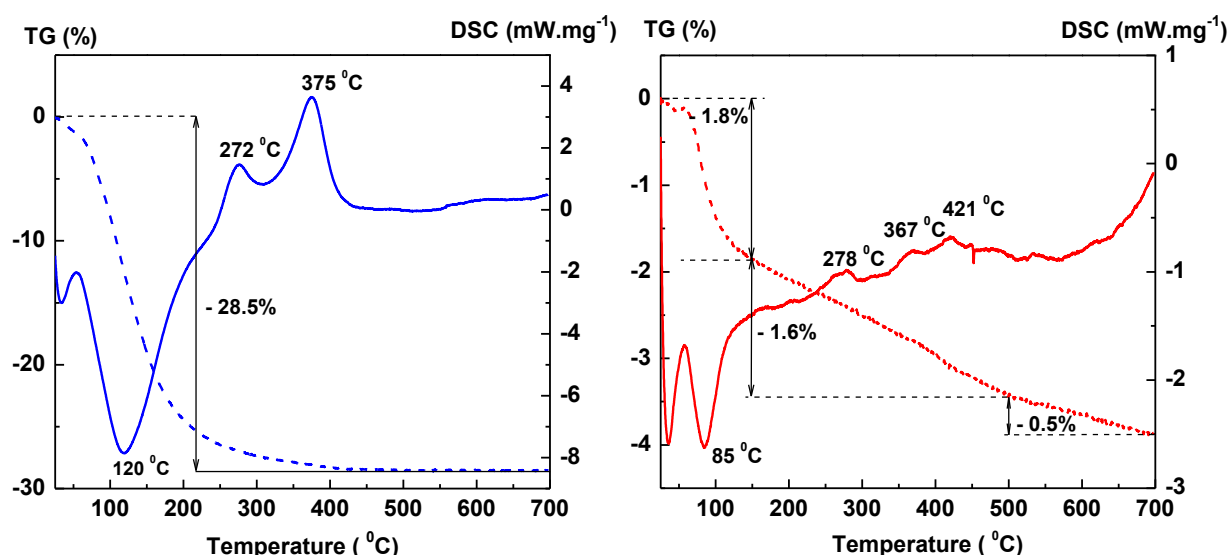


Figure 14. TG-DSC curves of (left) amorphous titania and (right) Brookite/Rutile mixture.

The TG-DSC curves of the as-prepared TiO₂ polymorphs until heating to 700 °C are shown in Figure 15. In case of Anatase, a total weight loss of *ca.* 8.3 wt% is observed (Figure 15a). The TG curve shows three main loss steps. Between RT and 150 °C, *ca.* 3.3 wt% is desorbed which is related to the physically adsorbed water with an endothermic DSC peak at 86 °C. The second weight loss of *ca.* 4.4 wt% is observed between 150 and 500 °C with an intermediate step at 270 °C. This weight loss is due to two exothermic DSC peaks at *ca.* 232 and 384 °C. They are related to a combined dehydroxylation/condensation process. Above 440 °C, the further weight loss proceeds slowly due to the dehydroxylation/condensation of remained surface hydroxyl groups.

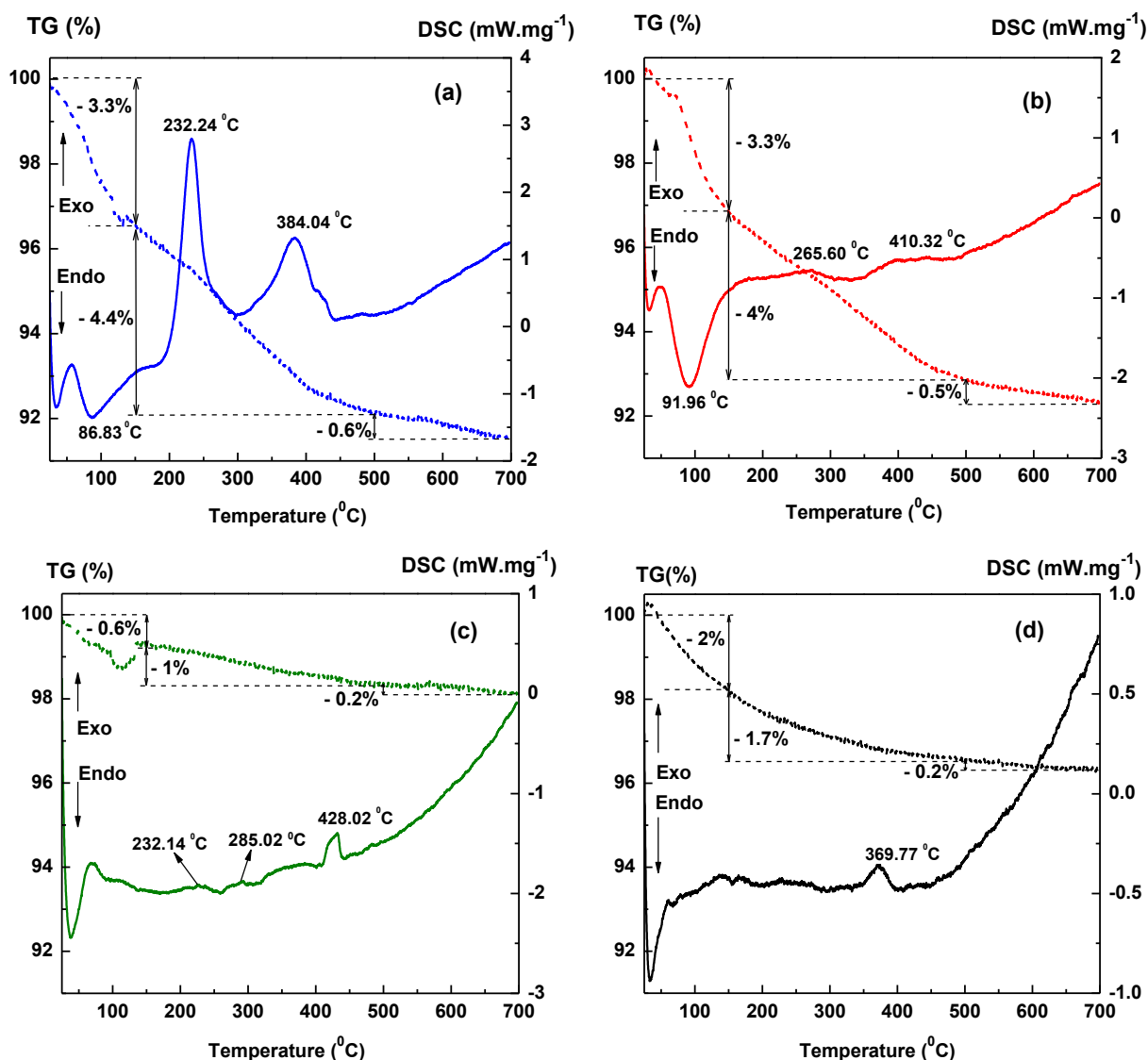


Figure 15. TG-DSC curves of (a) Anatase, (b) Brookite, (c) Rutile, and (d) titania P25.

The TG-DSC curve of Brookite shows in principle a similar behaviour especially in the weight loss (Figure 15b). The first weight loss is similar with an endothermic DSC peak slightly extended to higher temperature (*ca.* 92 °C). This indicates stronger bonding of adsorbed water on the surface of Brookite compared to Anatase. The second weight loss step is accompanied by two weak exothermic DSC peaks at *ca.* 265 and 410 °C. However, their intensities are quite low. These findings reflect the different connectivity of TiO₆ octahedra in both structures as shown in Figure 7.

With Rutile, similar weight loss steps occur up on heating with endothermic desorption of water and exothermic dehydroxylation/condensation at higher temperature. The processes are less pronounced. As a result, the weight loss is very small (Figure 15c). Rutile is the denser phase and the bulk density increases in the order: Anatase (3.89 g/cm³) < Brookite (4.12 g/cm³) < Rutile (4.27 g/cm³).^[135,160] For comparison, the TG-DSC curve of titania P25 (a

mixture of Anatase and Rutile) synthesized at high temperature is studied. It shows weak features with the exothermic DSC peaks at *ca.* 370 and 420 °C (Figure 15d), which likely belong to Anatase and Rutile, respectively. Based on the weight loss and the specific surface area, the densities of the physisorbed water and chemisorbed OH⁻ groups are calculated.^[110] Rutile is covered with larger amounts of physisorbed water (*ca.* 2 times) and chemisorbed OH⁻ groups (*ca.* 3 times) than with Anatase and Brookite (Table 7). This property is correlated with the surface hydroxylation which might explain the difference in the photocatalytic performances between titania polymorphs Anatase, Brookite, and Rutile.^[112]

Table 7: The densities of the physisorbed water and chemisorbed OH⁻ groups calculated based on the weight loss and S_{BET} for Anatase, Brookite, Rutile, Brookite/Rutile mixture, and titania P25.

Sample	Weight loss (%)		S _{BET} (m ² /g)	Amount of physisorbed water (molecules/nm ²)	Amount of chemisorbed OH ⁻ groups (molecules/nm ²)
	RT-150 °C	150-500 °C			
Brookite/Rutile	1.8	1.6	49	12.3	11.6
Anatase	3.3	4.4	132	8.4	11.8
Brookite	3.3	4.0	116	9.5	12.2
Rutile	0.6	1.0	12	16.7	29.5
Titania P25	2.0	1.7	46	14.5	13.1

3.2.4 Scanning electron microscopy (SEM)

The morphology (shape and size) of synthesized titania polymorphs has been studied by scanning electron microscopy (SEM). Figure 16 shows SEM images of amorphous titania as starting material and the hydrothermal products Anatase, Brookite, and Rutile, respectively. The amorphous titania particles are spherical in shape, *ca.* 75 nm in size. By changing hydrothermal conditions, Anatase and Brookite particles consist of agglomerated sphere-shaped nanoparticles, *ca.* 10 nm. These results are in agreement with XRD results which show crystallite sizes of *ca.* 10 nm for Anatase and *ca.* 12 nm for Brookite. In contrast, Rutile TiO₂ powders are large rod-like nanocrystals with some spherical particles. The rod-like Rutile crystals have a width of *ca.* 50-100 nm and a length of *ca.* 300-500 nm. Beside large rod-like nanocrystals, spherical nanoparticles are *ca.* 50 nm. These particles could be identified as non-reacted amorphous titania or small spherical Rutile nanoparticles. Figure 17 compares the SEM images of Brookite samples obtained after the first and second peptization with water. It shows that a second peptization is required to remove also very small Rutile impurities.

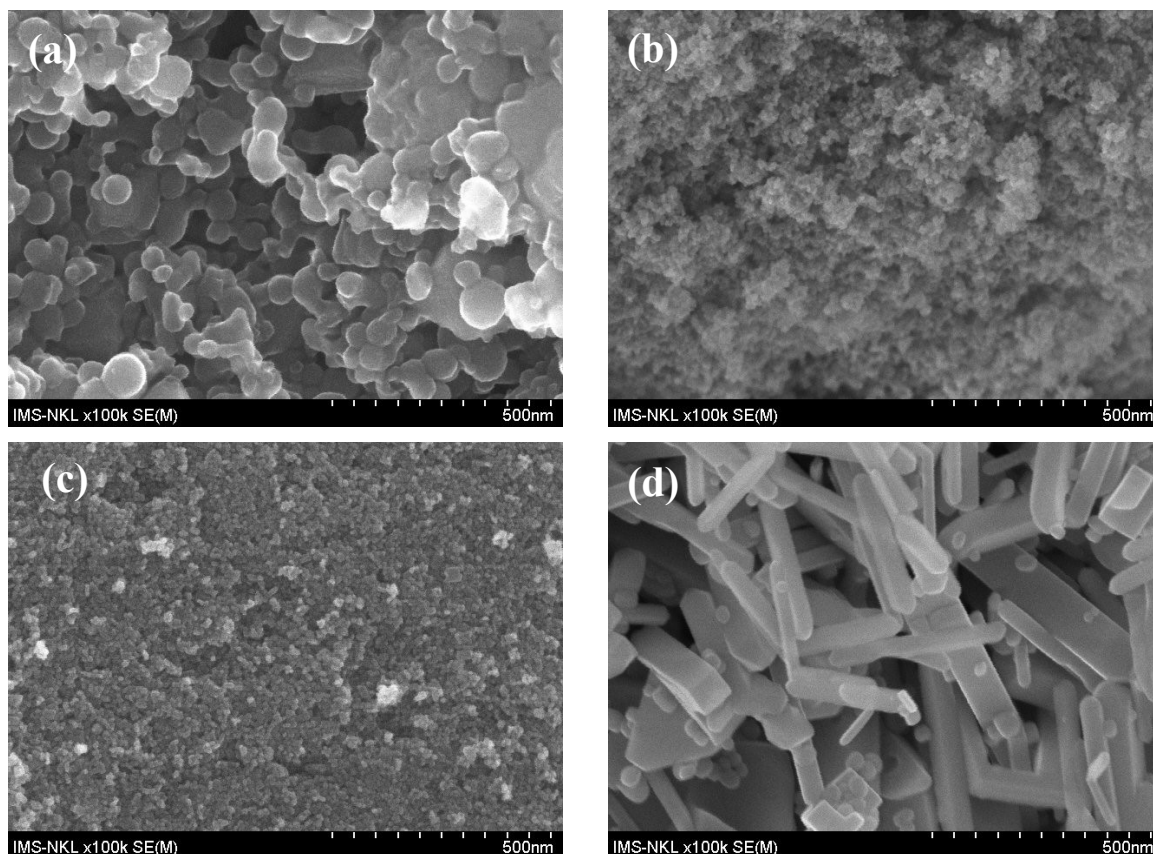


Figure 16. SEM images of (a) amorphous titania, (b) Anatase, (c) Brookite, and (d) Rutile.

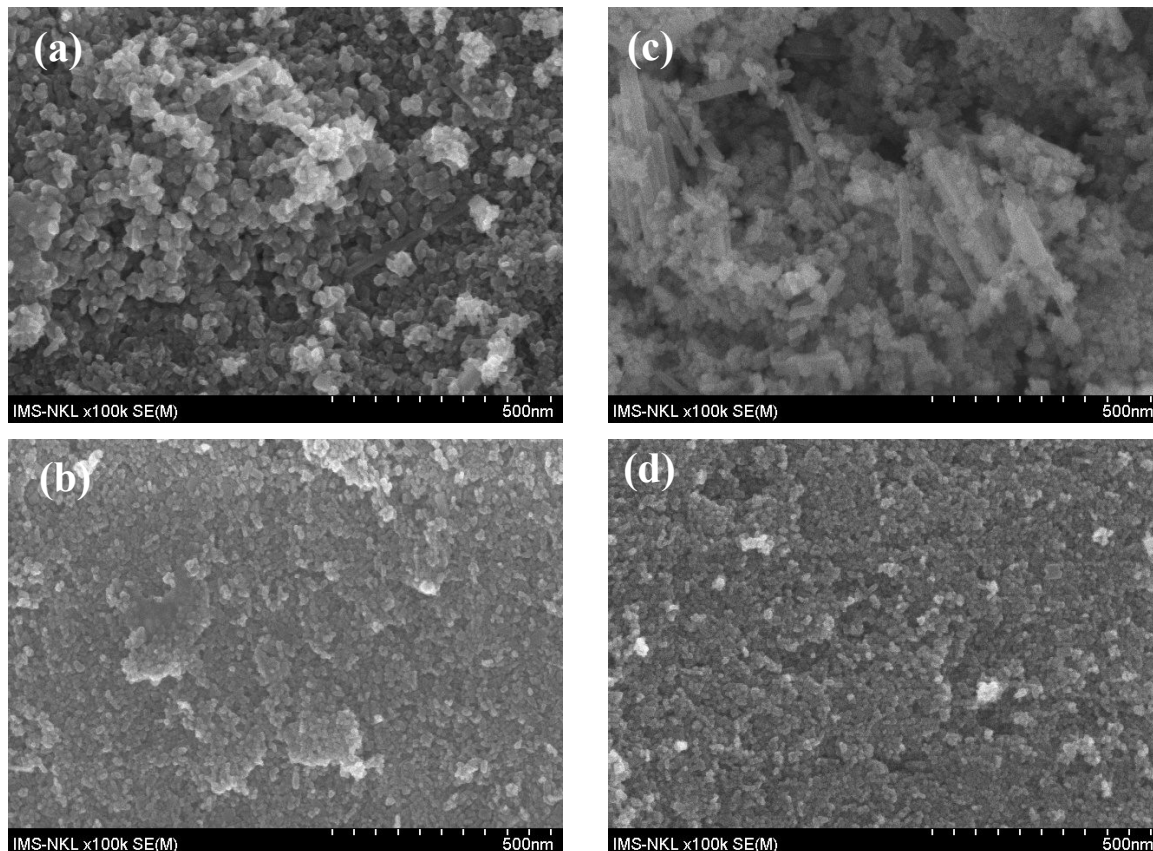


Figure 17. SEM images of Brookite samples obtained after (left) the first and (right) the second peptization with H_2O . Images (a, c) represent precipitates and (b, d) represent corresponding liquids obtained after centrifugation of the Brookite supernatant liquids.

After the second peptization with water, a Rutile-containing precipitate could be removed by centrifugation (Figure 17c). It contains elongated Rutile crystals which could not be removed in the first peptization step (Figure 17a). So, Figure 17d represents the final pure Brookite sample. Obviously some small amounts of Rutile are peptized as long as the liquid is sufficiently acidic. The second dilution with water increases the pH to a critical value where Rutile is not more peptised.

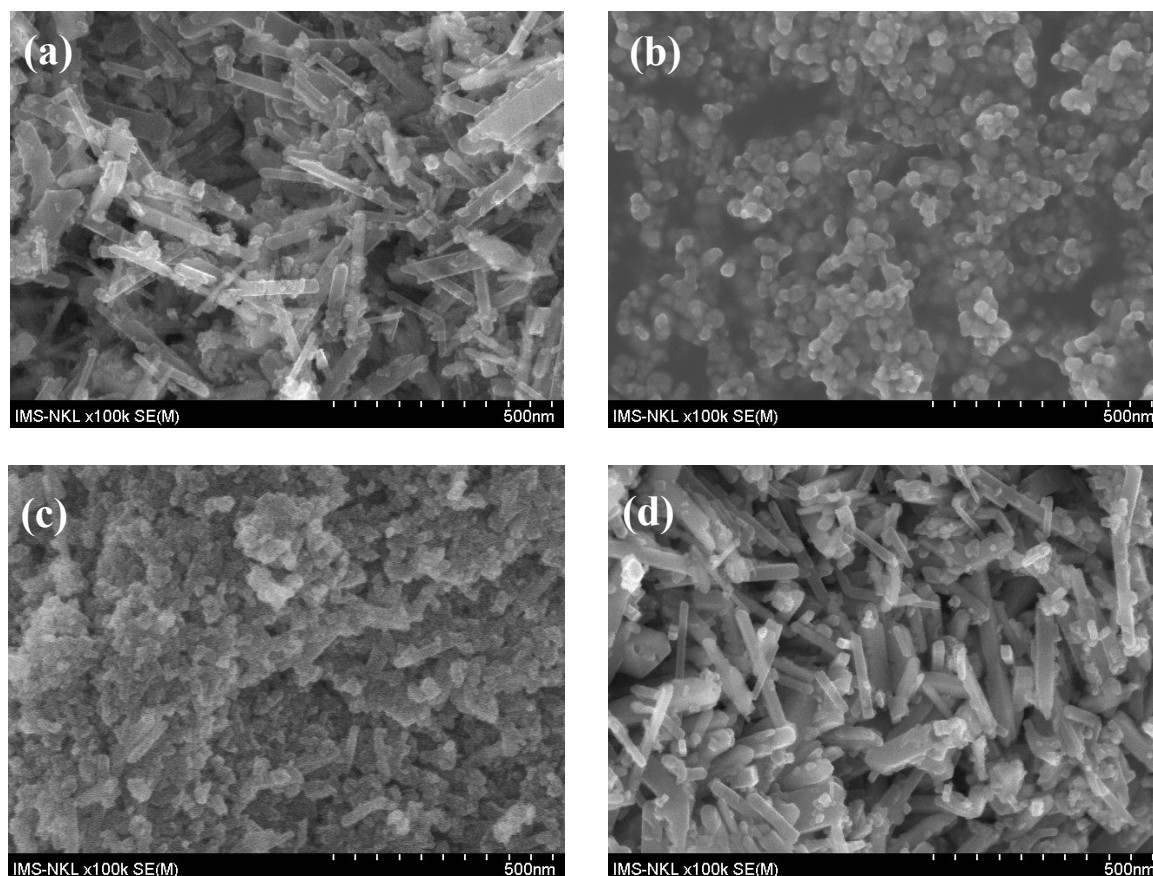


Figure 18. SEM images of the (a) synthesized Brookite/Rutile mixture, (b) titania P25, (c) Brookite-rich, and (d) Rutile-rich recovered by peptization with HNO_3 .

Figure 18a shows the SEM image of Brookite/Rutile mixture. The mixture consists of spherical particles ascribed to Brookite and rod-shaped particles assigned to Rutile. The size of spherical particles is *ca.* 10 nm and the rods have a width of *ca.* 20-50 nm and a length of *ca.* 150-300 nm. Figure 18b shows the SEM image of titania P25, the Anatase/Rutile mixture. The mixture contains spherical particles with a mean particle size of *ca.* 25 nm. The peptization with HNO_3 only is less efficient for separation of Brookite from the mixture. The Brookite-rich sample recovered from the white suspension with HNO_3 (Figure 18c) contains spherical Brookite nanoparticles (*ca.* 10 nm) and a significant amount of Rutile nanorods (37% Rutile as given in Table 6). Rutile nanorods almost completely appeared in precipitate obtained by peptization with HNO_3 have a width of *ca.* 20-50 nm and a length of *ca.* 150-300 nm (Figure 18d).

3.2.5 UV-vis diffuse reflectance

The band gap energies of the synthesized titania polymorphs have been determined from the absorption edge observed from the UV-vis diffuse reflectance spectra. Figure 19 (top) shows the UV-vis diffuse reflectance spectra of amorphous titania, synthesized titania polymorphs, and titania P25. A steep increase of absorption is observed below 450 nm. The spectra show that the absorption is shifted to longer wavelength (bathochromic shift) in the order:

Amorphous titania < Titania P25 < Anatase \approx Brookite < Rutile.

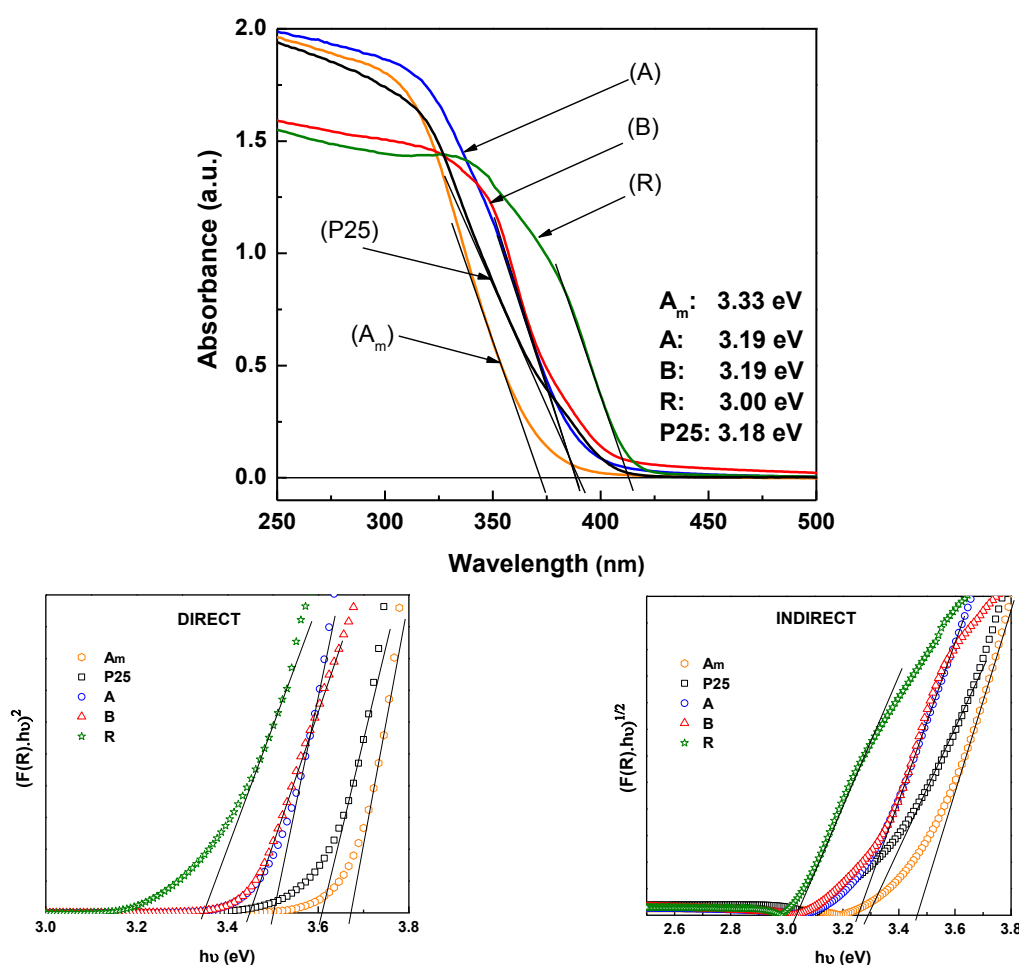


Figure 19. UV-vis diffuse reflectance spectra of the amorphous titania, the as-prepared titania polymorphs, and titania P25 (top). Tauc plots for the determination of the band gap energy E_g for direct and indirect transitions (bottom). A_m, A, B, and R represent amorphous titania, Anatase, Brookite, and Rutile, respectively.

To calculate the band gap energy, the Kubelka-Munk function and Tauc plots were used. The $[F(R) \cdot h\nu]^2$ versus $h\nu$ plot for a direct transition and the $[F(R) \cdot h\nu]^{1/2}$ versus $h\nu$ plot for an indirect transition, where $F(R)$ is the Kubelka–Munk absorption coefficient, $h\nu = 1240/\lambda$ is the photon energy (eV), and λ is the absorption wavelength (nm). E_g was determined as the energy coordinate of the point on the low energy side of $F(R)$ curve at which the linear increase starts.^[101,124,142] In the present work, the band gap energies of the amorphous titania,

the as-prepared titania polymorphs Anatase, Brookite, Rutile, and the commercial photocatalyst titania P25 have been determined for both cases (direct and indirect transitions). The band gap energy decreases in the following order:

$$\text{Amorphous titania} > \text{Titania P25} > \text{Anatase} \geq \text{Brookite} > \text{Rutile}.$$

The obtained band gap energy for direct transitions is larger than the value for indirect transitions (Table 8). Band gap values which are estimated simply from the absorption edge of the UV-vis diffuse reflectance spectra are smaller than the values obtained by using Tauc plots for both types of transitions. The band gap of Rutile is determined by direct transitions ($E_g = 3.34$ eV). The band gap energies of Anatase and Brookite ($E_g = 3.25$ eV) calculated for indirect transitions are larger than the value of 3.2 eV usually reported for the bulk TiO_2 . The band gap energy obtained for titania P25 Degussa of 3.29 eV compares to Anatase. These values compare well with those found in the literatures.^[123,161,162]

Table 8: The band gap energies of the amorphous titania, the as-prepared titania polymorphs, and titania P25 calculated by the Kubelka–Munk absorption function.

Sample	E_g (eV)	
	Direct transition	Indirect transition
Amorphous titania	3.67	3.46
Anatase	3.50	3.25
Brookite	3.44	3.25
Rutile	3.34	3.03
Titania P25 Degussa	3.61	3.29

3.2.6 Nitrogen adsorption-desorption

The N_2 adsorption-desorption isotherms and the corresponding pore size distributions of the synthesized TiO_2 polymorphs Anatase, Brookite, Rutile and commercial photocatalyst titania P25 Degussa are shown in Figure 20. The shapes of isotherms belong to type-V for Anatase, Rutile, titania P25 and type-IV for Brookite. They are characterized by a low uptake of nitrogen at the onset of adsorption followed by a slight increase of adsorption due to the monolayer coverage of the titania surface until p/p_0 ca. 0.3, followed by multilayer adsorption. At high relative pressure of $p/p_0 > 0.8$, a steep increase of nitrogen uptake is observed. This uptake is assigned to the filling of inter particle meso- and nanopores of titania agglomerates. The onset of this step varies somewhat for the different titania polymorphs indicating different particle size and agglomeration. The specific surface area, pore diameter and pore volume have been derived by BET and BJH analysis (compare Experimental part).

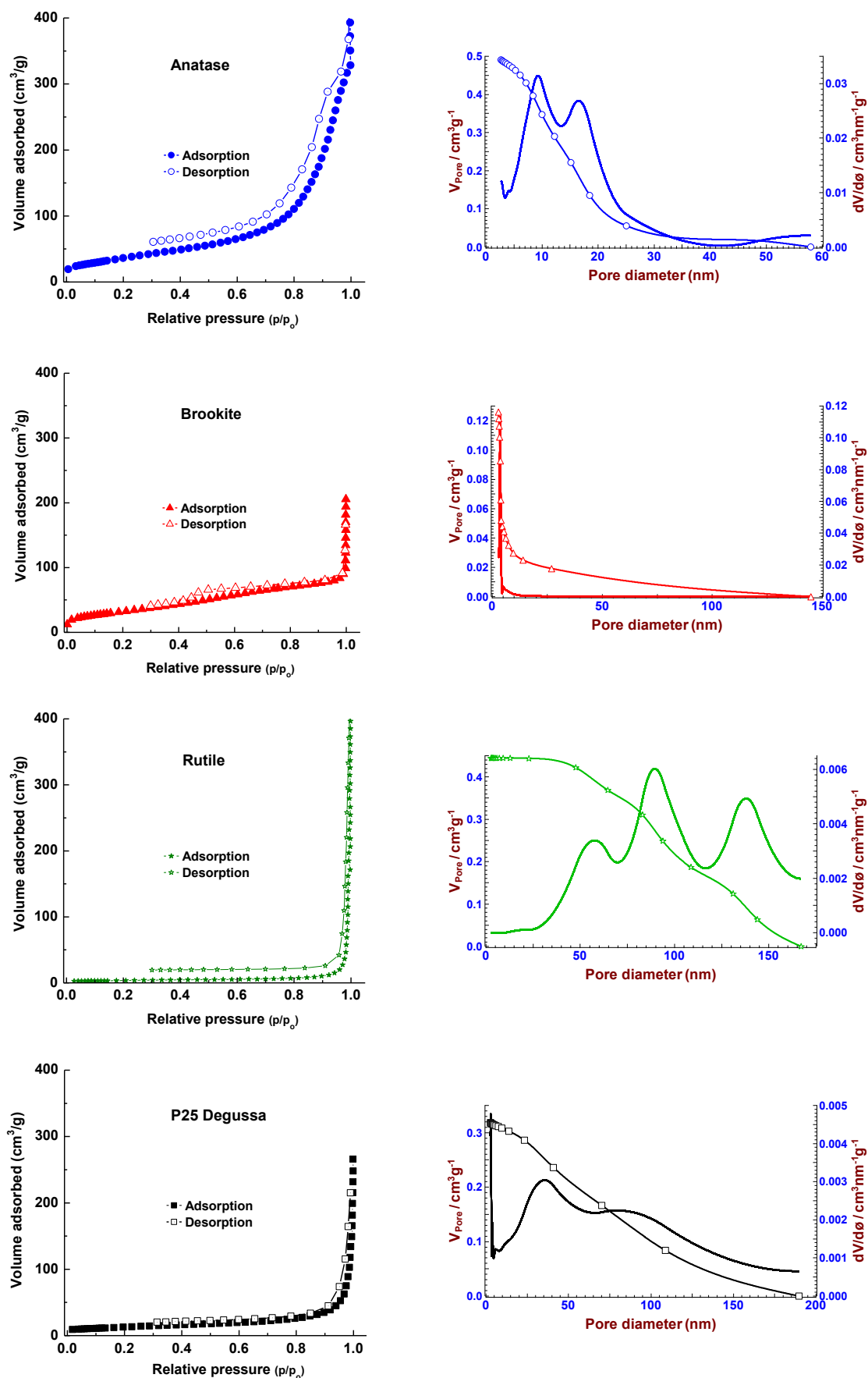


Figure 20. (Left) N_2 sorption isotherms and (right) corresponding pore size distribution curves of Anatase, Brookite, Rutile, and titania P25 (from top to bottom).

Anatase and Brookite show higher specific surface areas of 132 and 116 m²/g, respectively, due to the small particle size of *ca.* 11-12 nm. In contrast, titania P25 Degussa and Rutile show distinctly lower specific surface areas of 46 and 12 m²/g due to their larger particle sizes of *ca.* 31 and 117 nm, respectively. They are in line with the particle sizes observed in the SEM images of the titania samples as shown in Table 9.

It is possible to estimate average particle sizes from specific surface area by assuming that all the particles are non-porous, spherical shaped and of similar size. The particle size, D, is given by following equation:^[163,164]

$$D = \frac{6}{S_{\text{BET}} \cdot \rho}, \quad (15)$$

where S_{BET} is the specific surface area, ρ is the bulk density.

Table 9: The specific surface area, pore diameter, pore volume and average particle size of Anatase, Brookite, Rutile, and titania P25.

Sample	SSA (m ² /g)	Pore diameter (nm)	Pore volume (cm ³ /g)	Average particle size (nm)
Anatase	132	14	0.4908	11
Brookite	116	4	0.1260	12
Rutile	12	99	0.4480	117
Titania P25	46	73	0.3186	31

In summary, the structural and textural characterization of the amorphous titania; the synthesized titania polymorphs Anatase, Brookite, and Rutile; the as-prepared Brookite/Rutile mixture; and the commercial photocatalyst titania P25 Degussa are summarized in Table 10.

- The three synthesized polymorphs Brookite, Anatase, and Rutile show their distinctive crystal phases as well as morphology (shapes and sizes): agglomerated sphere-shaped nanoparticles for Brookite and Anatase with small crystallite size of *ca.* 10 nm, while rod-like large nanocrystals for Rutile with larger crystallite size of *ca.* 98 nm. The particle size observed by SEM, crystallite size estimated by XRD, and average particle size determined by S_{BET} values of small Brookite and Anatase particles are similar.

- Both the direct band gap (3.44 eV) and the indirect band gap (3.25 eV) of Brookite are determined. These band gap energies are between those of Anatase and Rutile.

Table 10: The characteristics of the as-prepared titania powders and titania P25.

Sample		Phase content (%)			S_{BET} (m^2/g)	Pore volume (cm^3/g)	E_g (eV)	Particle size (D, nm)		
		A	B	R				S_{BET}	SEM	XRD
Amorphous titania					530	0.1706	3.67^2	-	50	-
Anatase		100			132	0.4908	3.25^1	11	10	10
Brookite/Rutile			23	77	49	0.3107	3.43^2	29	Width: 20-30 Length: 150-300	-
Brookite (Peptization)	H ₂ O		100		116	0.1260	3.25^1	12	10	12
	HNO ₃		63	37	73	0.1583	-	20	10	-
Rutile (Peptization)	H ₂ O			100	-	-	-	-	Width: 20-30 Length: 150-300	56
	HNO ₃		14	86	-	-	-	-	Width: 20-30 Length: 150-300	-
Synthesized Rutile				100	12	0.4480	3.34^2	117	Width: 50-100 Length: 300-500	98
Titania P25		80		20	46	0.3186	3.29^1	31	25	21^3 67^4

- 1: calculated for the indirect transitions
2: calculated for the direct transitions
3: calculated for the Anatase (101) peak
4: calculated for the Rutile (110) peak
-: not determine

3.3 Photocatalytic performance of Brookite (B), Anatase (A), and Rutile (R)

The photocatalytic performance of the titania polymorphs Brookite (B), Anatase (A), and Rutile (R) obtained by a similar hydrothermal treatment of the amorphous titania precursor, have been comparatively studied in the photocatalytic degradation of organic compounds in water. Solarium UV-vis light lamps of low intensity (60 W) simulating the UV part of sun light were used as irradiation sources. It has to be noticed that in this work the photocatalytic degradation of contaminations which are rarely considered in the literature so far, has been studied. Additionally, compared to literature a very low catalyst concentration combined with comparatively high loading of pollutant (catalyst-to-substrate ratio of four) has been applied. A set of different reactive organic molecules has been chosen as model compounds: ibuprofen (IBP), cinnamic acid (CA), phenol (Ph), diatrizoic acid (DA) as well as the dyes rhodamine B (RhB) and rose bengal (RB).

3.3.1 Brookite

The photocatalytic performance of Brookite has been evaluated and compared with that of commercial titania P25 Degussa (Evonik). Firstly, the photocatalytic degradation of ibuprofen (IBP) has been considered. As shown in Figure 21, the UV-vis absorption spectrum of the starting IBP solution exhibits two main absorption bands located at 190 nm and 221.5 nm, respectively, which are related to the aromatic ring.

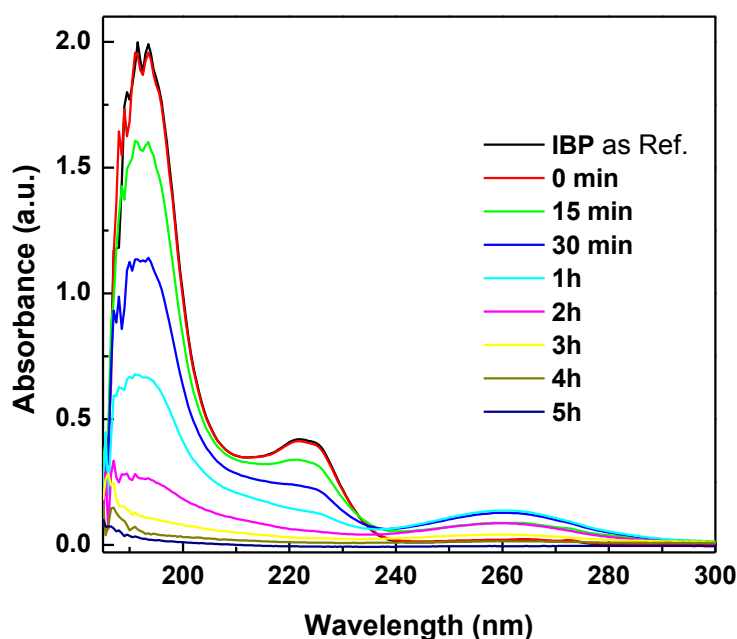


Figure 21. The UV-vis absorption spectra of the IBP solutions photocatalytically treated with Brookite. Reaction conditions: RT, IBP conc.: 10 ppm, aqueous reaction solution: 250 ml, catalyst loading: 10 mg.

In this work, the photocatalytic abatement of IBP was followed by the change in the intensity of the absorption band at 221.5 nm. This band decreases rapidly with photocatalytic treatment, indicating fast decomposition of IBP and oxidative aromatic ring opening. Simultaneously, a new absorption band appears at 262 nm. This band is assigned to the formed intermediates and is used as a measure for the formation and decomposition of reaction intermediates with high intensity depending on the UV-vis irradiation time.^[8,9]

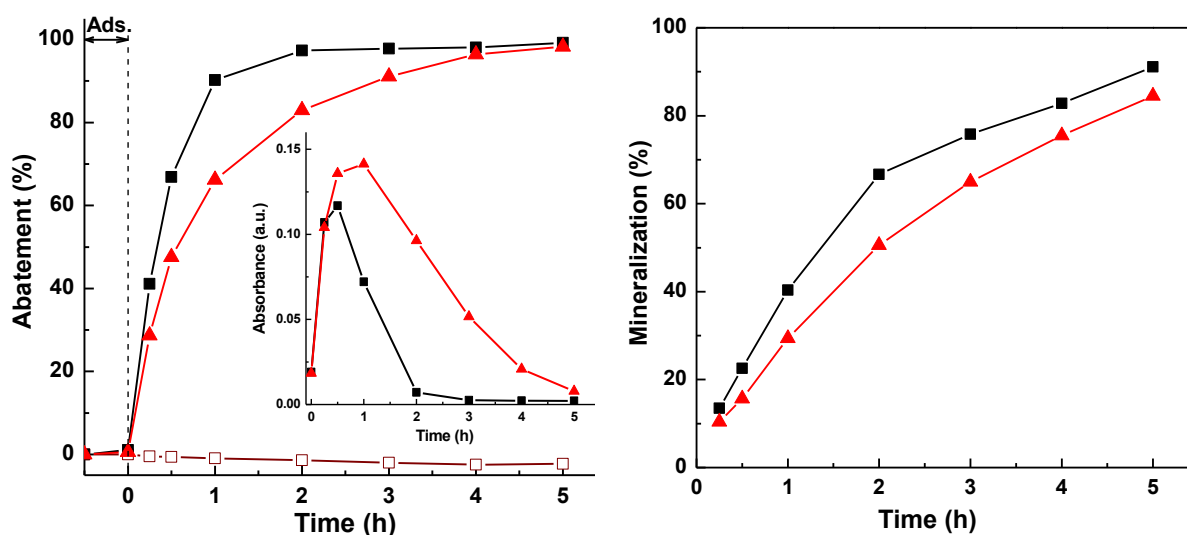


Figure 22. (Left) Photocatalytic abatement and (right) mineralization of IBP over (▲) Brookite and (■) titania P25. (□) Photolysis of IBP. Formation and decomposition of IBP intermediates (inset). Reaction conditions: RT, IBP conc.: 10 ppm, aqueous reaction solution: 250 ml, catalyst loading: 10 mg.

The photocatalytic degradation starts immediately as shown by the abatement curve (Figure 22, left). After 1 h of treatment *ca.* 65% of IBP is abated, and total degradation is achieved after 5 h according to the UV-vis spectra. The abatement is accompanied by a strong increase in the absorbance at 262 nm, which is related to intermediates. It reaches maximum intensity after 1 h of reaction and then decreases continuously during 5 h of reaction. The blank curve (no catalyst) shows that the abatement is due to the photocatalytic degradation only. Adsorption or photolysis has only a small impact of the abatement. After 30 min dark (adsorption) the amount of IBP absorbed onto the surface of Brookite is negligible, *ca.* 0.6%. For comparison, the photocatalytic degradation of IBP over commercial catalyst P25 Degussa has been evaluated. The IBP concentration decreases rapidly during the course of photocatalytic reaction. Even the Brookite shows high activity, titania P25 Degussa is slightly more active. After 2 h, already *ca.* 97% of IBP is degraded over titania P25. The photocatalytic degradation is fully completed after 5 h. In addition, the rapid decrease of the formed intermediates related to the high activity of Brookite (the inset of Figure 22, left).

These results confirm that Brookite shows high activity in the photocatalytic degradation of IBP at low concentration, which is close to that of titania P25.

Although the UV-vis spectra are sensitive to the destruction of the ibuprofen by detecting the corresponding absorbance of the aromatic ring, they give no information on the achieved degree of mineralization. The total conversion to carbon dioxide and water can be visualized by the decrease of TOC content (total organic carbon). The TOC is monitored in order to know to what extent the photocatalytic degradation results in a complete oxidation of pollutants to CO₂ and H₂O. Figure 22 (right) shows the mineralization of IBP over Brookite and P25 for comparison. Up to 85% of IBP over Brookite is oxidized to CO₂ and H₂O, while *ca.* 91% are oxidized with titania P25 after 5 h of reaction. Again the activity of Brookite is close to that of the commercial photocatalyst titania P25 showing its high potential in water treatment. Compared to the photocatalytic degradation of the aromatic ring, the mineralization proceeds markedly slower. Especially, at the onset of reaction, the degradation of aromatic pollutants is overestimated by considering the UV-vis absorption spectra alone. This finding implies that there are a lot of highly stable intermediates formed during the course of treatment. Therefore, it can be expected that total mineralization is achieved with longer irradiation time only.

In order to identify by-products of IBP in the abatement over Brookite, the photocatalytically treated solutions collected at various time intervals are analysed by means of ESI-TOF-MS spectra in the negative ion mode (Figure 23). Beside the [M-H]⁻ peak at m/z 205 ascribed to the deprotonated IBP,^[9,11,89] lower and higher [M-H]⁻ peaks are observed at m/z 89, 137, 433, 661, and 889, respectively, in the starting solution. These peaks indicate the presence of agglomerated IBP or oxidation IBP species.^[9] The intensity of the [M-H]⁻ peak at m/z 205 decreases continuously with increasing treatment time and disappears completely after 5 h of reaction. At the same time, the higher mass peaks at m/z 433, 661 and 889 decrease gradually with prolonged UV-vis irradiation and nearly disappear finally. While the lower mass peaks at m/z 81, 170 still remain with low intensity. The obtained ESI-TOF-MS results further confirm the high activity of Brookite in the photocatalytic degradation of IBP, the formation of reaction intermediates/by-products and their efficient decomposition.

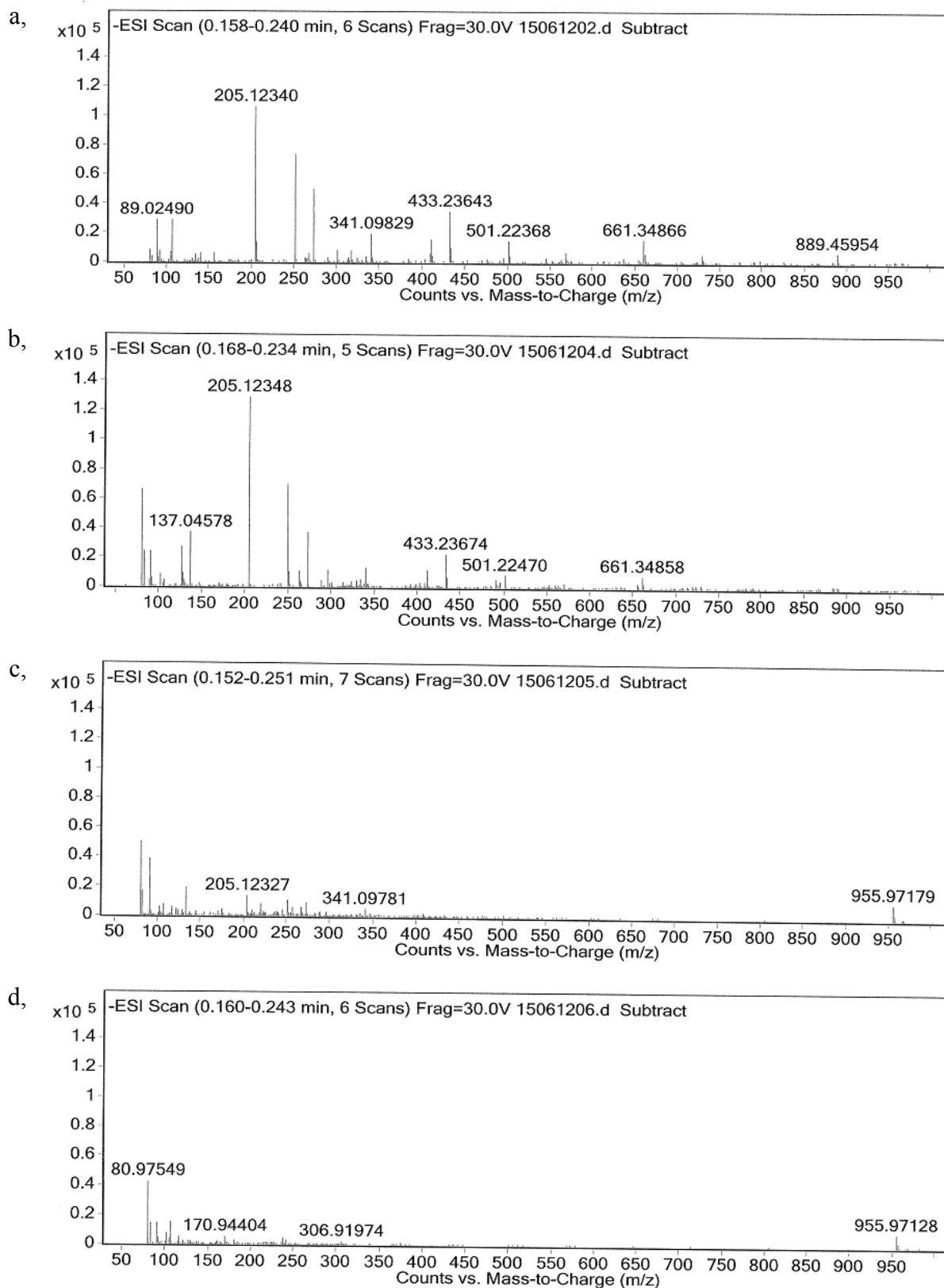


Figure 23. Negative ESI-TOF-MS spectra of the aqueous IBP solutions after photocatalytic treatment with Brookite: (a) starting solution, the photocatalytically treated solutions after (b) 0 min, (c) 1 h and (d) 5 h. Reaction conditions: RT, IBP conc.: 10 ppm, aqueous reaction solution: 250 ml, catalyst loading: 10 mg.

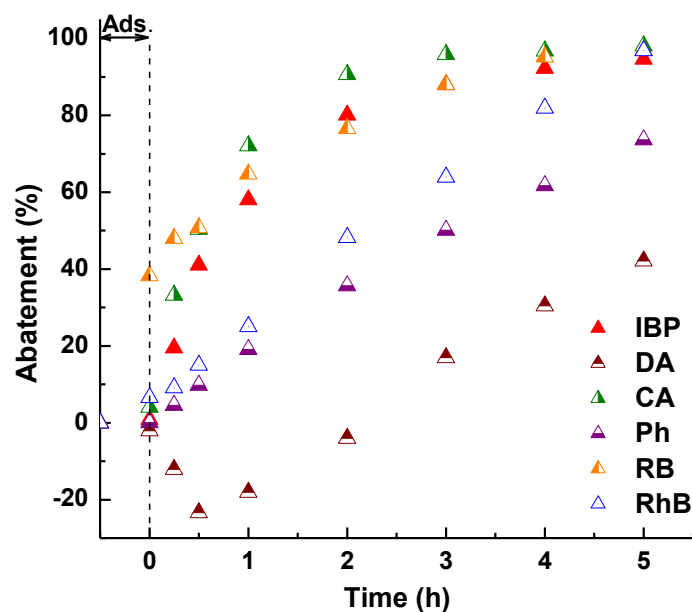


Figure 24. Photocatalytic abatement of different organic compounds cinnamic acid (CA), phenol (Ph), diatrizoic acid (DA) and the dyes rose bengal (RB) and rhodamine B (RhB) over Brookite. RhB and RB curves represent decolourization. Reaction conditions: RT, organic conc.: 10 ppm, aqueous reaction solution: 250 ml, catalyst loading: 10 mg.

In addition to ibuprofen a series of the photocatalytic degradation experiments have been carried out with other different reactive molecules cinnamic acid (CA), phenol (Ph), diatrizoic acid (DA) and the dyes rose bengal (RB), and rhodamine B (RhB) as given in Figure 24. This approach allows evaluating the photocatalytic performance of the synthesized Brookite in more detail. Although Brookite is active in the photocatalytic degradation of all studied compounds, marked differences in the degree of degradation are observed. Abatements from 40% to 98% are achieved after 5 h of treatment. High conversions are observed for CA, IBP, RB and RhB. In contrast, phenol and, especially, the halogenated diatrizoic acid (DA) behave more recalcitrant. Nevertheless, the iodide-substituted DA is degraded by 18% over Brookite. The abatement (conversion) decreases in the order (abatements after 3 h of photocatalytic treatment in brackets):

$$\text{CA (95\%)} > \text{IBP (89\%)} > \text{Ph (53\%)} > \text{DA (18\%)}$$

This order reflects the reactivity of the molecules. In case of CA, the aromatic ring is substituted with a reactive olefinic propylene group (Table 2). Phenol is resonance stabilized and DA is stabilized by M^+ effect of the iodide substituents.

ESI-TOF-MS spectra are also studied to identify by-products formed in the photocatalytic degradation of CA and DA over Brookite. The $[M-H]^-$ peak at m/z 147 related to the CA anion in the starting solution is rapidly decreased in the intensity under UV-vis irradiation (Figure 25). Simultaneously, a new intense peak appears at m/z 121, which might be due to

the formation of hydroxybenzaldehyde or benzoic acid. At the end of treatment process (5 h), this peak disappears completely showing the total conversion of CA over Brookite.

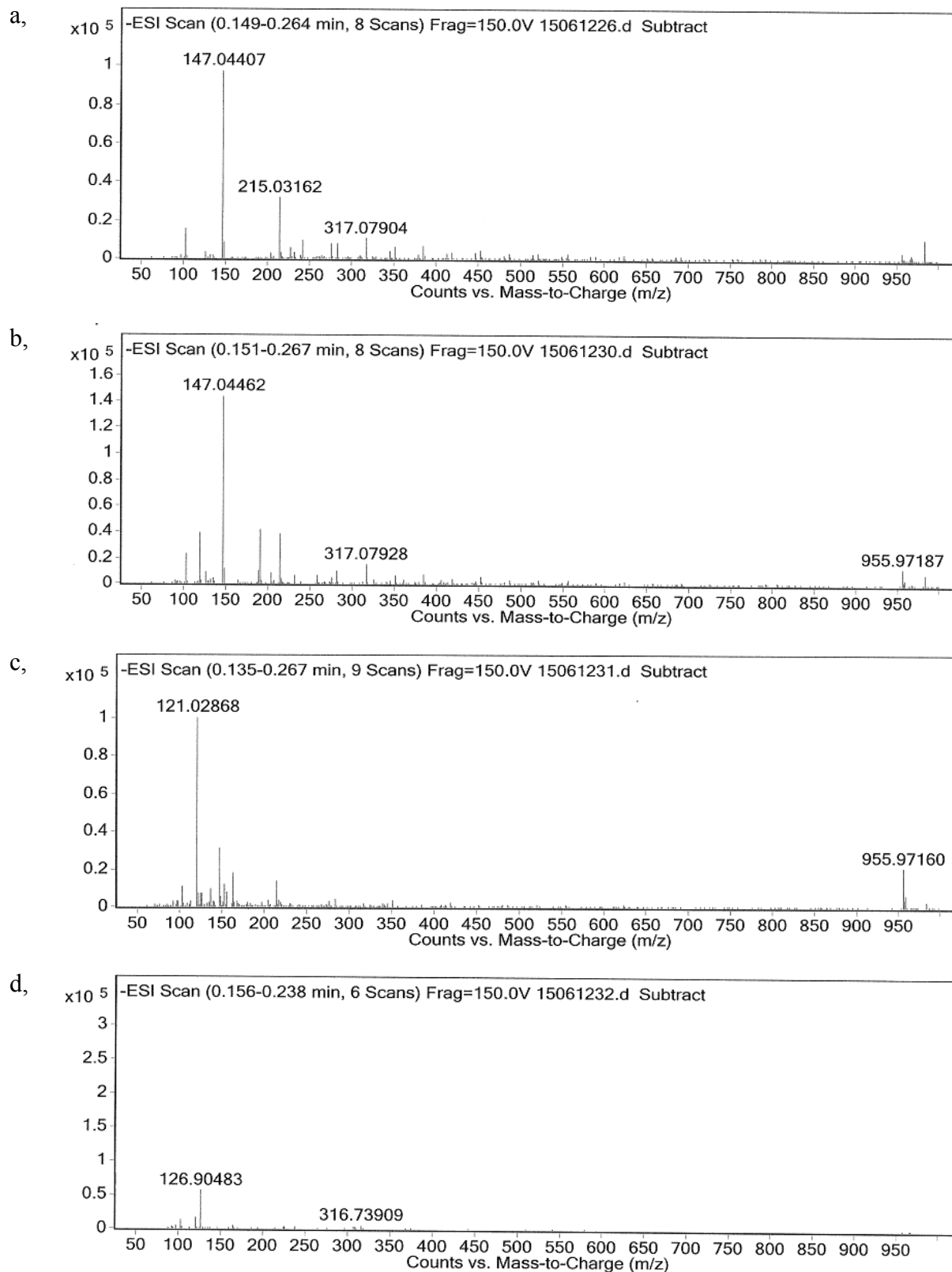


Figure 25. Negative ESI-TOF-MS spectra of the aqueous CA solutions after photocatalytic treatment with Brookite: (a) starting solution, the photocatalytically treated solutions after (b) 0 min, (c) 1 h and (d) 5 h. Reaction conditions: RT, CA conc.: 10 ppm, aqueous reaction solution: 250 ml, catalyst loading: 10 mg.

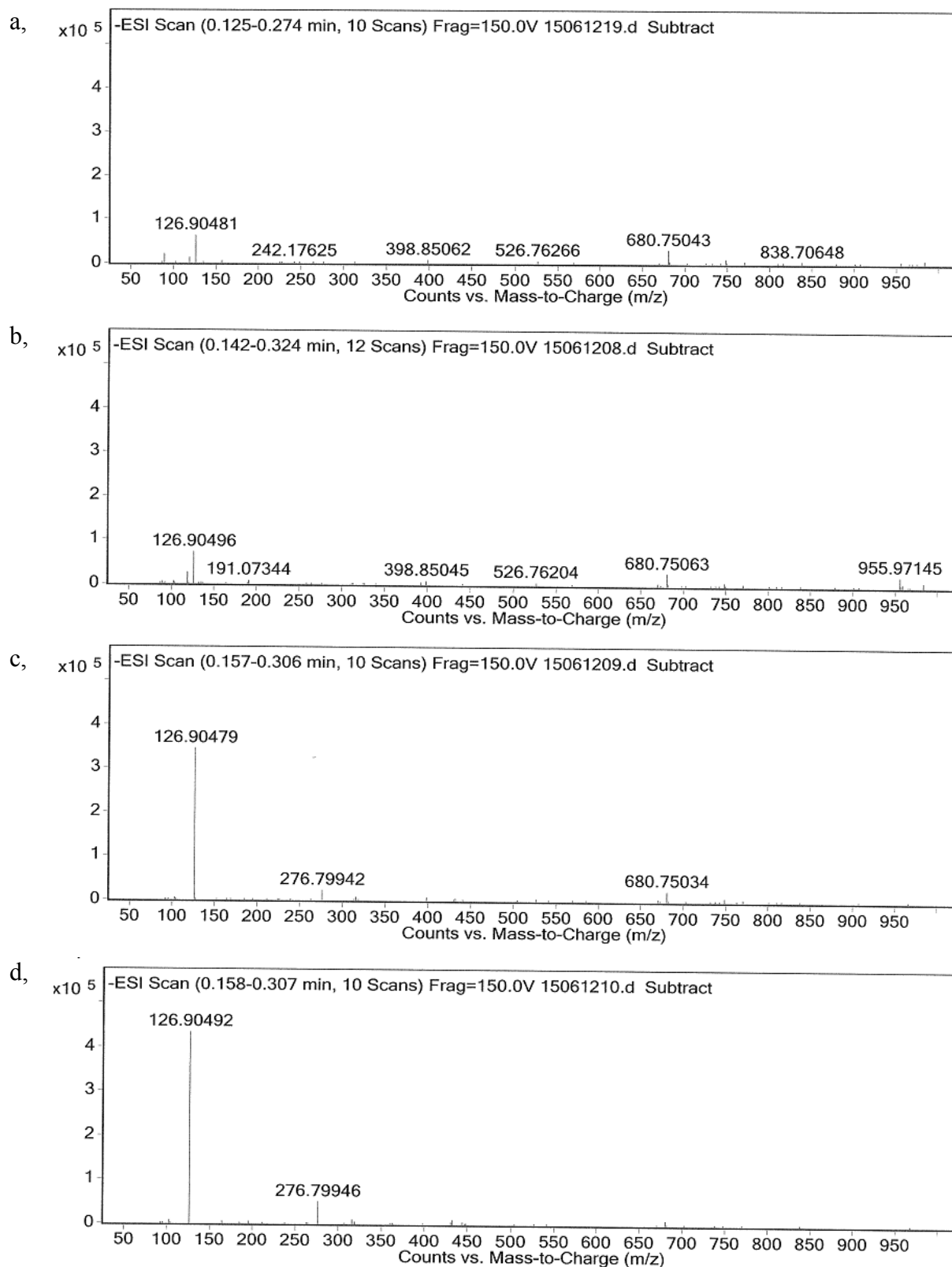


Figure 26. Negative ESI-TOF-MS spectra of the aqueous DA solutions after photocatalytic treatment with Brookite: (a) starting solution, the photocatalytically treated solutions after (b) 0 min, (c) 1 h and (d) 5 h. Reaction conditions: RT, DA conc.: 10 ppm, aqueous reaction solution: 250 ml, catalyst loading: 10 mg.

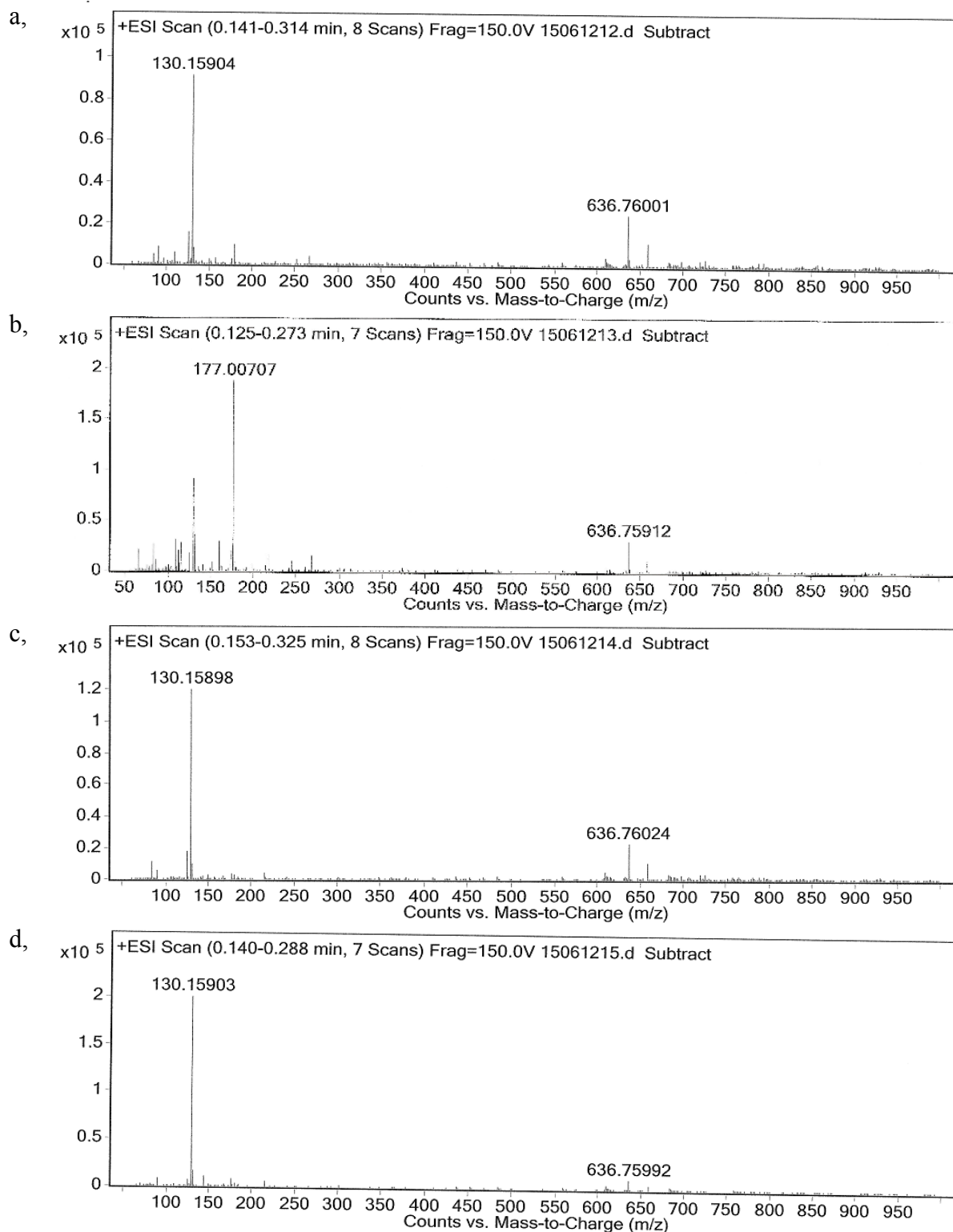


Figure 27. Positive ESI-TOF-MS spectra of the aqueous DA solutions after photocatalytic treatment with Brookite: (a) starting solution, the photocatalytically treated solutions after (b) 0 min, (c) 1 h and (d) 5 h. Reaction conditions: RT, DA conc.: 10 ppm, aqueous reaction solution: 250 ml, catalyst loading: 10 mg.

Figure 26 and 27 show the ESI-TOF-MS spectra of starting DA aqueous solution and photocatalytically treated solutions after the photocatalytic degradation of DA over Brookite.

The intensity of the $[M-H]^-$ peak at m/z 126 (negative mode) corresponding to the iodine ions increases with photocatalytic reaction time (Figure 26). It indicates that DA molecules are decomposed and iodide ions are liberated from the aromatic ring, which is broken. A new low intense $[M-H]^-$ peak appears at m/z 276 after 1 h of photocatalytic reaction. This peak is also observed after 5 h with increase in intensity (even though negligible). Importantly, the negative spectrum of DA obtained after 5 h of reaction is cleaner than those of IBP and DA, which cannot explain low photocatalytic abatement and mineralization of DA over Brookite derived from UV-vis spectra and TOC measurement, respectively. Therefore, the positive ESI-TOF-MS spectra of DA have been studied. As shown in Figure 27, the intensity of the mass peak at m/z 636 decreases slowly with prolonged photocatalytic treatment time, which indicates the low degradation of DA. The presence of this peak belongs to the diatrizoate sodium salt (3,5-Diacetamido-2,4,6-triiodobenzoic acid, sodium salt). Beside this peak, a lower $[M-H]^+$ peak at m/z 130 is permanently present in the starting solution and increases during the course of photocatalytic degradation of DA. It is assigned to the side product which may show the low conversion of DA. The ESI-TOF-MS results further confirm that diatrizoic acid behaves highly recalcitrant against photocatalytic treatment.

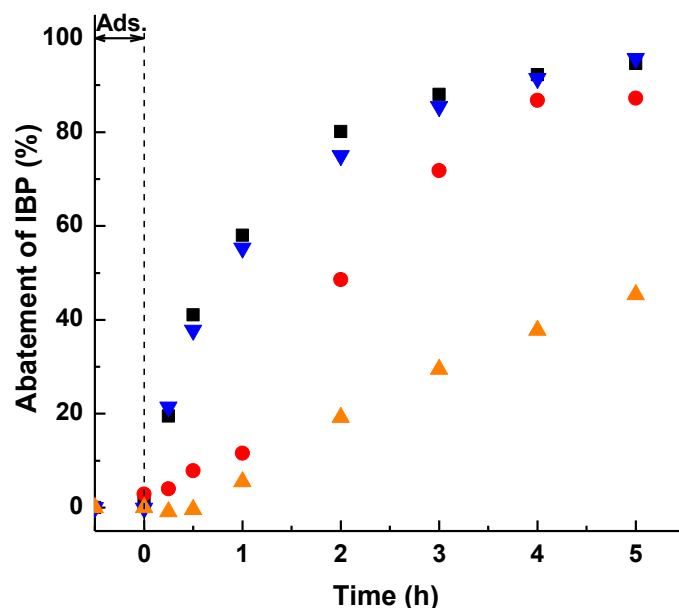


Figure 28. Impact of different scavengers on the photocatalytic abatement of IBP over Brookite. Reaction conditions: RT, IBP conc.: 10 ppm, aqueous reaction solution: 250 ml, catalyst loading: 10 mg. (■) No scavenger. Scavengers: (●) 1.46 mg EDTA, (▼) 0.1 ml *t*-BuOH, and (▲) 2.704 mg 1,4-BQ.

The nature of active species formed in the photocatalytic performance of Brookite has been studied. A series of trapping experiments have been carried out with adding different scavengers.^[45,63] EDTA (ethylenediaminetetraacetic acid) acts as a hole (h^+) scavenger,^[80]

t-BuOH acts as a hydroxyl ($\cdot\text{OH}$) radical scavenger,^[84] and 1,4-BQ (1,4-Benzoquinone) acts as a superoxide ($\text{O}_2^{\cdot-}$) radical scavenger.^[85] Figure 28 shows the impact of different scavengers on the photocatalytic degradation of IBP over Brookite. The addition of *t*-BuOH has nearly no influence showing that $\cdot\text{OH}$ radicals are not major species. In contrast, addition of EDTA or 1,4-BQ leads to a markedly drop of the conversion after 1 h of reaction indicating that electron holes in Brookite and $\text{O}_2^{\cdot-}$ (or $\cdot\text{OOH}$) radicals are the main active species.

The effect of thermal pre-treatment on the photocatalytic activity of Brookite in the abatement of IBP is shown in Figure 29. Gradual increase in the annealing temperature to 100–300 °C causes a substantial decrease in activity. Further increase in the temperature to 500 °C causes only a minor decrease. Calcination at 700 °C leads to a complete deactivation of Brookite. Remarkably, severe loss in activity is observed already under mild thermal treatment even Brookite is reported to be stable until 400 °C.^[103,152] Possible structural changes of Brookite after thermal treatment process in the range of 100–700 °C have been studied by Raman spectroscopy and XRD pattern.

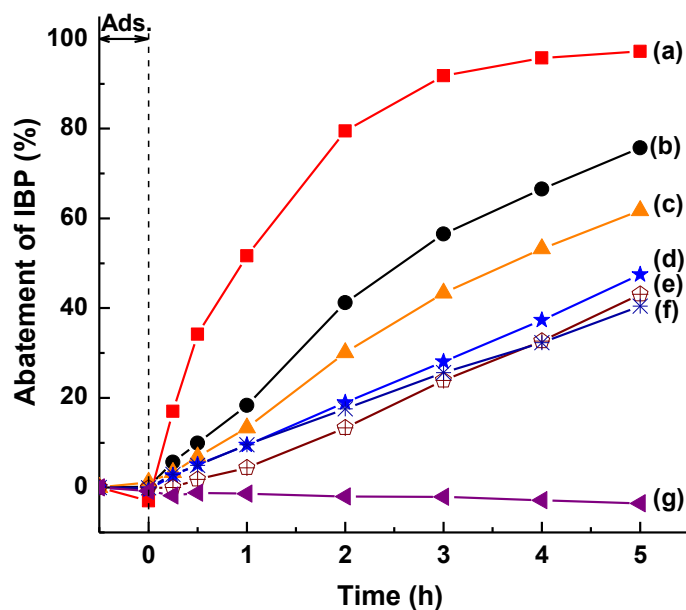


Figure 29. The effect of thermal pre-treatment on photocatalytic activity of Brookite: (a) as-prepared and calcined at (b) 100 °C, (c) 200 °C, (d) 300 °C, (e) 400 °C, (f) 500 °C, (g) 700 °C for 2 h in air. Reaction conditions: RT, IBP conc.: 10 ppm, aqueous reaction solution: 250 ml, catalyst loading: 10 mg.

The Raman spectrum of the starting material (synthesized Brookite) reflects on pure Brookite structure (Figure 30a-left). With increasing temperature to 100–300 °C, the appearance is nearly not changed. Only slightly shift of the strong Raman band at 153 cm^{-1} to 146 cm^{-1} after treatment at elevated temperatures is observed. Some Rutile is formed at 400 °C, as indicated by the XRD reflection at $2\theta = 27.4^\circ$ (110) (Figure 30e-right). Starting Rutile formation between 400-500°C is obviously responsible for minor decrease in photocatalytic activity. A

clear phase change from Brookite to Rutile is observed after calcination at 700 °C. The Raman band of Brookite at 153 cm⁻¹ completely disappears. The Raman spectrum is now characterized by the presence of three Raman-active modes at 234 cm⁻¹, 437 cm⁻¹, 604 cm⁻¹ related to the Rutile phase (Figure 30g-left). These findings are confirmed by the XRD patterns (Figure 30, right). They show that Brookite phase is present until 500 °C.

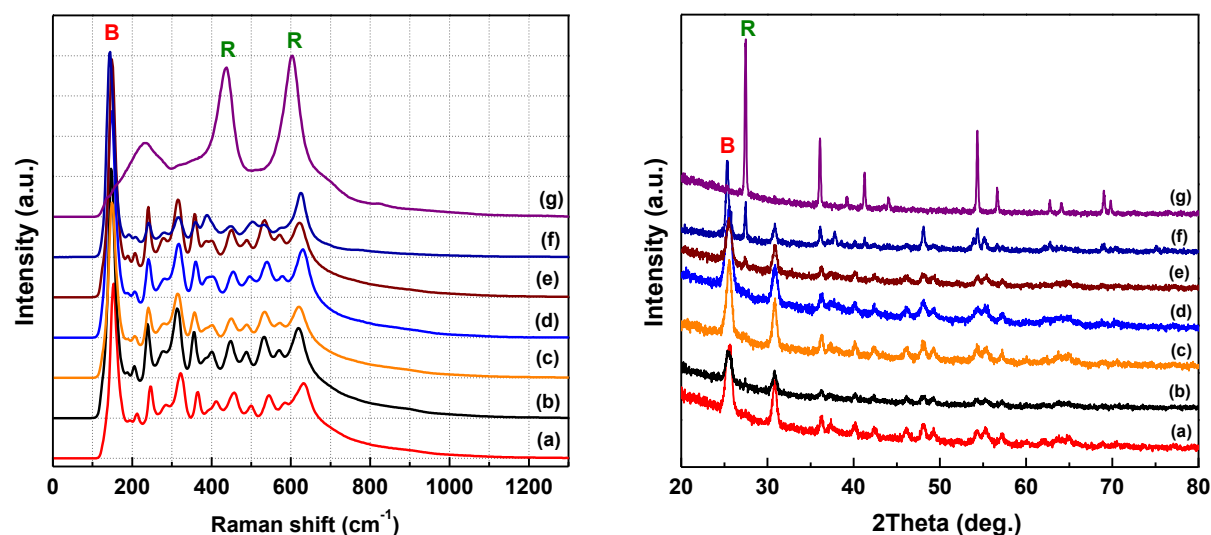
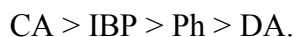


Figure 30. The effect of thermal pre-treatment on (left) Raman spectra and (right) XRD patterns of Brookite samples: (a) as-prepared and calcined at (b) 100 °C, (c) 200 °C, (d) 300 °C, (e) 400 °C, (f) 500 °C, (g) 700 °C for 2 h in air. B and R represent Brookite and Rutile, respectively.

At 700 °C, Brookite is completely converted to Rutile, which explains the drastic activity loss of the sample. As Brookite is stable until 300–400 °C, the observed activity loss after annealing is likely due to the dehydroxylation at the surface. Calcination at higher temperature does not improve the photocatalytic activity. The photocatalytic degradation activity is completely diminished by the phase transformation of Brookite to Rutile.

Conclusion to the photocatalytic activity of Brookite:

- Brookite is highly active and even high recalcitrant diatrizoic acid is slowly degraded.
- Abatement is related to the chemical reactivity of the organic molecules (substituted aromatic rings) with a general recalcitrant order (obtained after 5h of treatment):



- ESI-TOF-MS and TOC measurements confirm nearly complete conversion of organic compounds after 5h of the photocatalytic reaction.
- Main active species are the valence band holes (h^+) and superoxide radicals ($O_2^{\bullet-}$). Hydroxyl ($\bullet OH$) radicals are of minor importance.
- Brookite is sensitive to heating. Surface hydroxylation is important for activity.

- UV-vis vs. TOC: Titania P25 Degussa is not active as expected from the aromatic ring opening observed from UV-vis absorption spectra. The mineralization determined by TOC measurement proceeds much more slowly at the onset of reaction (1 h: 90% vs. 40% for P25, 2 h: 65% vs. 30% for Brookite).

3.3.2 Anatase

Anatase is usually considered to be the most photocatalytic active titania polymorph. In this work, Anatase has been prepared by hydrothermal treatment of amorphous titania under acidic condition using 1.5 molar acetic acid. The photocatalytic behaviour of Anatase has been studied in the abatement of IBP used as a model compound and other molecules for comparison like CA, Ph, DA and the dyes RB and RhB. Additionally, the photocatalytic performance of Anatase has been compared with that of the commercial photocatalyst titania P25 Degussa. The photocatalytic degradation of IBP over Anatase has been followed by the decrease in intensity of absorption band at 221.5 nm related to the aromatic ring (Figure 31).

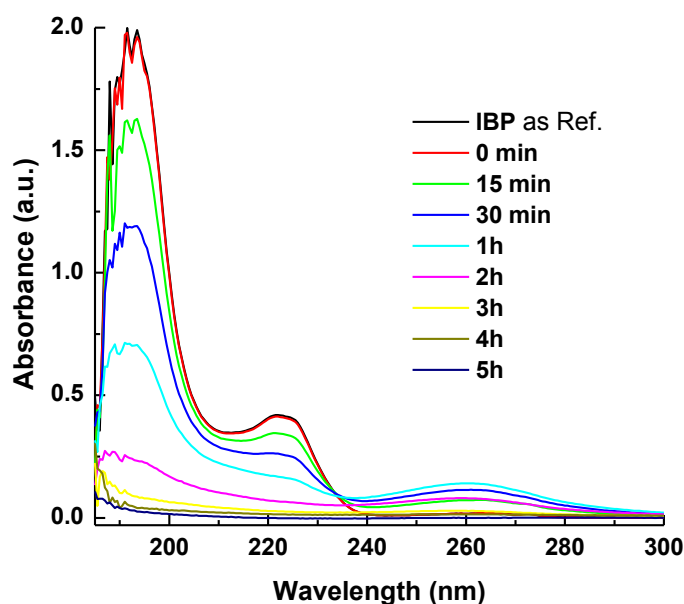


Figure 31. The UV-vis absorption spectra of the IBP solutions photocatalytically treated with Anatase. Reaction conditions: RT, IBP conc.: 10 ppm, aqueous reaction solution: 250 ml, catalyst loading: 10 mg.

During the course of photocatalytic treatment, a markedly decrease in the IBP absorbance is observed which is accompanied by the simultaneous appearance of a new absorbance at 262 nm. It is assigned to the formation of intermediate oxidation products of IBP. After 1 h, the absorption band of intermediates at 262 nm reaches maximum intensity. After 5 h of reaction, the IBP molecules and formed intermediates are nearly decomposed (Figure 32 left). A basis

for comparison with titania P25 shows that the synthesized Anatase is highly active, reaches IBP decomposition, and is close to that of titania P25. But the photocatalytic abatement over Anatase is somewhat slower at the onset of the photocatalytic reaction (Figure 32, left). Namely, *ca.* 85% of IBP over Anatase is degraded, while *ca.* 95% of IBP is abated with titania P25 after 2 h. This finding is further confirmed by TOC (total organic carbon) measurements which determine the remaining TOC content of photocatalytically treated IBP solutions (degree of mineralization) with photocatalytic reaction time (Figure 32, right).

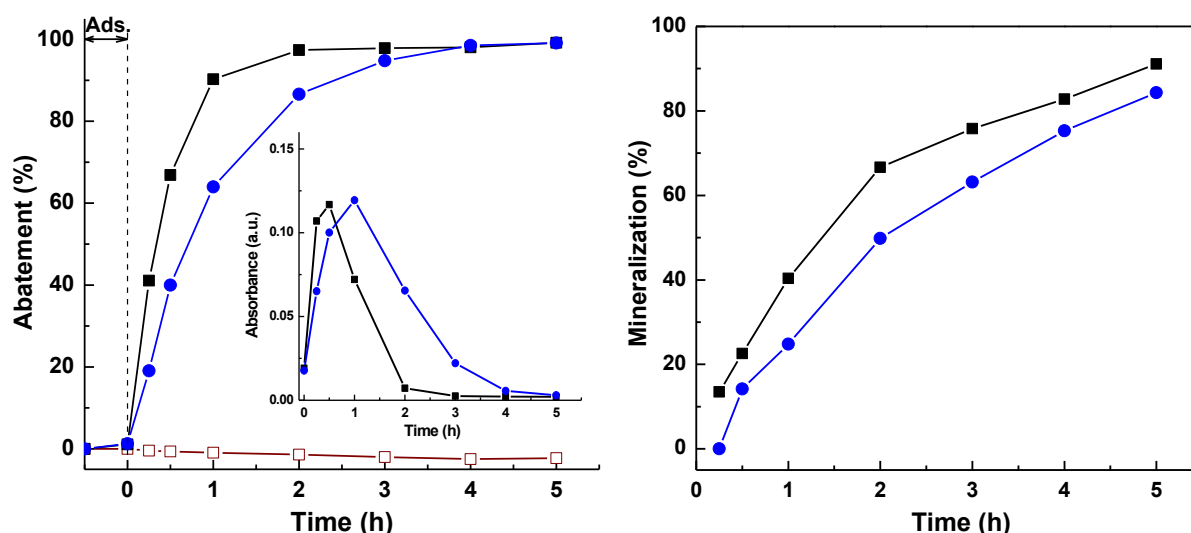


Figure 32. (Left) Photocatalytic abatement and (right) mineralization of IBP over (●) Anatase and (■) titania P25. (□) Photolysis of IBP. Formation and decomposition of IBP intermediates (inset). Reaction conditions: RT, IBP conc.: 10 ppm, aqueous reaction solution: 250 ml, catalyst loading: 10 mg.

Figure 32 (right) shows that *ca.* 84% of IBP over Anatase is mineralized to CO₂ and H₂O after 5 h of reaction, while *ca.* 91% with P25 Degussa. In contrast, the photocatalytic abatement determined by the strong decrease in intensity of the absorption band at 221.5 nm is *ca.* 99% (Figure 32, left). This means that mineralization is slower than degradation. The possible reasons are that intermediates are continuously formed during the course of photocatalytic treatment and after reaction finished, small molecular by-products still remain. Importantly, the TOC plots confirm the high efficiency of Anatase and titania P25 in the IBP degradation. It is well known that titania P25, the mixture of Anatase and Rutile, prepared by combustion of TiCl₄ is somewhat more active than the synthesized Anatase. The high activity of titania P25 is expected to be properly originating from Rutile content.

Figure 33 and 34 show the ESI-TOF-MS spectra of IBP solutions photocatalytically treated over Anatase. The spectra show a decrease in the intensities of the [M-H]⁻ peak at *m/z* 205 related to IBP anion (negative mode, Figure 33) and of the [M-H]⁺ peak *m/z* 251 ascribed to a carboxylated IBP by-product (mass difference to IBP = 44, COO) (positive mode, Figure 34)

during the course of reaction. After 5 h, these peaks nearly disappeared. Besides, some higher or lower mass peaks still remain indicating the presence of IBP by-products which are not fully decomposed leading to the lower mineralization compared to the oxidative ring opening.

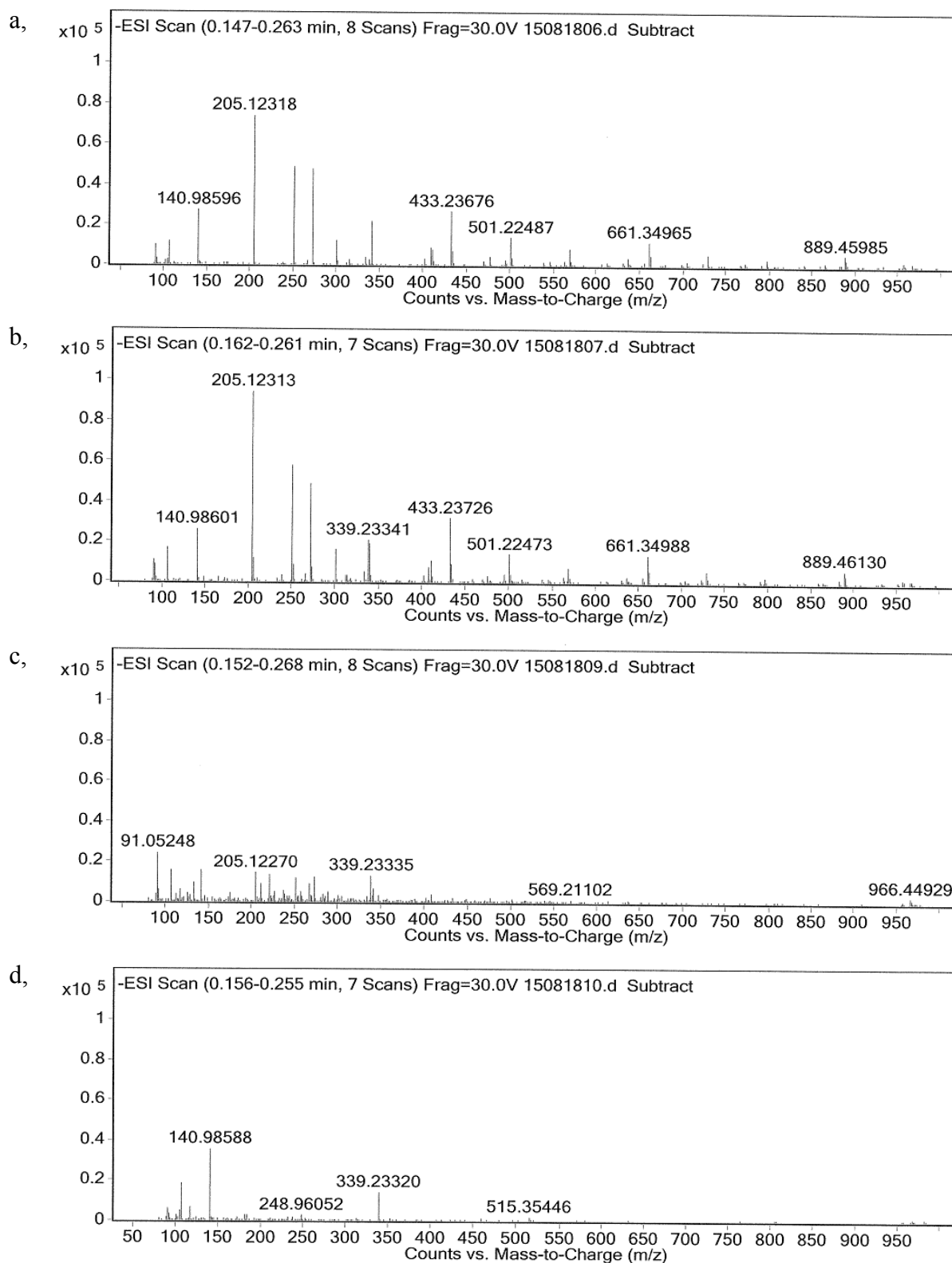


Figure 33. Negative ESI-TOF-MS spectra of the aqueous IBP solutions after photocatalytic treatment with Anatase: (a) starting solution, the photocatalytically treated solutions after (b) 0 min, (c) 1 h and (d) 5 h. Reaction conditions: RT, IBP conc.: 10 ppm, aqueous reaction solution: 250 ml, catalyst loading: 10 mg.

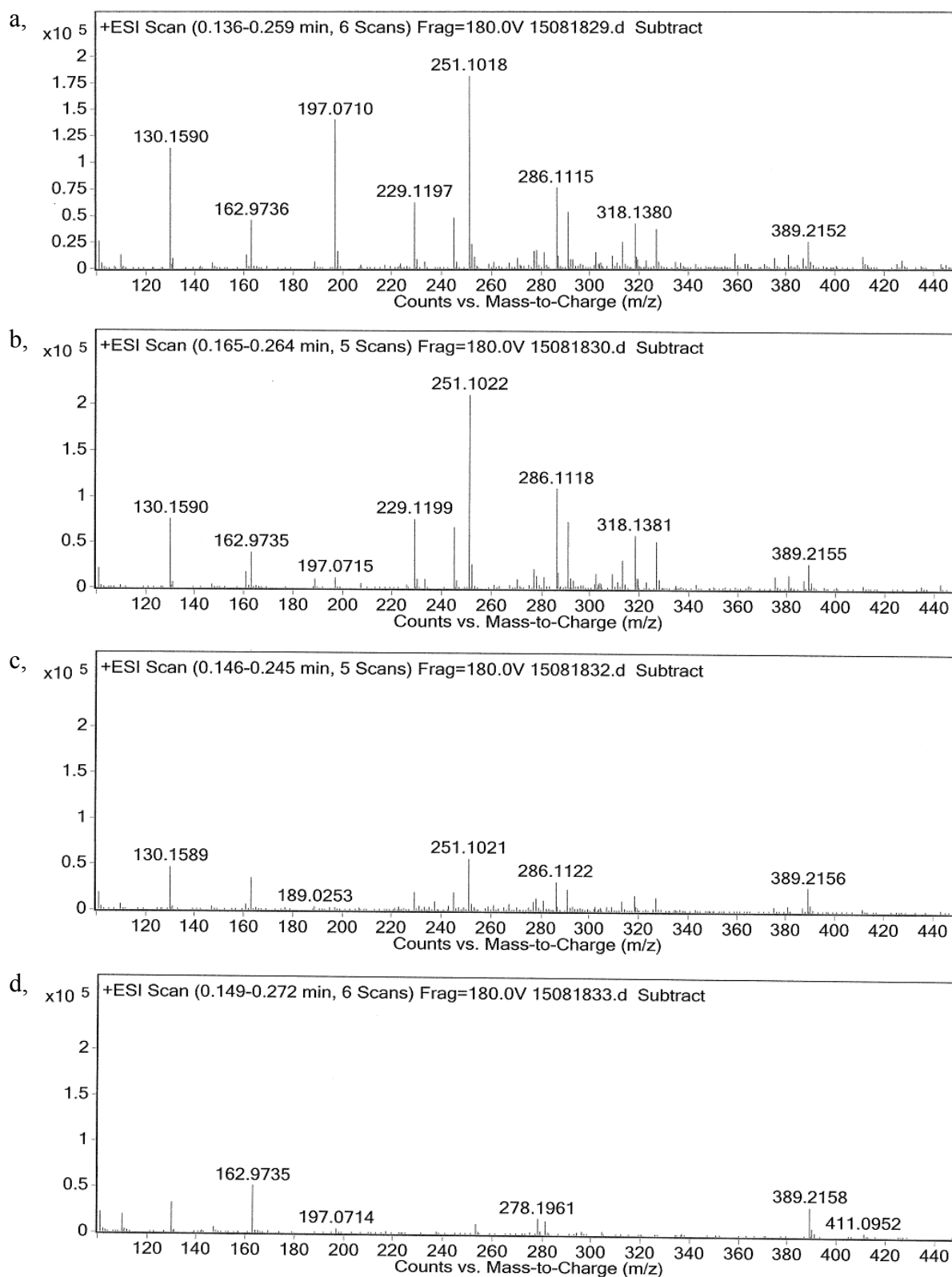


Figure 34. Positive ESI-TOF-MS spectra of the aqueous IBP solutions after photocatalytic treatment with Anatase: (a) starting solution, the photocatalytically treated solutions after (b) 0 min, (c) 1 h and (d) 5 h. Reaction conditions: RT, IBP conc.: 10 ppm, aqueous reaction solution: 250 ml, catalyst loading: 10 mg.

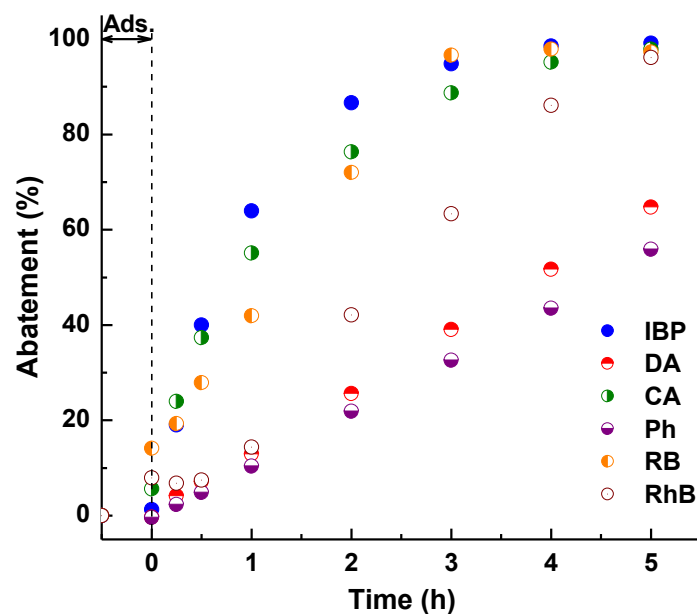


Figure 35. Photocatalytic abatement of different organic compounds cinnamic acid (CA), phenol (Ph), diatrizoic acid (DA) and the dyes rose bengal (RB) and rhodamine B (RhB) over Anatase. RhB and RB curves represent decolourization. Reaction conditions: RT, organic conc.: 10 ppm, aqueous reaction solution: 250 ml, catalyst loading: 10 mg.

Figure 35 shows the activity of Anatase in the photocatalytic degradation of various organic compounds. *Ca.* 90% of IBP, 75% of CA and 70% of RB are decomposed after 2 h, while lower conversion of Ph, DA, and RhB are obtained, only *ca.* 20-30%. After 5 h, nearly complete degradation of CA, IBP, RB and RhB are achieved. This result shows the different reactivity of organic compounds and the recalcitrant behaviour of Ph and DA. The photocatalytic abatement decreases in the order (abatements after 3 h of photocatalytic treatment in brackets):

$$\text{IBP (95\%)} > \text{CA (89\%)} > \text{DA (39\%)} > \text{Ph (32\%)}.$$

The contribution of the different reactive species to the photocatalytic abatement of IBP over Anatase has been determined by the addition of selective scavengers. Figure 36 shows that *ca.* 87% of IBP is rapidly decomposed with Anatase after 2 h of treatment, while only *ca.* 30% of IBP is abated after addition of the holes scavenger EDTA or the superoxide radicals scavenger 1,4-BQ. In contrast, the addition of *t*-BuOH, the $\cdot\text{OH}$ hydroxyl radicals scavenger, leads only to a slight decrease to *ca.* 73%. The EDTA is an efficient hole scavenger (blocking these sites). The strong decrease in the conversion of IBP after addition of EDTA points to the major contribution of holes which facilitate the aromatic ring opening. The similar strong decrease is achieved with the 1,4-BQ, the $\text{O}_2^{\cdot-}$ superoxide radical scavenger. It is concluded that both VB holes and $\text{O}_2^{\cdot-}$ radicals are the main active species in the photocatalytic degradation of IBP over Anatase, whereas $\cdot\text{OH}$ radicals play a comparatively minor role.

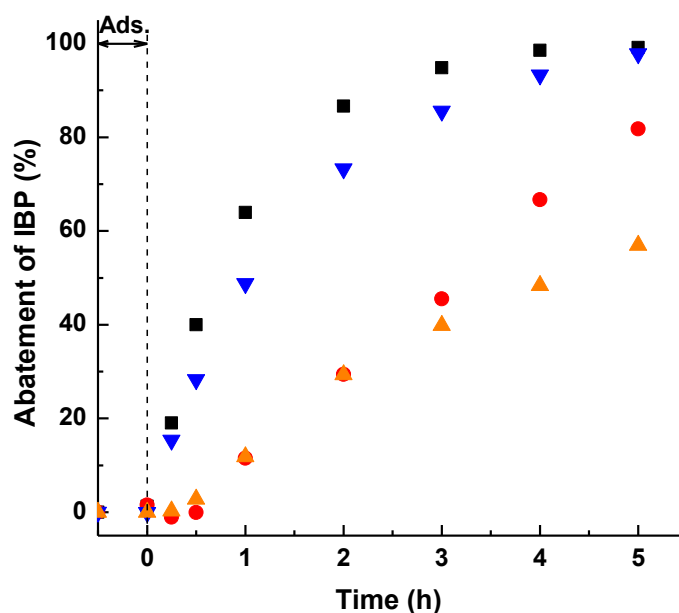


Figure 36. Impact of different scavengers on the photocatalytic abatement of IBP over Anatase. Reaction conditions: RT, IBP conc.: 10 ppm, aqueous reaction solution: 250 ml, catalyst loading: 10 mg. (■) No scavenger. Scavengers: (●) 1.46 mg EDTA, (▼) 0.1 ml *t*-BuOH, and (▲) 2.704 mg 1,4-BQ.

3.3.3 Rutile

Rutile is known as a catalyst having lower photocatalytic activity than Anatase due to larger crystallite size and lower specific surface area, even its band gap energy is close to that of Anatase. In this work, Rutile has been prepared by hydrothermal treatment of amorphous titania in aqueous HCl solution. Hence, the starting material and synthesis procedure are very similar to that of Anatase and Brookite. Therefore, the photocatalytic performance of the different prepared titania polymorphs can be reasonably compared. A possible influence of the synthesis procedure is diminished.

The UV-vis absorption spectra of IBP solutions obtained after photocatalytic treatment with Rutile (Figure 37). Different from Anatase or Brookite, the intensities of IBP absorbance decrease gradually with irradiation time. At the same time, the absorbance of intermediates at 262 nm is nearly linear increased. *Ca.* 80% of IBP is gradually decomposed during 5 h of irradiation (Figure 38, left). The conversion of IBP with Anatase proceeds significantly slower than that with titania P25. After 2 h of reaction only *ca.* 30% IBP is decomposed, compared to *ca.* 98% with the commercial photocatalyst titania P25. Even Rutile has larger particle size than titania P25, the adsorption of IBP on the surface of titania P25 and Rutile (kept in the dark for 30 min before starting the photocatalytic reaction) are similar, *ca.* 1.08% and 0.45%, respectively.

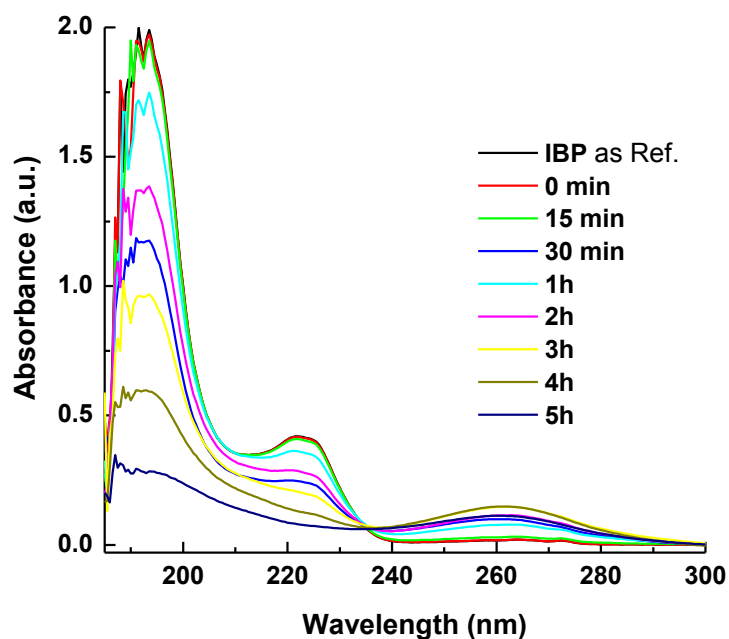


Figure 37. The UV-vis absorption spectra of the IBP solutions photocatalytically treated with Rutile. Reaction conditions: RT, IBP conc.: 10 ppm, aqueous reaction solution: 250 ml, catalyst loading: 10 mg.

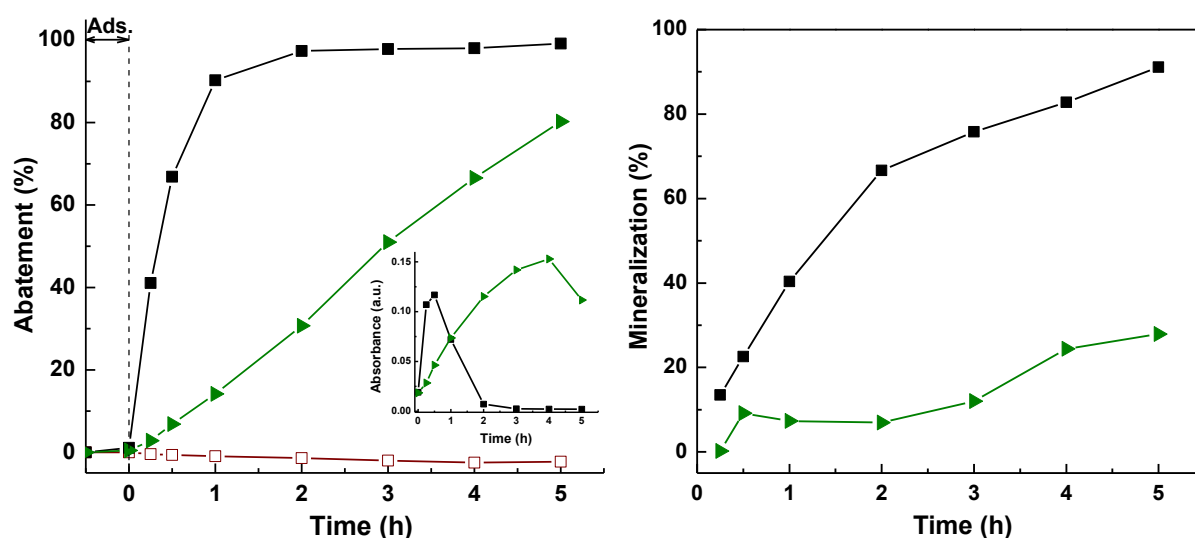


Figure 38. (Left) Photocatalytic abatement and (right) mineralization of IBP over (►) Rutile and (■) titania P25. (□) Photolysis of IBP. Formation and decomposition of IBP intermediates (inset). Reaction conditions: RT, IBP conc.: 10 ppm, aqueous reaction solution: 250 ml, catalyst loading: 10 mg.

Hence, the impact of low surface area of Rutile alone cannot explain its comparatively low photocatalytic activity. The latter is also reflected in the permanent increase of formed intermediates during the photocatalytic treatment. This behaviour of Rutile is different from titania P25 in which initial rapid degradation of intermediates is observed. A higher number of intermediate species are generated over Rutile and the increased tendency exhibits with prolonged irradiation time (4 h) by the increased intensity of the absorbance at 262 nm. The markedly lower photocatalytic activity of Rutile is confirmed by the distinctly lower degree of

IBP mineralization compared to the abatement curve determined by UV-vis absorption measurement, which is sensitive to the aromatic ring opening (Figure 38, left). They show that mineralization over Rutile is markedly lower than expected from the UV-vis results. The extent of mineralization of IBP with Rutile is also much lower than with titania P25. *Ca.* 28% IBP is mineralized with Rutile after 5 h of reaction compared to *ca.* 91% with titania P25 (Figure 38, right). These results are confirmed by the ESI-TOF-MS measurements.

Negative ESI-TOF-MS spectra of IBP over Rutile are shown in Figure 39. The results show that the $[M-H]^-$ peak at m/z 205 related to the IBP anion appearing in the spectrum of starting solution still remains after photocatalytic treatment. Beside this mass peak, lower and higher mass peaks at m/z 140, 341, 433, 501, 661 and 889 are observed indicating the presence of oxidation products and agglomerated IBP species. E.g., the mass peak at m/z 433 is assigned to $Na(IBP)_2$ anion. The distribution of these mass peaks regarding mass and intensity (pattern) is not changed, but the absolute intensity of peaks decrease with extended photocatalytic treatment. Especially, after reaction finished (5 h), the $[M-H]^-$ peak at m/z 205 still present with low intensity combined with the lower and higher mass peaks which show the presence of IBP by-products. The ESI-TOF-MS results observed for synthesized Rutile again confirm the lower mineralization compared to the aromatic ring opening.

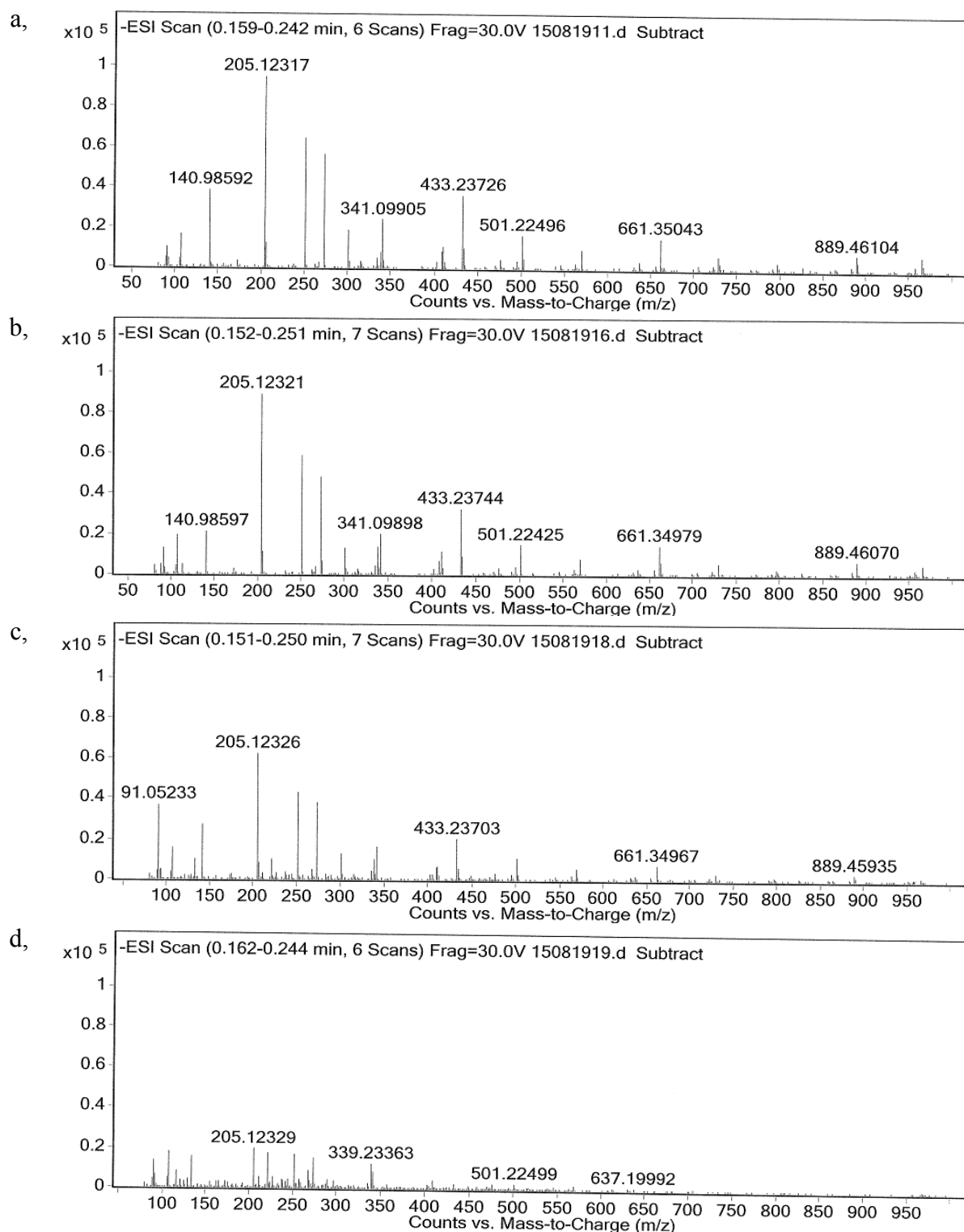


Figure 39. Negative ESI-TOF-MS spectra of the aqueous IBP solutions after photocatalytic treatment with Rutile: (a) starting solution, the photocatalytically treated solutions after (b) 0 min, (c) 1 h and (d) 5 h. Reaction conditions: RT, IBP conc.: 10 ppm, aqueous reaction solution: 250 ml, catalyst loading: 10 mg.

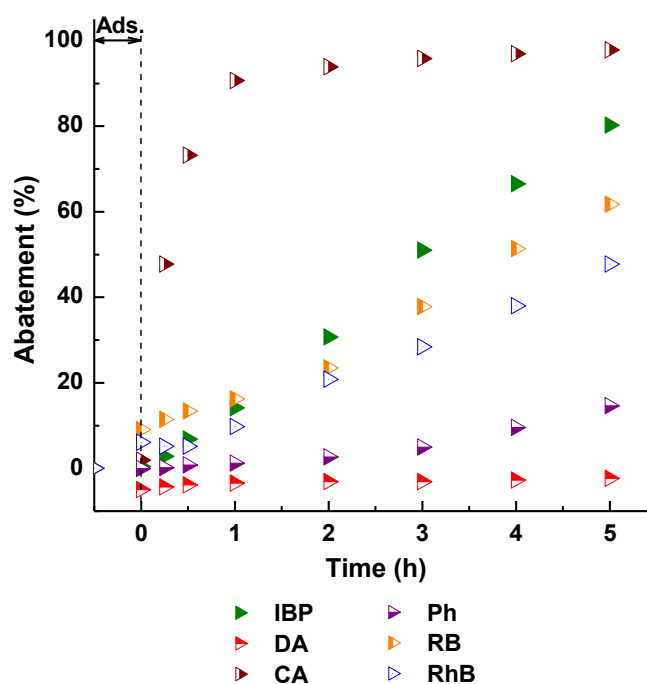


Figure 40. Photocatalytic abatement of different organic compounds cinnamic acid (CA), phenol (Ph), diatrizoic acid (DA) and the dyes rose bengal (RB) and rhodamine B (RhB) over Rutile. RhB and RB curves represent decolourization. Reaction conditions: RT, organic conc.: 10 ppm, aqueous reaction solution: 250 ml, catalyst loading: 10 mg.

The photocatalytic activity of Rutile is also studied in the photocatalytic degradation of different organic compounds such as CA, IBP, Ph, DA and the dyes RB and RhB. Figure 40 shows the difference in the course of photocatalytic degradation of these organic molecules over Rutile and the adsorption as well. After 2 h of UV-vis irradiation, the order of recalcitrance is as follows:

$$DA > Ph > RhB \geq RB > IBP > CA.$$

In contrast, CA is rapidly degraded with *ca.* 48% after 15 min and *ca.* 94% after 2 h of the treatment, whereas the photocatalytic abatement of the other molecules proceeds distinctly slower. Diatrizoic acid is nearly not converted under used reaction conditions. That means the final activity may be affected not only by the specific surface area, but also by the chemical reactivity of organics. Obviously, the mass transfer of reacting molecules from the solution to the catalyst is not the limiting factor. Adsorption proceeds very speedy providing sufficient amount of pollutant molecules located at the surface of large crystal Rutile. In comparison, Rutile exhibited the highest activity in degradation of CA.

It is essential to deeply understand the role of active species during the photocatalytic degradation of IBP over Rutile. Therefore, hole and reactive oxygen radical trapping experiments have been performed. Figure 41 shows the impact of addition of *t*-BuOH ($\cdot\text{OH}$

scavenger), EDTA (holes scavenger) and 1,4-BQ ($O_2^{\bullet-}/\bullet OOH$ scavenger), respectively, on the photocatalytic abatement of IBP over Rutile. The addition of $O_2^{\bullet-}$ radical scavenger inhibits the IBP degradation nearly completely. This indicates that superoxide ($O_2^{\bullet-}$) or hydroperoxyl ($\bullet OOH$) radicals are the primary active species formed in the photocatalytic abatement of IBP over Rutile. The addition of $\bullet OH$ radical scavenger also reduces the photocatalytic abatement of IBP from originally 80% to 30% indicating the strong contribution of $\bullet OH$ radicals.

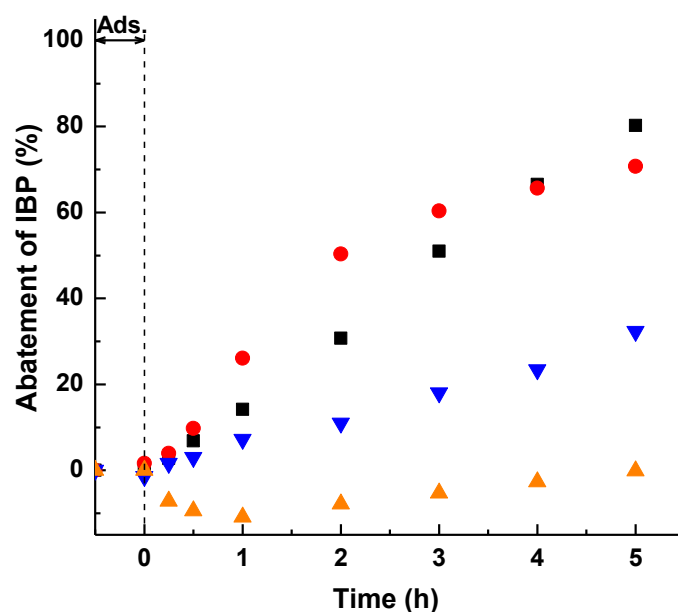


Figure 41. Impact of different scavengers on the photocatalytic abatement of IBP over Rutile. Reaction conditions: RT, IBP conc.: 10 ppm, aqueous reaction solution: 250 ml, catalyst loading: 10 mg. (■) No scavenger. Scavengers: (●) 1.46 mg EDTA, (▼) 0.1 ml *t*-BuOH, and (▲) 2.704 mg 1,4-BQ.

In contrast, the addition of the holes (h^+) scavenger does not affect the photocatalytic abatement. Therefore, it is concluded that valence band holes are not involved directly in the photocatalytic degradation of IBP over Rutile, but produce $\bullet OH$ radicals via oxidation reaction by holes and OH^- groups. Instead, the addition of enhanced amounts of EDTA gradually increases the photocatalytic abatement (compare Figure 48a). This effect implies that EDTA injects electrons into the valence band of Rutile thereby improving charge carrier separation by excitation of electrons to the conduction band. As a result, the formation of superoxide radicals is further enhanced. The photocatalytic abatement of IBP is increased from 30% (without addition of EDTA) to 50% (addition of EDTA) for 2 h of reaction. The order of affecting the rate for photocatalytic abatement of IBP over Rutile is as follows: $\bullet OH \approx O_2^{\bullet-}$, no hole contribution. However, the more reactive $\bullet OH$ radicals (high oxidation potential)^[70] act as “door openers” in the photocatalytic degradation of organics over Rutile (aromatic ring opening).

3.4 Comparison of the photocatalytic activity of titania polymorphs with different organic compounds

By using the different reactive organic compounds and from individual measurements of single titania polymorphs, it is concluded that the chemical reactivity of molecules towards photocatalytic degradation decreases in the order: CA > IBP > Ph > DA, whereby the more complex dyes show the order: IBP > RB ≥ RhB > Ph.

3.4.1 The photocatalytic degradation of cinnamic acid (CA)

The CA molecules are rapidly degraded under photocatalytic treatment. Figure 42 (left) shows the photocatalytic degradation of CA under UV-vis irradiation over different titania polymorphs. The conversion of CA is higher for Rutile (89%) after 2 h of reaction compared to Brookite (88%) and Anatase (75%) although the surface area of Rutile is markedly lower than that of Brookite (9.5 times) and Anatase (11 times). Titania P25 shows the highest activity (94%). The adsorption of CA on the surface of Anatase, Brookite, and titania P25 is 3.03%, 1.4%, 2.06%, respectively, while that of Rutile is still 1.33%. It is interesting to note that despite low specific surface area the loading of molecular CA on the Rutile is high. Obviously, the quite large planar crystal facets, which are *ca.* 50-100x300-500 nm in size, facilitate multilayer adsorption by alignment of CA molecules at the crystal surface (Langmuir-Blodgett layer).^[165] Therefore, the photocatalytic degradation of cinnamic acid over low surface area Rutile is not limited by mass transfer or adsorption.

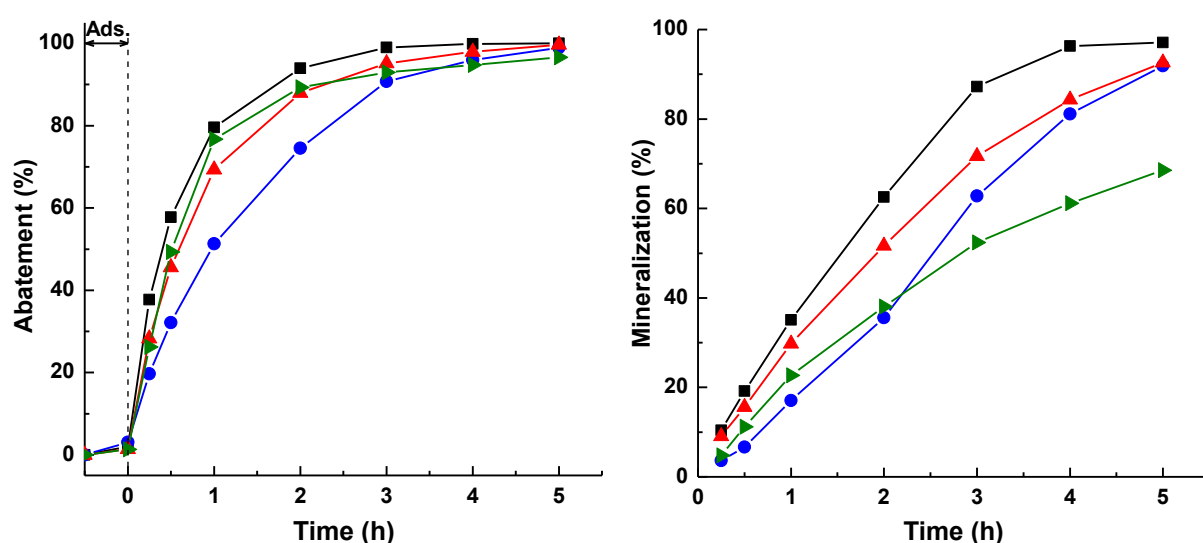


Figure 42. (Left) Abatement of CA and (right) mineralization during the course of photocatalytic performance of (■) titania P25, (●) Anatase, (▲) Brookite and (▼) Rutile. Reaction conditions: RT, CA conc.: 10 ppm, aqueous reaction solution: 250 ml, catalyst loading: 10 mg.

The photocatalytic activity of titania polymorphs in the CA degradation obtained after 2 h decreases in the order:

$$\text{Titania P25} > \text{Rutile} \approx \text{Brookite} > \text{Anatase}.$$

The rapid CA degradation over Rutile can be explained by the high reactivity of CA due to the presence of a reactive olefinic ($-\text{C}=\text{C}-$) bond^[23] in the side chain which facilitates rapid oxidation of CA by reactive oxygen species ($\cdot\text{OH}$ and $\cdot\text{OOH}$ radicals). However, formed intermediates are relatively recalcitrant. As a consequence, the mineralization is lower than the degradation. After 2 h of reaction, the TOC content decreases in the order: Titania P25 (63%) > Brookite (51%) > Anatase (36%) > Rutile (38%). Finally, Anatase and Brookite exhibit high degree of mineralization (*ca.* 90%) after 5 h of UV-vis irradiation, while the TOC removal efficiency is *ca.* 70% in the presence of Rutile (Figure 42, right). Cinnamic acid is totally mineralized over Anatase, Brookite, and titania P25 Degussa.

3.4.2 The photocatalytic degradation of ibuprofen (IBP)

Figure 43 shows the results on the photocatalytic abatement of IBP over titania polymorphs Anatase, Brookite, Rutile, and commercial photocatalyst titania P25 Degussa. All samples are active, again Anatase, Brookite, and titania P25 show distinctly higher activity than Rutile. Importantly, Anatase and Brookite show activities close to that of titania P25 which consists of Anatase (80%) and Rutile (20%). The photocatalytic abatement is very high at the onset of treatment followed by a slower abatement step at longer reaction time.

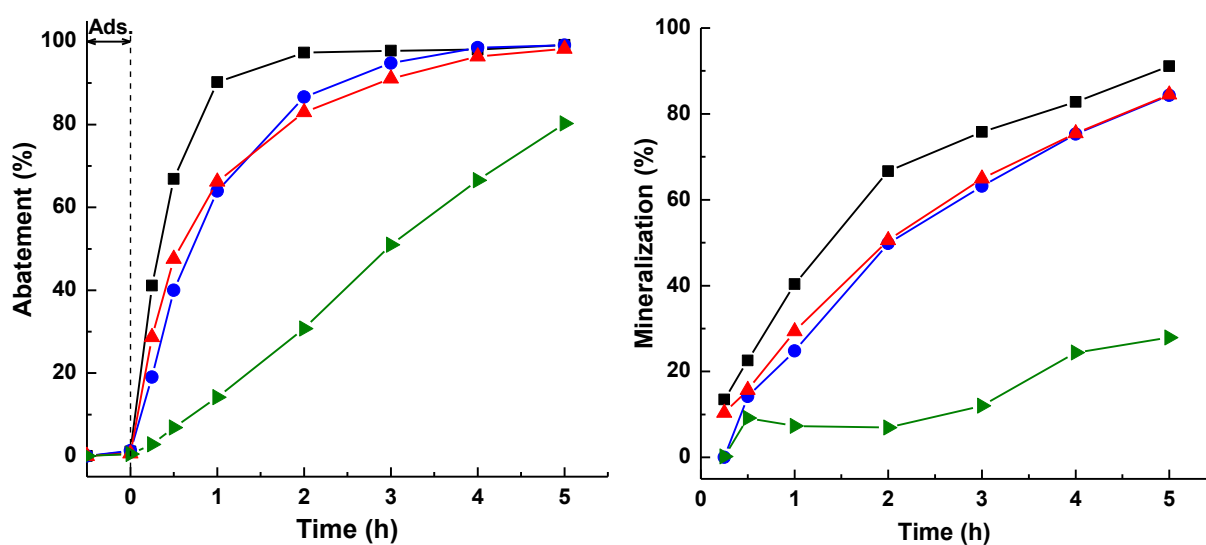


Figure 43. (Left) Abatement of IBP and (right) mineralization during the course of photocatalytic performance of (■) titania P25, (●) Anatase, (▲) Brookite and (▼) Rutile. Reaction conditions: RT, IBP conc.: 10 ppm, aqueous reaction solution: 250 ml, catalyst loading: 10 mg.

After 2 h of reaction, *ca.* 97%, 86%, 82%, 30% of IBP is abated over titania P25, Anatase, Brookite, and Rutile, respectively. Nearly full conversion is achieved after 5 h, but with Rutile *ca.* 80% of IBP is degraded (Figure 43, left). Compared to the high activity observed with Rutile in the photocatalytic degradation of cinnamic acid, its activity in the IBP degradation is now lowest. This finding is confirmed by the mineralization.

Figure 43 (right) shows the corresponding mineralization (TOC content) curves compared to the IBP abatement curves. They confirm the high mineralization capability of IBP with titania-based photocatalysts after 5 h of treatment. The mineralization decreases in the order:

$$\text{Titania P25 (91\%)} > \text{Anatase (84\%)} \approx \text{Brookite (85\%)} \gg \text{Rutile (28\%)}.$$

Again Rutile is markedly less efficient. The lower activity of Rutile is consistent with the lack of active species valence band holes (h^+). Obviously, the IBP is more recalcitrant than the CA. The alkyl substituents stabilize the aromatic ring. In contrast, the reactive olefinic substituent increases the reactivity and facilitates the photocatalytic degradation. Comparison of the abatement curve derived from UV-vis absorption spectra showing high degradation, the mineralization proceeds slowly. The UV-vis absorption spectroscopy is sensitive to the aromatic ring opening, which proceeds rapidly at the onset of reaction. It requires less but strong reactive species. In contrast, the mineralization detected by TOC measurements requires huge amounts of reactive species. Each carbon and hydrogen atom has to be oxidized to CO_2 and H_2O , respectively. Therefore, this process proceeds comparatively slow and is not detected in UV-vis absorption spectra. The latter shows only the decomposition of the remaining small amount of aromatics.

3.4.3 The photocatalytic degradation of phenol (Ph)

Figure 44 (left) shows the photocatalytic abatement of phenol over titania P25 Degussa, Anatase, Brookite, and Rutile, respectively. Phenol is hard to decompose under the UV-vis irradiation alone (presented in the experimental part). The degradation efficiency of Ph increases linearly with prolonged irradiation time. The highest conversion is observed for titania P25, *ca.* 98% of Ph is abated within 5 h of treatment. At the same time, only *ca.* 21% of Ph is degraded in the photocatalytic performance of Rutile. The photocatalytic activity of Brookite and Anatase are similar, *ca.* 65% after 5 h. The degradation efficiency of Ph over titania polymorphs decreases in the order:

$$\text{Titania P25} > \text{Anatase} \approx \text{Brookite} > \text{Rutile}.$$

The obtained mineralization of Ph determined by TOC measurement is shown in Figure 44 (right). Again it is observed that TOC removal proceeds markedly slower compared to the photocatalytic abatement monitored by UV-vis absorption spectroscopy. Interestingly, high and nearly linear mineralization of phenol during the course of photocatalytic treatment is observed with titania P25 (*ca.* 95% after 5 h), while only *ca.* 8% is achieved with Rutile. Anatase and Brookite show the same mineralization of Ph (*ca.* 45%). In the photocatalytic degradation of phenol, the differences in the photocatalytic activity between Anatase and Brookite are on one side and titania P25 are more pronounced.

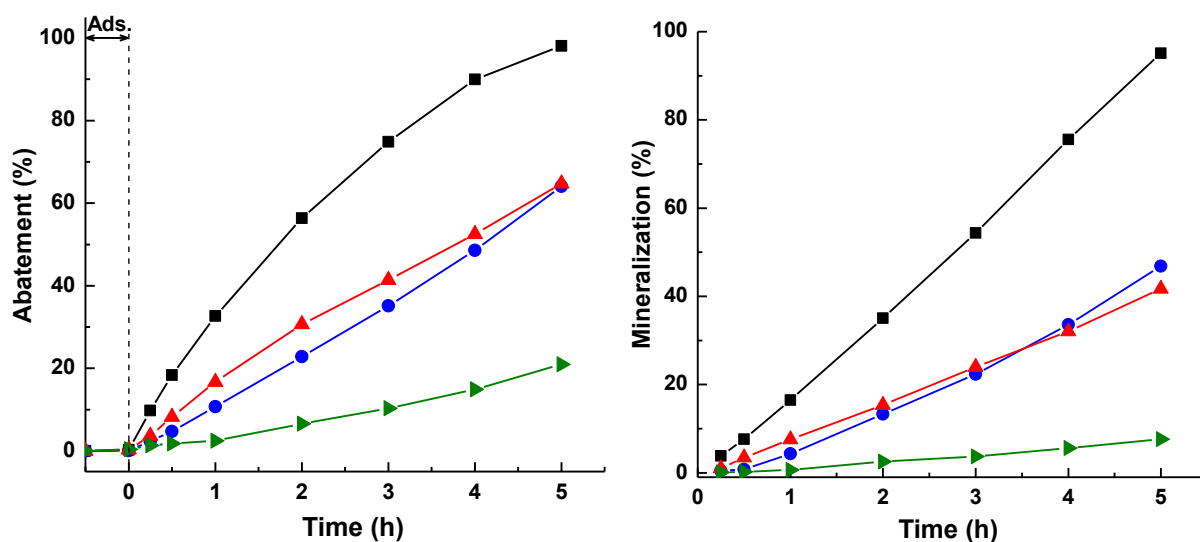


Figure 44. (Left) Abatement of Ph and (right) mineralization during the course of photocatalytic performance of (■) titania P25, (●) Anatase, (▲) Brookite and (►) Rutile. Reaction conditions: RT, Ph conc.: 10 ppm, aqueous reaction solution: 250 ml, catalyst loading: 10 mg.

3.4.4 The photocatalytic degradation of diatrizoic acid (DA)

Diatrizoic acid (DA), a recalcitrant organic compound, exhibits no significant the photolysis under UV-vis irradiation as given in experimental part. Figure 45 (left) shows that after 5 h of the photocatalytic treatment, *ca.* 79%, 64%, and 40% of DA is abated over titania P25 Degussa, Anatase, and Brookite, respectively. Remarkably, Rutile is not active in the photocatalytic degradation of DA.

The extent of mineralization of DA is comparatively low with Anatase and Brookite, even with titania P25 (Figure 45, right). Namely *ca.* 59%, 53%, 50% of total organic carbon content is mineralized after 5 h of photocatalytic reaction with titania P25, Anatase, and Brookite, respectively. Very low mineralization is observed for Rutile.

The photocatalytic activity decreases in the order: Titania P25 > Anatase > Brookite >>> Rutile.

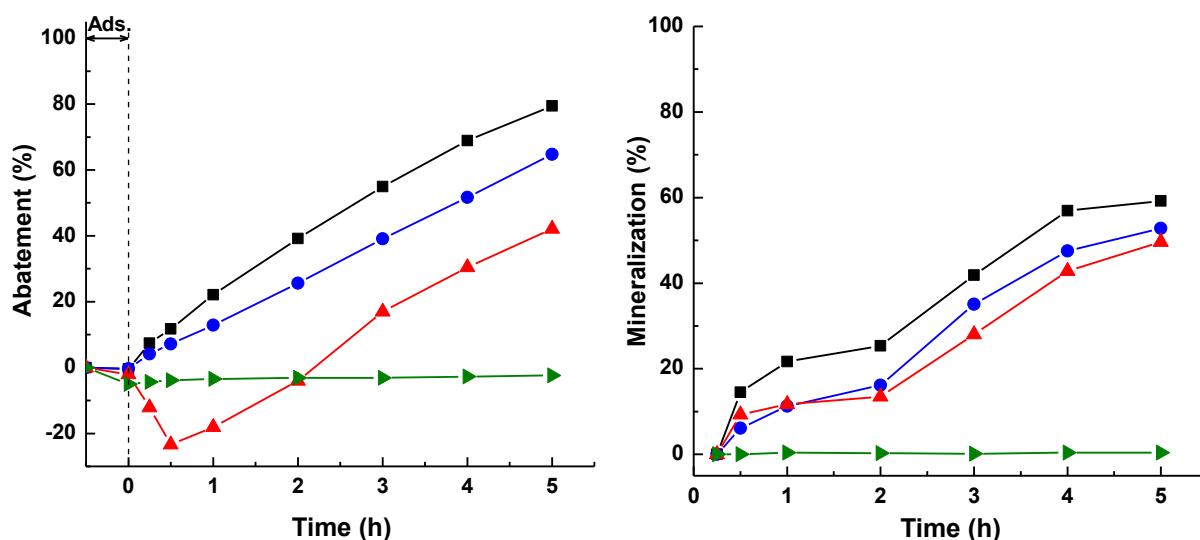


Figure 45. (Left) Abatement of DA and (right) mineralization during the course of photocatalytic performance of (■) titania P25, (●) Anatase, (▲) Brookite and (►) Rutile. Reaction conditions: RT, DA conc.: 10 ppm, aqueous reaction solution: 250 ml, catalyst loading: 10 mg.

Both low degradation and mineralization of DA show its high recalcitrance compared to the other organic compounds (CA, IBP, Ph). This could be attributed to the stabilizing effect of the three iodide substituents on the aromatic ring. DA and their derivatives are used as X-ray contrast agents due to its high chemical stability and X-ray absorption behaviour.^[26]

3.4.5 The photocatalytic degradation of rose bengal (RB)

Rose bengal shows a characteristic absorption band at 523.5 nm causing its pink colour in aqueous solution. The change in intensity of this band (decolourization) is often used for the determination of the photocatalytic degradation with irradiation time. The photolysis of RB under the UV-vis light is shown in the experimental part. Photolysis amounts to *ca.* 20% within 5 h for UV-vis irradiation alone.

The activity of different titania polymorphs Anatase, Brookite, and Rutile in the photocatalytic degradation of RB is shown in Figure 46 (left). Anatase and Brookite exhibit higher activity than Rutile. The order of activity followed by decolourization after 3 h of reaction is as follows:

$$\text{Anatase} > \text{Titania P25} > \text{Brookite} \gg \text{Rutile}.$$

With Rutile, RB is weakly degraded (*ca.* 22%) after 2 h and reached *ca.* 60% after 5 h of treatment. With titania P25, the maximum photocatalytic degradation efficiency of *ca.* 94 % is achieved after 4 h, afterward its efficiency decreases. The decolourization of RB over Anatase and Brookite is nearly completed after 5 h showing high efficiency to oxidize dyes into colourless products. The low activity of Rutile is attributed to the absence of active species

holes as evidenced by the scavenger experiments (see section 3.5). The adsorption of RB is high for all titania photocatalysts (in the order 10%).

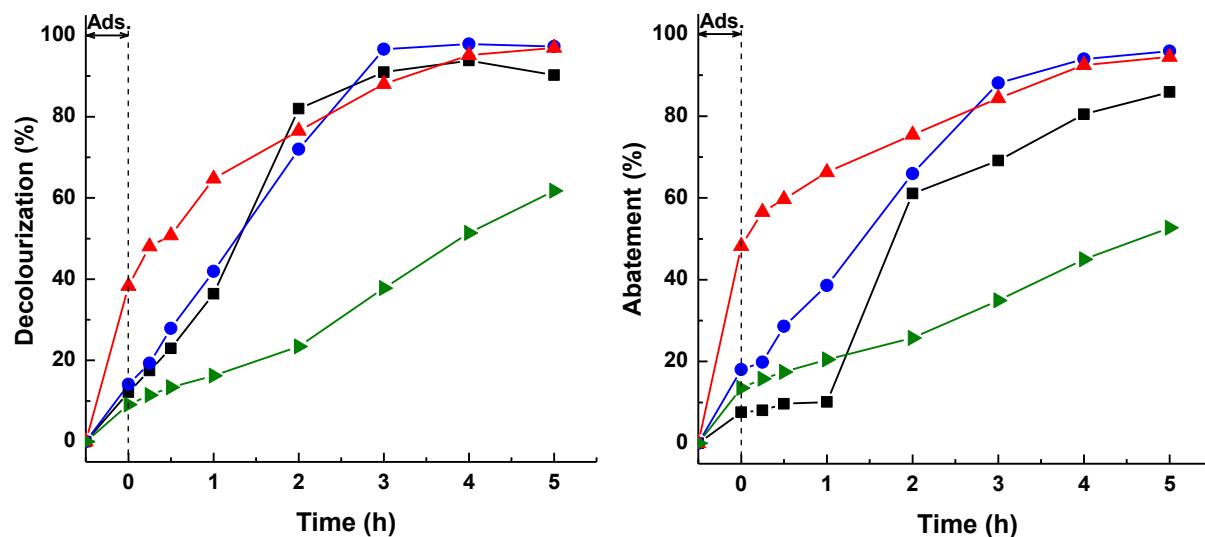


Figure 46. (Left) Decolourization of RB and (right) abatement of aromatic ring during the course of photocatalytic performance of (■) titania P25, (●) Anatase, (▲) Brookite, and (▼) Rutile. Reaction conditions: RT, RB conc.: 10 ppm, aqueous reaction solution: 250 ml, catalyst loading: 10 mg.

Table 11: Degree of mineralization of RB after photocatalytic treatment over titania photocatalysts.

Catalyst Time	Anatase	Brookite	Rutile	Titania P25 Degussa
2 h	36%	42%	-	37%
4 h	50%	47%	-	62%

Table 11 shows the degree of mineralization of RB obtained after 2 h and 4 h of reaction with Anatase, Brookite, Rutile, and titania P25 Degussa. The mineralization is usually lower than the degradation derived from UV-vis absorption spectroscopy. The latter refers only to the aromatic ring opening (destruction of the aromatic ring), whereas the TOC measurement allows to determine the decrease in TOC content which is mineralized to CO₂ as final product after photocatalytic treatment.

3.4.6 The photocatalytic degradation of rhodamine B (RhB)

The characteristic colour of RhB exhibits the maximum absorption band at 553.5 nm (in water). The decolourization of RhB is determined by the change in intensity of this band with prolonged reaction time. Figure 47 (left) shows that *ca.* 99% of RhB is decolorized in the photocatalytic performance of titania P25 Degussa after 5 h of reaction, whereas with Brookite, Anatase, and Rutile the decolourization efficiency is *ca.* 97%, 96%, 48%, respectively. This

means that Brookite and Anatase again show higher activity than Rutile and close to that of titania P25. Figure 47 (right) shows the photocatalytic abatement of aromatic ring during the course of reaction. The photocatalytic abatement of RhB is determined by the change in intensity of absorption band at 225 nm. Compared to Rutile, Brookite and Anatase are more effective for aromatic ring opening reaction in the photocatalytic degradation of RhB.

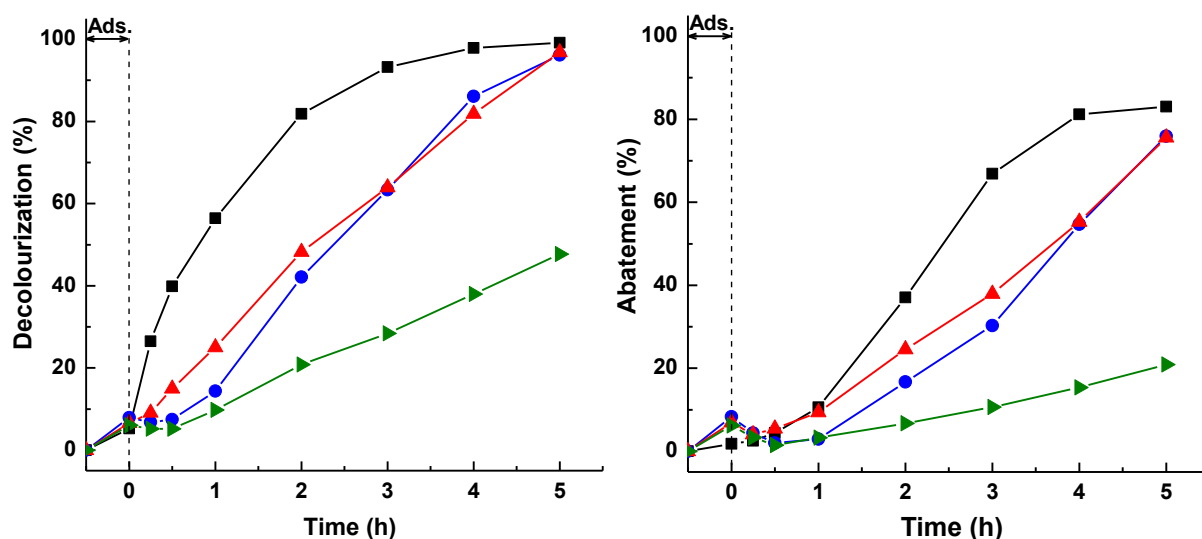


Figure 47. (Left) Decolourization of RhB and (right) abatement of aromatic ring during the course of photocatalytic performance of (■) titania P25, (●) Anatase, (▲) Brookite, and (▼) Rutile. Reaction conditions: RT, RhB conc.: 10 ppm, aqueous reaction solution: 250 ml, catalyst loading: 10 mg.

Table 12: Degree of mineralization of RhB after photocatalytic treatment over titania photocatalysts.

Catalyst Time	Anatase	Brookite	Rutile	Titania P25 Degussa
2 h	-	-	-	9%
4 h	24%	17%	-	61%

Table 12 shows the achieved mineralization of RhB after 2 h and 4 h in the photocatalytic treatment with Anatase, Brookite, Rutile, and titania P25. The low mineralization and low efficiency for oxidative ring opening reaction compared to high efficiency in colour removal are observed in the photocatalytic degradation of RhB. The result indicates the complex structure of RhB compound and the formation of stable intermediates as well.

Conclusion to the chemical reactivity of organic compounds:

- The abatement and mineralization obtained in the photocatalytic performance of Anatase (A), Brookite (B), Rutile (R), and titania P25 Degussa show that in tendency the chemical reactivity of the different pollutants decreases in the order: CA \approx IBP > Ph > DA.
- The synthesized titania polymorphs show following tendency of activity in the photocatalytic degradation of organics: General activity decrease P25 > A \approx B > R, with exceptions of CA and Ph, where A < B.

Rutile shows on average a markedly lower activity than Brookite or Anatase.

- The reactivity differences are due to the formed different active species (see Section 3.5): VB holes (h^+) formed in titania P25, Anatase, and Brookite perform aromatic ring opening, whereas $\cdot OH$ and $O_2^{\cdot -}$ radicals preferentially formed with Rutile. These radicals easily attack the olefinic double bond of cinnamic acid. Aromatic ring opening which is very efficient with h^+ in the photocatalytic performance of titania P25, Anatase, and Brookite is achieved after 2 h of treatment. Rutile behaves according to the chemical reactivity of the organic compounds.

Table 13: Summary of the obtained abatement and mineralization of different pollutants after photocatalytic treatment (2 h) over titania photocatalysts.

Pollutants	Abatement (%)				Mineralization (%)			
	A	B	R	P25	A	B	R	P25
IBP	87	83	31	97	50	51	7	67
CA	76	88	94	95	36	52	38	63
Ph	23	31	3	55	13	15	3	35
DA	26	2	0	39	13	13	0	25

Table 14: Summary of the obtained abatement and mineralization of different pollutants after photocatalytic treatment (5 h) over titania photocatalysts.

Pollutants	Abatement (%)				Mineralization (%)			
	A	B	R	P25	A	B	R	P25
IBP	99	98	80	99	84	85	28	91
CA	98	99	96	99	92	93	69	97
Ph	64	65	15	98	47	42	8	95
DA	56	42	0	79	53	50	0	59

The tendency of the chemical reactivity of various pollutants obtained after 2 h of photocatalytic treatment is shown below.

Abatement

Titania P25:	IBP (97%) \approx CA (95%) > Ph (55%) > DA (39%)
Anatase:	IBP (87%) > CA (76%) > DA (26%) \geq Ph (23%)
Brookite:	CA (88%) \geq IBP (83%) >> Ph (31%) >> DA (2%)
Rutile:	CA (94%) >> IBP (31%) > Ph (3%) \approx DA (0%)

Mineralization

Tiatania P25:	IBP (67%) \approx CA (63%) > Ph (35%) > DA (25%)
Anatase:	IBP (50%) > CA (36%) > DA (16%) \approx Ph (13%)
Brookite:	CA (52%) \approx IBP (51%) > Ph (15%) \approx DA (13%)
Rutile:	CA (38%) > IBP (7%) > Ph (3%) > DA (0%)

3.5 Comparison of the impact of hole/radical scavenger on the photocatalytic abatement of IBP over the titania polymorphs Brookite, Anatase, and Rutile

Various active species as photogenerated hole (h^+), hydroxyl radicals ($\bullet OH$), superoxide radicals ($O_2^{\bullet -}$), hydroperoxyl radicals ($\bullet OOH$), and singlet oxygen (1O_2) can be formed during the course of photocatalytic treatment with titania photocatalysts.^[80,81,166] Among reactive oxygen species (ROS), the $\bullet OH$ radical is a highly active species (redox potential +2.8 V vs. SHE).^[63,167] In this work, the nature of present active species has been investigated via selective trapping experiments as follows: EDTA (ethylenediaminetetraacetic acid) acts as a hole scavenger,^[80,81] *t*-BuOH (*tert*-butanol) acts as a $\bullet OH$ radical scavenger,^[84] and 1,4-BQ (1,4-Benzoquinone) acts as a $O_2^{\bullet -}$ radical scavenger.^[85] Ibuprofen has been used as model pollutant.

3.5.1 Impact of the hole scavenger on the photocatalytic abatement of ibuprofen

The impact of the hole scavenger on the photocatalytic abatement of IBP over titania P25 Degussa, Anatase, Brookite, and Rutile has been investigated by the addition of EDTA. The result shows a markedly decrease in the photocatalytic degradation of IBP with Anatase, Brookite, and titania P25 as shown in Table 15.

Table 15: Relative decrease of the photocatalytic abatement of IBP (%) over titania polymorphs and titania P25 after addition of the hole (h^+) scavenger EDTA^a.

Irradiation time	Anatase	Brookite	Rutile	Titania P25 Degussa ^b
1 h	83	82	-	67
2 h	67	40	-	53

^aReaction conditions: RT, IBP conc.: 10 ppm, aqueous reaction solution: 250 ml, catalyst loading: 10 mg, addition of EDTA: 1.46 mg, ^b5.72 mg – four times increase in scavenger addition.

The decrease in activity reaches *ca.* 82% with Anatase and Brookite. In case of titania P25, the amount of EDTA has to be increased by a factor four in order to achieve a similar high decrease (Table 15). It is therefore concluded that titania P25 provides significantly more active holes (h^+) than single components Anatase or Brookite. It also indicates that holes are main active species in the photocatalytic performance of Anatase and Brookite, which could directly oxidize the adsorbed organic pollutants.^[84]

Surprisingly, the addition of EDTA results in an increase in activity of Rutile (Figure 48a). This means that these holes are not directly involved in the oxidation of organics. Obviously, the EDTA injects electrons into valence band. Thereby, charge separation is improved, because the excited electrons located in conduction band cannot recombine and migration to the catalyst surface is facilitated. As a result, the formation of $O_2^{\bullet-}$ radicals (or $\bullet OOH$ radicals) via reduction of oxygen molecules by conduction band electrons is enhanced. They take part in the oxidation process of IBP and lead to an increase in the abatement of IBP by addition of EDTA. It cannot be excluded possible that some $\bullet OH$ radicals might be generated by multistep reduction of $O_2^{\bullet-}$ radicals via an $e^- \rightarrow O_2^{\bullet-} \rightarrow H_2O_2 \rightarrow \bullet OH$ pathway (Eq. 4-8).^[2,34,86] Furthermore, an enhancement of the activity of Rutile is observed with increasing amount of EDTA from 30% (no scavenger) to 39%, 50%, and 47% after adding 0.73 mg, 1.46 mg, and 2.92 mg of EDTA, respectively, after 2h of the photocatalytic reaction (Figure 48a).

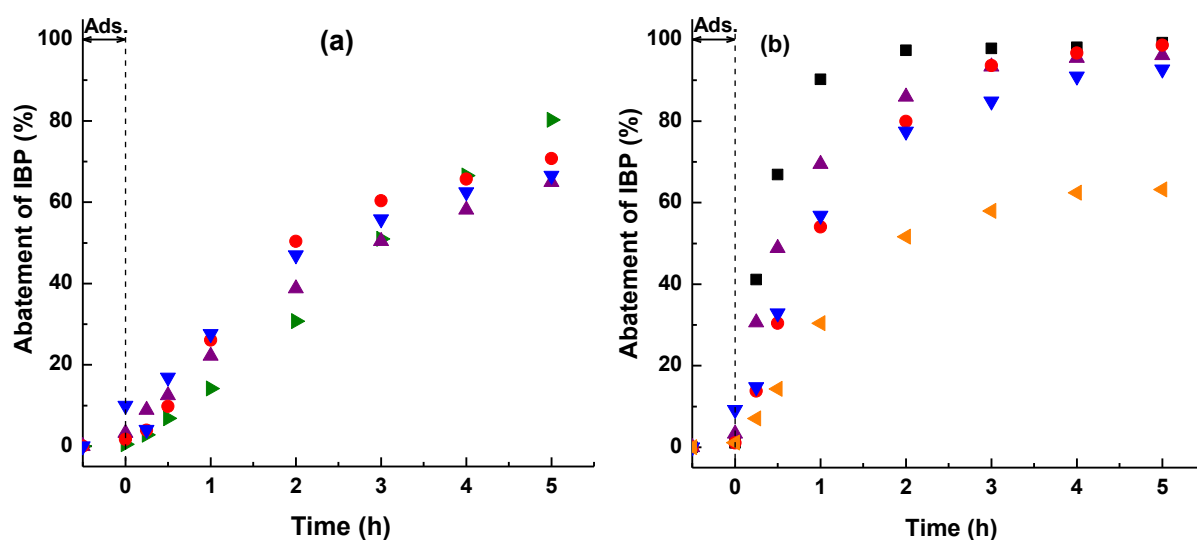


Figure 48. Photocatalytic abatement of IBP over (a) Rutile and (b) titania P25 by changing amount of the addition of EDTA: (\blacktriangle) 0.73 mg, (\bullet) 1.46 mg, (\blacktriangledown) 2.92 mg, (\blacktriangleleft) 5.72 mg. No scavenger with (\blacktriangleright) Rutile and (\blacksquare) titania P25. Reaction conditions: RT, IBP conc.: 10 ppm, aqueous reaction solution: 250 ml, catalyst loading: 10 mg.

In summary, the impact of the holes on the photocatalytic abatement of ibuprofen (activity) decreases in the order: Titania P25 > Anatase \geq Brookite \gg Rutile. Obviously, valence band holes (h^+) play no or only a minor role with Rutile, whereas titania P25 differs from Anatase or Brookite by an enhanced contribution of strong oxidative valence band holes.

3.5.2 Impact of the $\bullet OH$ radical scavenger on the photocatalytic abatement of ibuprofen

The impact of $\bullet OH$ radical scavenger on the photocatalytic abatement of IBP over titania P25, Anatase, Brookite, and Rutile has been studied by the addition of *t*-BuOH. The addition causes

a reduction in the activity of titania P25, Anatase and a remarkable decrease in the activity of Rutile (Table 16). The lowest influence is observed for Brookite. It implies that the $\cdot\text{OH}$ radical, the most active oxygen species, effectively contributes to the photocatalytic performance of Rutile and is of minor importance in the abatement of IBP over Anatase and titania P25.

Table 16: Relative decrease of the photocatalytic abatement of IBP (%) over titania polymorphs and titania P25 after addition of the $\cdot\text{OH}$ radical scavenger $t\text{-BuOH}^a$.

Irradiation time	Anatase	Brookite	Rutile	Titania P25 Degussa
1 h	23	17	50	24
2 h	16	9	64	9

^aReaction conditions: RT, IBP conc.:10 ppm, $t\text{-BuOH}$: 0.1 ml, aqueous reaction solution: 250 ml, catalyst loading: 10 mg.

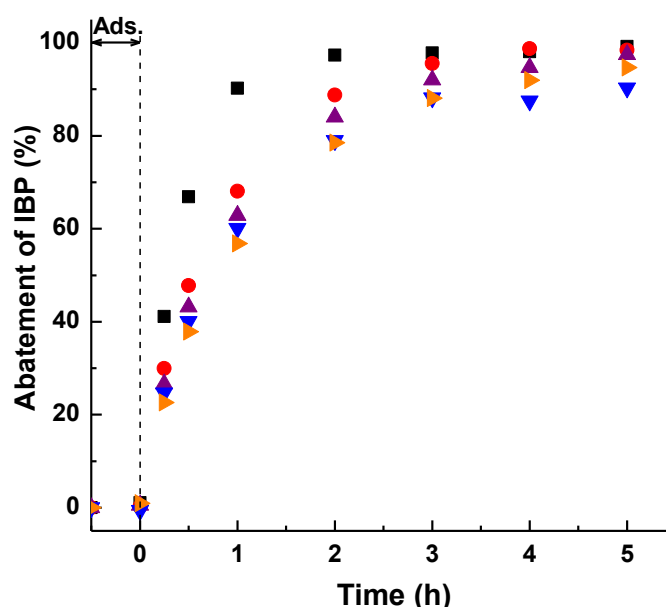


Figure 49. Photocatalytic abatement of IBP over titania P25 by increasing addition of $t\text{-BuOH}$: (●) 0.1 ml, (▲) 0.2 ml, (▼) 0.3 ml, (►) 0.4 ml. (■) No scavenger. Reaction conditions: RT, IBP conc.: 10 ppm, aqueous reaction solution: 250 ml, catalyst loading: 10 mg.

Further $\cdot\text{OH}$ radical trapping experiments have been carried out to investigate the impact of $\cdot\text{OH}$ radical scavenger in the photocatalytic degradation of IBP over titania P25 with various amounts of $t\text{-BuOH}$. Figure 49 shows a decrease in the activity of titania P25 with increasing amount of added $t\text{-BuOH}$. When 0.4 ml of $t\text{-BuOH}$ is added, *ca.* 55% of IBP is decomposed after 1 h of reaction, while 90% of IBP is abated without scavenger (39% relative decrease in activity after addition of $t\text{-BuOH}$). This effect is not so strong compared to the addition of only 0.1 ml of $t\text{-BuOH}$ (24%).

In summary, the relative contribution of $\bullet\text{OH}$ radicals on the photocatalytic abatement of ibuprofen (activity) decreases in the order: Rutile \gg Titania P25 \approx Anatase $>$ Brookite. Remarkably, the contribution of $\bullet\text{OH}$ radicals is somewhat lower with Brookite than Anatase.

3.5.3 Impact of the $\text{O}_2^{\bullet-}$ radical scavenger on the photocatalytic abatement of ibuprofen

The impact of $\text{O}_2^{\bullet-}$ (or $\bullet\text{OOH}$) radical scavenger on the photocatalytic abatement of IBP over Anatase, Brookite, Rutile, and titania P25 has been investigated by addition of 1,4-BQ. The addition causes a strong decrease in the activity of all titania polymorphs. This means the importance of $\text{O}_2^{\bullet-}$ (or $\bullet\text{OOH}$) radicals for degradation process, even it has low redox potential. The concentration of $\text{O}_2^{\bullet-}$ ($\bullet\text{OOH}$) radicals seems to be suppressed also with prolonged irradiation time (compare Figure 28, 37, 42). The order of activity in the IBP degradation after 2 h is as follows: Titania P25 (97%) $>$ Anatase (86%) $>$ Brookite (83%) \gg Rutile (31%) and the relative decrease in activity after addition of the $\text{O}_2^{\bullet-}$ ($\bullet\text{OOH}$) radicals (Table 17) follows the order: Rutile $>$ Brookite $>$ Anatase \approx Titania P25. The differences between the titania polymorphs become more pronounced when a lower amount of 1,4-BQ is added (0.5 mg): Rutile (78%) $>$ Brookite (65%) $>$ Anatase \approx Titania P25 (40%), respectively, after 1 h, confirming also the importance of the holes (h^+) at the onset of the photocatalytic degradation.

Table 17: Relative decrease of the photocatalytic abatement of IBP (%) over titania polymorphs and titania P25 after addition of the $\text{O}_2^{\bullet-}$ radical scavenger 1,4-BQ^a.

Irradiation time	Anatase	Brookite	Rutile	Titania P25
1 h	81	92	90	82
2 h	67	77	90	63

^aReaction conditions: RT, IBP conc.:10 ppm, 1,4-BQ: 2.704mg, aqueous reaction solution: 250 ml, catalyst loading: 10 mg.

In summary, over all titania catalysts sufficient amounts of $\text{O}_2^{\bullet-}$ ($\bullet\text{OOH}$) radicals are formed and contribute to the photocatalytic abatement although there are differences between the titania catalysts. But these radicals have the lowest oxidation potential and cannot perform the aromatic ring opening alone (Table 3 and Figure 2).

Conclusion to the impact of active species: The analysis of the contribution of active species derived from quenching experiments with various scavengers could give a detailed view of the different activity of synthesized titania polymorphs. Figure 50 shows the decrease in the

photocatalytic abatement of IBP (activity) over the synthesized titania polymorphs and commercial photocatalyst titania P25 after 2 h of the treatment. The impact of different active species is summarized in Table 18. It shows:

- Highest impact of valence band holes (h^+) for the most active photocatalyst titania P25 Degussa, followed by Anatase and Brookite which have similar activities.
- Marginal impact of holes with the lowest active catalyst Rutile.
- Formation of hydroxyl ($\cdot OH$) radicals is highest with Rutile.
- With Brookite, the impact of $\cdot OH$ radicals is only low.
- Superoxide ($O_2^{\cdot -}$) radicals have a high impact with all titania catalysts.

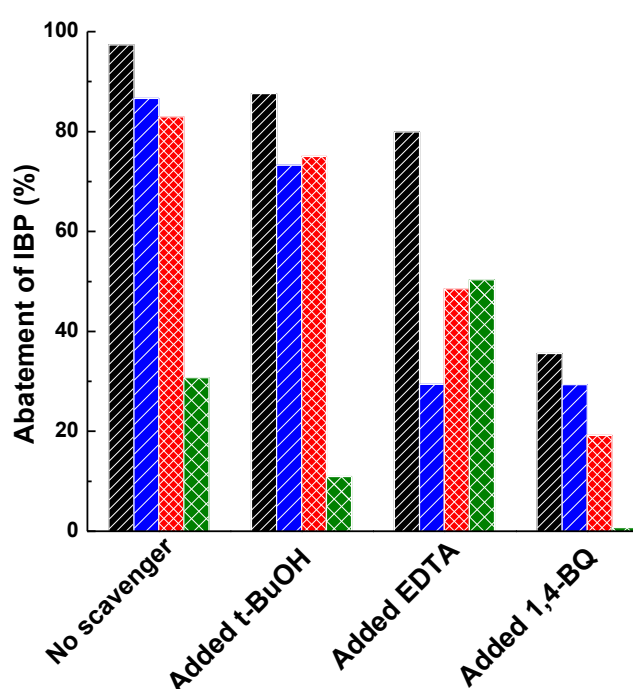


Figure 50. Summary of the photocatalytic abatement of IBP over (▨) titania P25, (▤) Anatase, (▥) Brookite, (▧) Rutile, respectively, and hole/radical trapping experiments with three different scavengers (under UV-vis irradiation for 2 h).

Table 18: The order of relative contribution of different active species in the IBP abatement over the synthesized titania polymorphs and titania P25 obtained after 2 h of the photocatalytic treatment.

Active species	The order of relative contribution in activity
h^+	Titania P25 > Anatase \geq Brookite >> Rutile
$\cdot OH$	Rutile >> Titania P25 \approx Anatase > Brookite
$O_2^{\cdot -}$	Rutile >> Brookite > Anatase \approx Titania P25

3.6 Origin of different activity of Rutile compared to Anatase and Brookite

The photocatalytic degradation activities of titania polymorphs decrease in the order: Titania P25 \geq Anatase > Brookite \gg Rutile. With the exception of CA, it is highly degraded even by Rutile. The achieved degradation decreases with increasing recalcitrance of the substrates in the order: CA > IBP > Ph > DA. The differences in the activity are more pronounced in the mineralization of the organics to CO₂ and H₂O compared to the degradation determined by UV-vis absorption spectroscopy, which is sensitive to the cleavage of the aromatic ring.

The radical and hole scavenger experiments show that Rutile suffers from the active VB holes (h^+) in the direct oxidation of organics, which explains its low activity (Table 18). Instead, the addition of hole scavenger EDTA leads to an enhancement of the activity. This is assigned to the effect of electron injection into the VB and subsequently increase charge separation, which leads to enhance the formation of O₂^{•-} radicals via reduction of O₂ by photogenerated electrons at the CB. It is concluded that the nature of holes of Rutile is different from that of Anatase and Brookite, e.g., they differ in the local structure or surface hydroxylation.

Rutile is highly active with reactive pollutants like cinnamic acid which do not require strong oxidative valence band sites but react with •OH radicals which are less strong than the VB holes. This shows that charge separation and migration of electron-hole pairs to the surface of catalysts are not main limiting factors explaining the lower activity of Rutile compared to other titania polymorphs.^[104,112,119] The importance of present active species is also reflected in the stronger dependency of the photocatalytic degradation on the recalcitrance (reactivity) of the pollutants observed with Rutile, e.g., DA is not converted over Rutile (Figure 51).

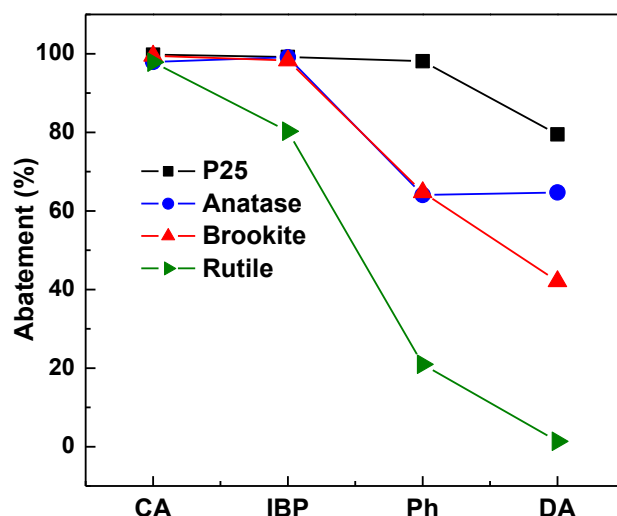


Figure 51. Recalcitrance of organic compounds against photocatalytic degradation. Photocatalytic abatement of cinnamic acid (CA), ibuprofen (IBP), phenol (Ph), and diatrizoic acid (DA) over (■) titania P25, (●) Anatase, (▲) Brookite, and (▼) Rutile.

The larger crystal size and correspondingly distinctly lower specific surface area of Rutile compared to Anatase, Brookite or titania P25 (Table 10) could explain the lower activity of Rutile. Therefore, a series of photocatalytic IBP degradation experiments have been carried out with different sized Rutile samples. Figure 52 shows that only *ca.* 20% of IBP over grinded Rutile R3 (short-time milled R1) is degraded after 5 h of reaction, while IBP is remarkably abated with the synthesized Rutile R1 (*ca.* 80%). For comparison, the photocatalytic activities of Rutile R2 separated from the synthesized mixture of Brookite/Rutile and Rutile R4 obtained by calcination of synthesized Brookite at 700 °C have been studied. The result shows that the photocatalytic activity decreases in the following order: R1 > R2 > R3 > R4, which is opposite to the order of crystal size: R1 > R2 > R4 > R3 (Table 19). Largest crystals (R1) show the highest activity. Basically, the particle size reduction is accompanied by an increase of the specific surface area and is expected to lead to an enhancement in the photocatalytic activity.

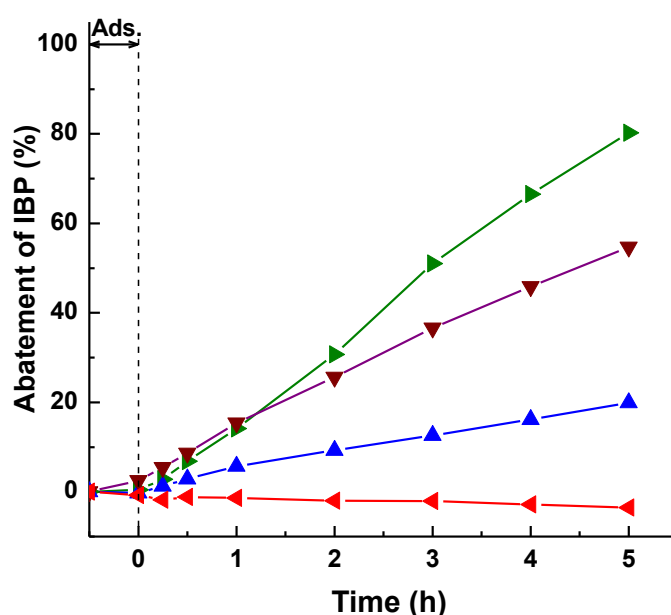


Figure 52. Photocatalytic abatement of IBP over (►) synthesized Rutile R1, (▼) Rutile R2 obtained by peptization with water, (▲) Rutile R3 obtained by grinding, and (◄) Rutile R4 obtained by calcination of synthesized Brookite at 700 °C. Reaction conditions: RT, IBP conc.: 10 ppm, aqueous reaction solution: 250 ml, catalyst loading: 10 mg.

Table 19: Crystal and crystallite size of different Rutile crystals determined by SEM and XRD.

Sample	Particle size (SEM)	Crystallite size (XRD)
R1	Width: 50-100 nm Length: 300-500 nm	98 nm
R2	Width: 20-30 nm Length: 150-300 nm	67 nm
R3	<i>ca.</i> 55 nm	93 nm
R4	<i>ca.</i> 50-180 nm	116 nm

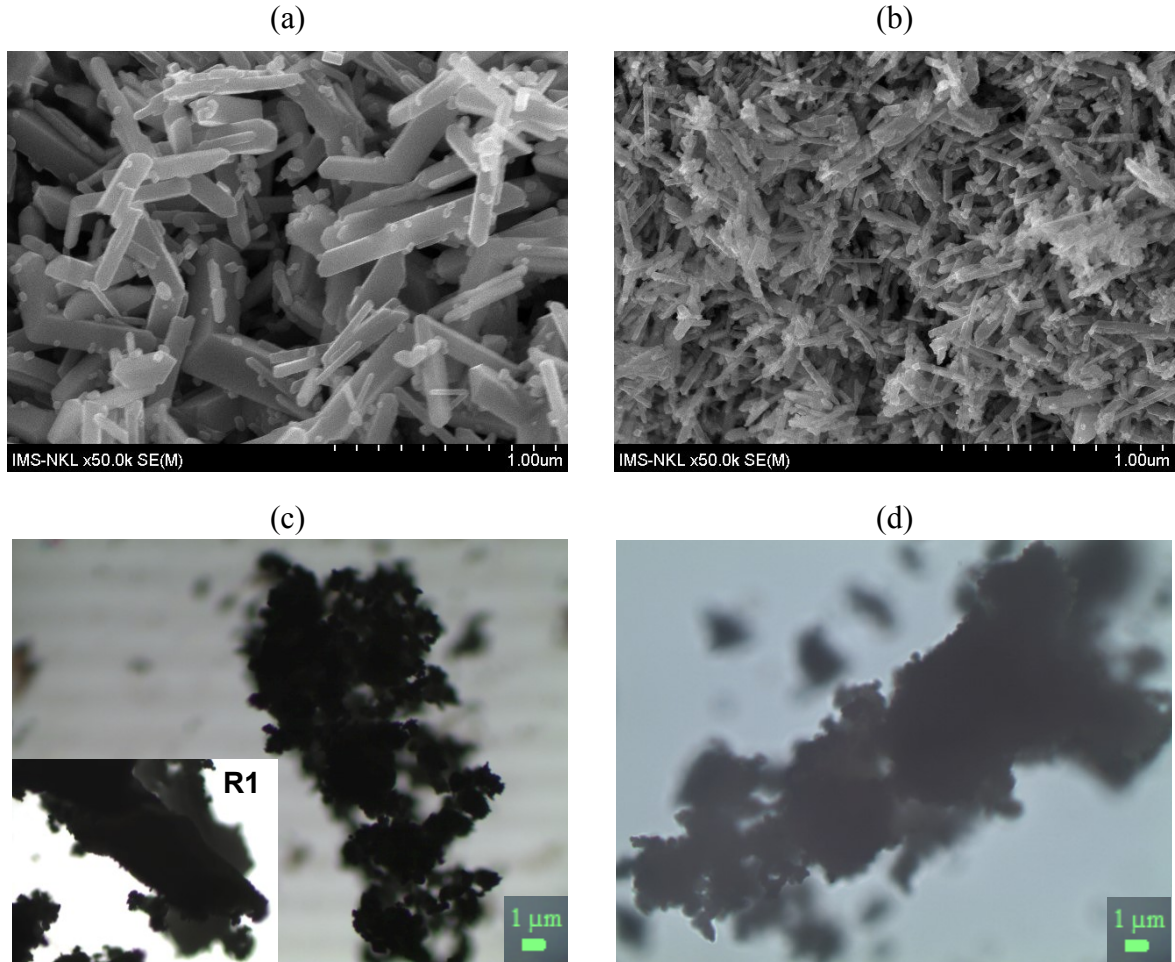


Figure 53. SEM images of (a) synthesized Rutile R1 and (b) Rutile R2 obtained by peptization with water. Raman microscopic images of (c) Rutile R3 obtained by grinding and (d) Rutile R4 obtained by calcination of synthesized Brookite at 700 °C.

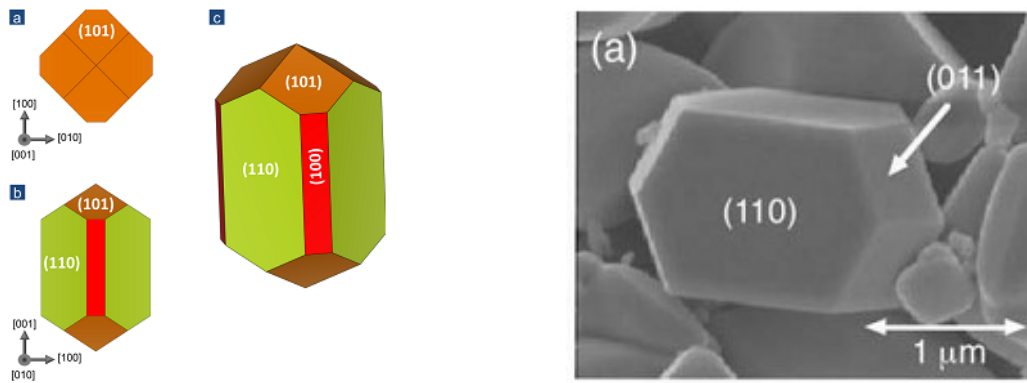


Figure 54. (Left) Predicted equilibrium shape of a Rutile TiO_2 nanocrystal obtained using the DFT calculated surface energies and the Wulff construction and (right) SEM image of Rutile (taken from Ref. [168,169], respectively).

According to the XRD patterns, all samples are highly crystalline. They show narrow reflections and larger crystallite sizes. The difference in size and shape of studied Rutile samples is shown in Figure 53 and Table 19. They show that with large Rutile (R1) crystals

the {110} facets are the dominating crystal faces. Compared to other facets of Rutile (Figure 54), the {110} facets are considered to be the most active regarding surface trapping of VB holes (h^+) formed by photo-excitation process of electrons to the conduction band.^[77,168,170] The relative contribution of the {110} facets to the surface area of the crystals is diminished with decreasing crystal size and/or change of the crystal shapes. Rutile R4 particles are irregular shaped and show a broad size distribution. As a result, the photocatalytic activity is decreased unexpectedly with decreasing particle size (decrease of the aspect ratio).

Finally, it is concluded that the origin of different (or lower) activity of Rutile compared to Anatase, Brookite, and the commercial photocatalyst titania P25 Degussa is the different nature of formed VB holes (h^+). The holes of all titania polymorphs exhibit high oxidation power of *ca.* 2.8 eV which is suitable for the cleavage of the aromatic ring of pollutants, a key step in degradation. However, the VB holes (h^+) of Rutile form mainly $\bullet OH$ radicals. The markedly higher surface hydroxylation density of synthesized Rutile compared to other titania polymorphs can be contribute to the behaviour of hydrophilicity (Table 7). It is concluded that the nature of holes, e.g., the coordination environment or hydroxylation state is special with Rutile.^[92] The high impact of the $O_2^{\bullet -}$ radical scavenger already at the onset of photocatalytic reaction, where aromatic ring opening is indicated by the UV-vis spectra, points to an involvement of the $O_2^{\bullet -}$ radicals in the cleavage of the aryl group. Hence, VB holes and $O_2^{\bullet -}$ radicals formed by reduction of oxygen by photogenerated electrons at conduction band, play major role in the photocatalytic oxidative degradation process. This conclusion is supported by recent ^{18}O -labelling experiments which point to the incorporation of oxygen molecules from the $O_2^{\bullet -}$ radicals into hydroxylation and aromatic ring opening products during the photocatalytic degradation process.^[92]

3.7 The photocatalytic activity of mixed-phase TiO_2 composites

The photocatalytic activities of the titania polymorphs Anatase, Brookite, and Rutile have been investigated and showed different performance depending on the chemical reactivity of the organic compounds as described in the previous section: Anatase \geq Brookite \gg Rutile (see Section 3.4). The efficiency of photocatalysis depends markedly on the charge carrier separation of formed electron-hole pairs. Therefore, the coupling of two kinds of titania polymorphs might be an efficient approach for improving electron-hole separation by diminishing electron-hole recombination.^[106,171,172] The high photocatalytic activity of commercial photocatalyst, titania P25 Degussa (Evonik) which represents a mixture of Anatase and Rutile, has been possibly attributed to synergetic effect.^[106,173] It is prepared at

very high temperature by combustion of titanium tetrachloride. However, the origin of the high efficiency of titania P25 in the photocatalytic degradation is still under discussion and remains unclear.^[20,113,125,174] A recent study, using layered Anatase/Rutile titania thin-films prepared by chemical vapour deposition, pointed also for a synergetic effect in the Anatase/Rutile interface of the thin films.^[175] The enhancement could be assigned to an Anatase/Rutile band alignment effect, which led to electron transfer from the conduction band of Rutile to the CB of Anatase.^[174–176] This evidence is based on the photocatalytic degradation tests of octadecanoic (stearic) acid in air. Therefore, it was worth to examine whether a similar positive effect on the photocatalytic degradation of aromatic compounds like Ibuprofen can be achieved by heterojunction of Anatase with Rutile or Brookite agglomerated composites in aqueous solution. Anatase or Brookite was coupled with a minor amount of Rutile or Brookite. In this work, Anatase/Brookite (A80B20), Anatase/Rutile (A80R20), and Brookite/Rutile (B80R20) agglomerated composites have been prepared by physical mixing. Also a synthesized Brookite/Rutile mixture has been involved. The photocatalytic degradation of IBP has been studied to compare the photocatalytic performance (aromatic ring opening and carbon mineralization) of the titania composites with that of the single components Anatase, Brookite, and Rutile, respectively. Additionally, the impact of active species (h^+ , $\bullet OH$, $O_2^{\bullet -}$) on the abatement of IBP has been investigated.

Anatase/Brookite

Figure 55 (left-top) shows the abatement of IBP over A80B20 composites and the single components Anatase, Brookite for comparison. Anatase and Brookite exhibits high and similar activity with *ca.* 87% and 83% abatement after 2 h of treatment. Surprisingly, the A80B20 composite shows distinctly lower activity with 74% abatement, although both the starting components are highly active. Nearly full conversion ($> 90\%$) is achieved in abatement of IBP after 5 h of reaction. The order of the photocatalytic activity after 2 h of reaction is as follows: Anatase \approx Brookite $>$ A80B20.

The observed differences are more pronounced in the mineralization efficiency. Although the photocatalytic conversion of A80B20 composite in IBP degradation is comparatively high (74%), the extent of respective mineralization (28%) is distinctly lower (Table 20). TOC measurements show that only *ca.* 67% of total organic carbon content is mineralized to CO_2 in the photocatalytic degradation of IBP over A80B20 after 5 h of reaction (Figure 55, right-top). Based on mineralization, the activity of titania photocatalysts decreases in the order:

$$\text{Anatase} \approx \text{Brookite} > \text{A80B20}.$$

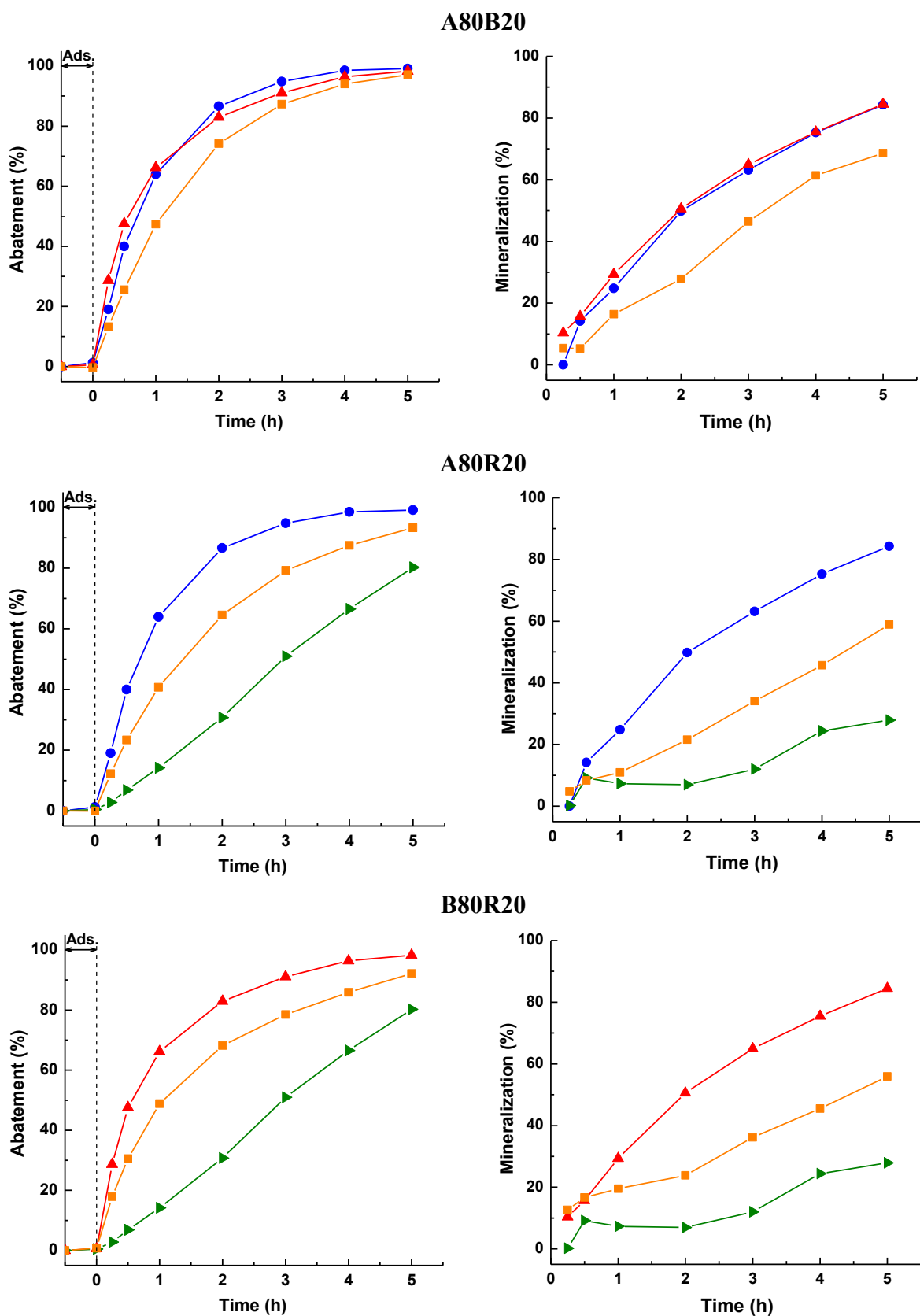


Figure 55. (Left) Abatement and (right) mineralization in the photocatalytic degradation of IBP over (top) A80B20, (middle) A80R20, and (bottom) B80R20 composites, respectively. Reaction conditions: RT, IBP conc.: 10 ppm, aqueous reaction solution: 250 ml, catalyst loading: 10 mg. Single components (●) Anatase, (▲) Brookite, (▼) Rutile, and (■) composite.

Table 20: Calculated and experimental abatement and mineralization of IBP over the titania polymorphs and composites after 2 h of the photocatalytic treatment.

Catalyst	Anatase	Brookite	Rutile	A80B20		A80R20		B80R20	
				Calc. ¹	Exp. ²	Calc. ¹	Exp. ²	Calc. ¹	Exp. ²
Abatement (%)	87	83	31	86	74	76	65	72	68
Mineralization (%)	50	51	7	50	28	41	22	42	24
1: Calculation based on the numerical sum of obtained photocatalytic efficiencies of single components 2: Experiment									

Anatase/Rutile

Figure 55 (left-middle) illustrates the photocatalytic activity of A80R20 composite compared to the single components Anatase and Rutile. After 2 h, *ca.* 87%, 65%, 38% of IBP is degraded over Anatase, A80R20, and Rutile, respectively. Again the composite shows a markedly lower activity than the main active component Anatase and the expected value from the calculated numerical sum of two components in the composite. The order of the photocatalytic activity decreases in the order: Anatase > A80R20 > Rutile

Again the decrease in activity is more pronounced in the mineralization as shown in Figure 55 (right-middle). Only *ca.* 60% IBP is mineralized in the photocatalytic degradation of IBP over A80R20 after 5 h of reaction.

Brookite/Rutile

Figure 55 (left-bottom) shows the abatement of IBP over Brookite/Rutile composite compared to single components Brookite and Rutile. Additionally, a R77B23 mixture of Rutile (77%) and Brookite (23%) prepared by hydrothermal synthesis, is presented for comparison as shown in Figure 56. Interestingly, the activity of the component Brookite is markedly enhanced by separating of the synthesized mixture into its purified components. Also the B80R20 composite which contains 80% of Brookite and 20% of Rutile obtained by hydrothermal treatment shows a markedly lower activity than single component Brookite. Again a markedly decrease in photocatalytic degradation activity is observed for the Brookite/Rutile composite compared to the main component Brookite. The photocatalytic activity decreases in the order:

$$\text{Brookite} > \text{B80R20} > \text{Rutile} > \text{R77B23}.$$

Interestingly, the synthesized mixture shows the lowest activity. Herein, Brookite and Rutile crystallize simultaneously in the reaction mixture forming agglomerates. This confirms that the observed decrease in photocatalytic activity of mixture is due to the effect of coupling. The B80R20 composite exhibits low mineralization capability. The degree of mineralization is only *ca.* 24% after 2 h of reaction (Table 20).

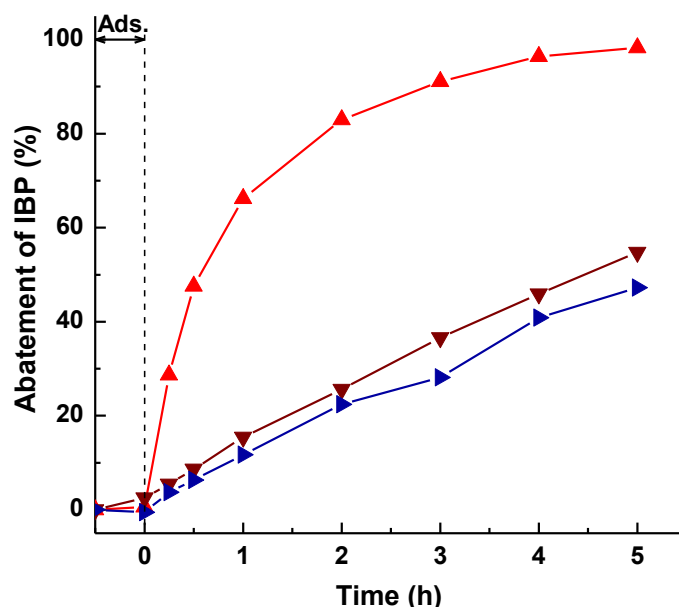


Figure 56. Photocatalytic abatement of IBP over (▲) Brookite, (▼) Rutile obtained from synthesized Brookite/Rutile mixture after peptization with water, and (►) synthesized Brookite/Rutile mixture. Reaction conditions: RT, IBP conc.: 10 ppm, aqueous reaction solution: 250 ml, catalyst loading: 10 mg.

Impact of active species

The contribution of the active species h^+ , $\cdot OH$, and $O_2^{\cdot -}$ radicals has been studied by addition of the different scavengers EDTA, *t*-BuOH, and 1,4-BQ, respectively, as shown in Figure 57. The data show a similar high impact of h^+ and $O_2^{\cdot -}$ radicals on the photocatalytic degradation of IBP. After 2 h of reaction, *ca.* 40-69% relative decrease in activity after addition of the corresponding scavengers is achieved with the different titania composites as given in Table 21. With the exception of Rutile, no contribution of holes is observed. The impact of $\cdot OH$ radicals is lower and the abatement of IBP after addition of *t*-BuOH decreases in the order:

$$\text{Brookite} < \text{A80R20} < \text{Anatase} < \text{A80B20} < \text{B80R20} < \text{Rutile}.$$

Although Rutile is only a minor component in the composites, the impact of $\cdot OH$ radicals is also high since $\cdot OH$ radicals are the main active species in the photocatalytic performance of Rutile. In general, both the direct oxidation of organic matters (aromatic ring opening) and the formation of $\cdot OH$ radicals proceed by the holes. That means both reactions compete with each other during the course of the photocatalytic degradation. Therefore, the increased contribution

of $\cdot\text{OH}$ radicals diminishes the direct oxidation leading to lower activity of the composites compared to that of the single main components.

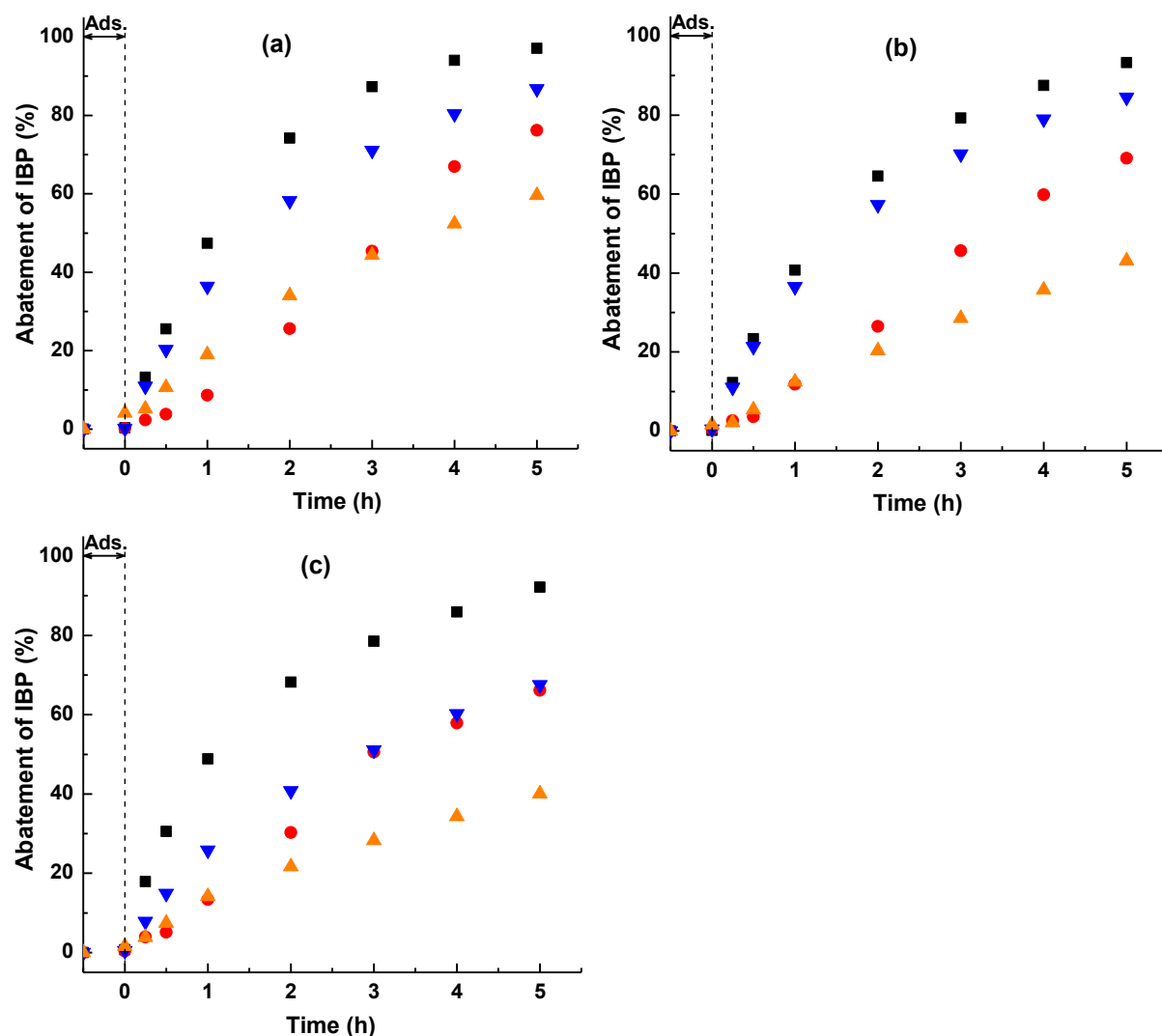


Figure 57. Impact of different scavengers on the photocatalytic abatement of IBP over (a) A80B20, (b) A80R20, and (c) B80R20 composites. Reaction conditions: RT, IBP conc.: 10 ppm, aqueous reaction solution: 250 ml, catalyst loading: 10 mg. (■) No scavenger. Scavengers: (●) 1.46 mg EDTA, (▼) 0.1 ml *t*-BuOH, and (▲) 2.704 mg 1,4-BQ.

Table 21: Relative decrease of the IBP abatement (%) after addition of various scavengers obtained after 2 h of the photocatalytic treatment.

Active species	Anatase	Brookite	Rutile	A80B20		A80R20		B80R20	
				Calc. ¹	Exp. ²	Calc. ¹	Exp. ²	Calc. ¹	Exp. ²
$\cdot\text{OH}$	16	6	64	14	22	26	12	18	40
$\text{O}_2^{\cdot-}$	67	77	79	69	54	69	69	77	68
h^+	67	40	0	62	65	54	60	32	56
1: Calculation based on the relative decrease in activity of single components obtained after addition of corresponding scavengers.									
2: Experiment									

Conclusion to the photocatalytic activity of physically mixed-phase TiO₂ composites

The obtained results can be summarized as follows:

- The coupling of Anatase and Brookite in nanocomposites by physical mixing with a minor amount of Rutile leads to a decrease in the photocatalytic activity, especially with the Brookite/Rutile composite. In contrast to expectation from experience with titania P25, an “opposite synergetic” effect is observed with hydrothermally synthesized titania.
- Although Anatase and Brookite show similar high photocatalytic activity, the activity of their composite is also diminished. The decrease in activity is larger than expected from the calculated numerical sum of the single active components. This is most pronounced in the mineralization behaviour.
- Active species: The influence of the addition of hole and radical scavenges on the abatement activity of Ibuprofen over A80R20, A80B20, and B80R20 catalysts is different from the numerical sum of the single components. Especially with B80R20, a decrease in the contribution of $\cdot\text{OH}$ radicals and holes is observed (larger relative decrease in activity after addition of the scavenger due to less number of active species present).
- In all cases, the coupling of different titania polymorphs causes a decrease in the activity, especially in the mineralization efficiency. This finding is similar to the result obtained in the photocatalytic degradation of the aromatic compound methylene blue in aqueous solution over Anatase and Anatase/Rutile physical mixtures.^[174] Obviously, findings obtained with biphasic titania thin films prepared in gas phase cannot be simply applied to agglomerated titania composites in aqueous solution. Although a heterojunction effect is observed in solution, the effect is negative. The decrease in activity is larger than should be expected from numerical sum of mixing highly active Anatase or Brookite with the lower active Rutile (“opposite synergetic” effect). More detailed investigations are required to clarify the origin of observed different heterojunction effects between titania polymorphs.

4 Final conclusion

- Phase-pure Brookite, Anatase, and Rutile have been prepared by hydrothermal synthesis in acid media followed by the same procedure and the same starting material (amorphous titania) at elevated temperatures between *ca.* 175 to 200 °C. Brookite and Anatase have small size of *ca.* 10-12 nm, while Rutile has large size of *ca.* 50-100x300-500 nm.
- Photocatalytic tests have been carried out under reliable photocatalytic conditions: low irradiation intensity (UV-vis 60W solarium lamps), low catalyst concentration, high organic loading (catalyst-to-substrate ratio = 4). Mineralization measurements and scavenger experiments to determine active species have been performed in detail.
- The complementary use of UV-vis spectroscopy and TOC measurements is required to obtain a comprehensive realistic assessment on the photocatalytic degradation of organics. The UV-vis absorption spectrum is sensitive to the aromatic ring opening, which leads to an overestimation of the degradation activity especially at the onset of reaction.
- Brookite is highly active in the photocatalytic degradation even of highly recalcitrant aromatic compounds like X-ray contrast agents. Brookite has similar activity as that of Anatase. The main active species are the valence band holes and superoxide radicals. The impact of hydroxyl radicals is low.
- Brookite and Anatase exhibit much higher activity than Rutile, which are followed in the order: Titania P25 \geq Anatase > Brookite \gg Rutile. The origin of low activity of Rutile is the different nature of valence band holes which facilitate the formation of hydroxyl radicals and not the direct oxidation of organic pollutants.
- The photocatalytic abatement and mineralization over the synthesized titania polymorphs decrease in tendency with the chemical reactivity of organics: CA > IBP > Ph > DA and IBP > RB \geq RhB > Ph, with the exception of the highly reactive cinnamic acid.
- Contribution of active species: With Brookite and Anatase, the valence band holes are directly involved in the oxidation of organic pollutants. Contrast to general expectation, the $\cdot\text{OH}$ radicals play here a minor role. Whereas $\cdot\text{OH}$ radicals play a major role with Rutile. Superoxide ($\text{O}_2^{\cdot-}$) radicals with all catalysts contribute in the oxidative cleavage of aromatic rings and oxidative degradation.
- Contrary to expectation, the coupling of Anatase/Brookite, Anatase/Rutile, Brookite/Rutile by physical mixing causes a decrease in the photocatalytic activity showing an “opposite synergetic” effect. The commercial photocatalyst titania P25 Degussa (Evonik) shows an enhanced concentration of valence band holes possibly explaining its high activity.

5 Appendix

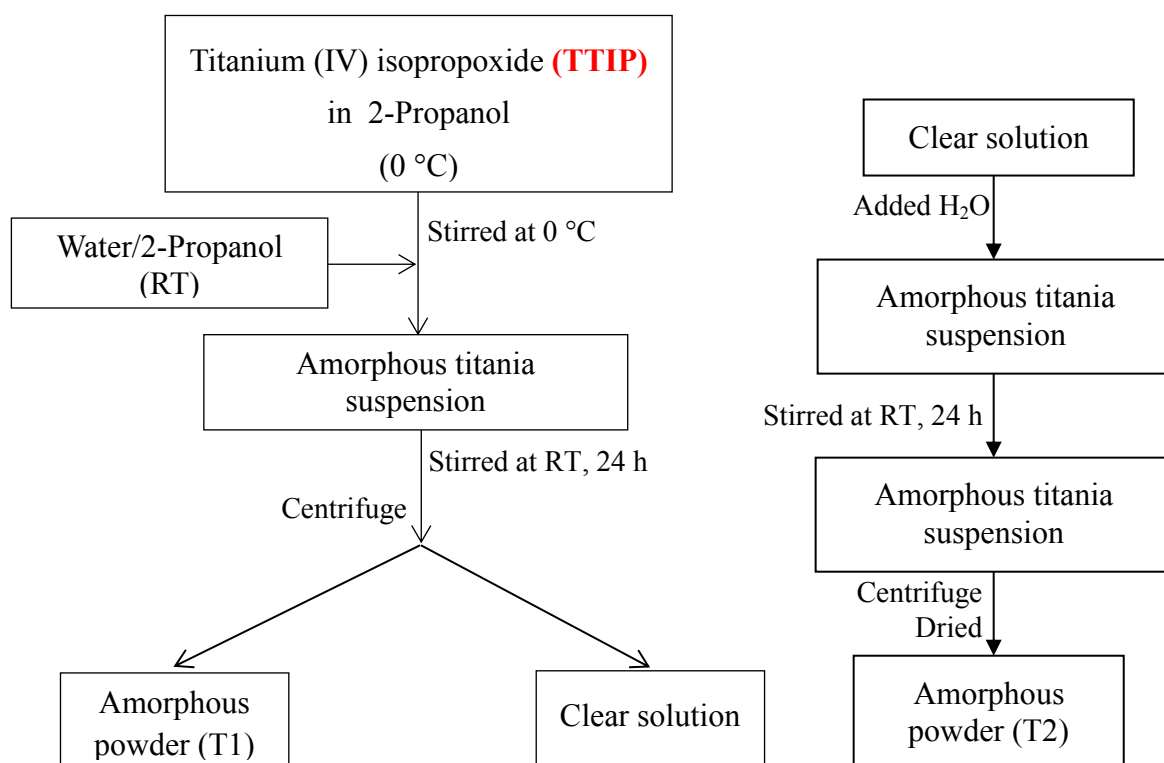
5.1 Material preparation

5.1.1 Amorphous sol-gel preparation

The amorphous titania powders were prepared following the steps reported earlier^[101] by hydrolysis and condensation processes of titanium(IV) *i*-propoxide (TTIP) in isopropanol (*i*-Propanol). The detailed synthetic process was as follows (Scheme 3).

- Firstly, 20 ml of TTIP was injected into 105 ml of isopropanol in an opened 500 ml round-bottom flask to obtain clear colourless solution (solution A). The solution A was cooled down to 0 °C by using an ice bath for 40 min.
- Secondly, a mixture containing 1.14 ml of distilled water and 105 ml of isopropanol (solution B) was slowly added dropwise into the solution A under vigorous stirring at 0 °C. After dropping for 4 h, the clear solution started to change to a white/milky solution (solution C, pH = 5-6). After 5 h for completely dropping step, the ice bath was removed allowing the reaction mixture to warm to room temperature (RT).
- Finally, the obtained solution C was continuously stirred at ambient condition for further 24 h. Hydrolysis of TTIP in small content of water was also accelerated in open air condition. Subsequently, the obtained milky suspension solution was centrifuged (7000 rpm, 5 min) to separate the white precipitate and the clear colourless solution (solution D):
 - + The separated/obtained white precipitate was washed twice with H₂O and finally once with ethanol. The first amorphous titania which is denoted T1, was dried in air over night and further dried in vacuum for a day.
 - + The clear colourless solution (solution D) was again diluted with 1000 ml of water and further stirred at RT for 24 h. Again a milky white suspension solution was immediately obtained when slowly adding water. The second amorphous titania which is denoted T2, was separated by centrifugation (10000 rpm, 10 min). Subsequently, it is washed twice with freshly distilled water and once with aqueous ethanol. Finally, it was dried in air over night and further dried in vacuum for a day.

The yield of amorphous TiO₂ powders can be optimized by changing the amount of TTIP (concentration of TTIP) which causes the increasing or decreasing of hydrolysis rate ([H₂O]/[Ti]) as well as the ratio of [isopropanol]/[Ti] (Table 22). Furthermore, the adding much more water to facilitate hydrolysis and condensation leading to formation of gel or precipitate rapidly. These modifies are not expected in this work. Solution D remaining TTIP was employed for further hydrolysis to form the second amorphous titania by adding of water.



Scheme 3. Steps in the synthetic pathway affording amorphous titania.

Table 22: Yield of the obtained amorphous TiO₂ powders.

T1		T2	
Amount of TTIP (ml)	Product (g)	Amount of water (ml)	Product (g)
5	0.938	10	0.310
10	2.140	100	0.379
20	2.878	200	1.901
		1000	5.039

5.1.2 Hydrothermal treatment

Phase formation of titania nanocrystals was achieved by hydrothermal treatment at high temperatures with acid solution using amorphous titania as a starting material.

- The second white precipitate was further hydrothermally treated. For this procedure, 1.0 g of amorphous titania was given into the 120 ml Teflon cup and then added 41.7 ml of the acid diluted solution to obtain the suspension having concentration of 0.3 M. The mixture was stirred at RT for 30 min to form white suspension.
- The Teflon cup was transferred into a stainless steel-lined autoclave. The autoclave was placed inside an oven operated for 7 h at different temperatures depending on the desired

phase composition, then left to cool down to RT by naturally before handling. The obtained white precipitate was decanted from the reaction solution.

- The precipitate was washed twice with distilled water and centrifuged (10000 rpm, 10 min) to remove the remaining unwanted species and finally washed with absolute ethanol in an attempt to alleviate agglomeration among the particles. The solid was dried at ambient temperature overnight, then further in vacuum for a day.

Titania polymorphs Anatase, Brookite and Rutile have been prepared from the same starting material by changing hydrothermal conditions (kind of acid, concentration of acid, temperature and time for treatment) which summarized in the Table 23.

Table 23: Hydrothermal conditions to form different crystalline titania.

Phase composition	Temperature (°C)	Time (h)	Kind of acid	Concentration (M)
Anatase	200	7	CH ₃ COOH	1.5
Brookite + Rutile	175	7	HCl	3.0
Rutile	200	7	HCl	4.0

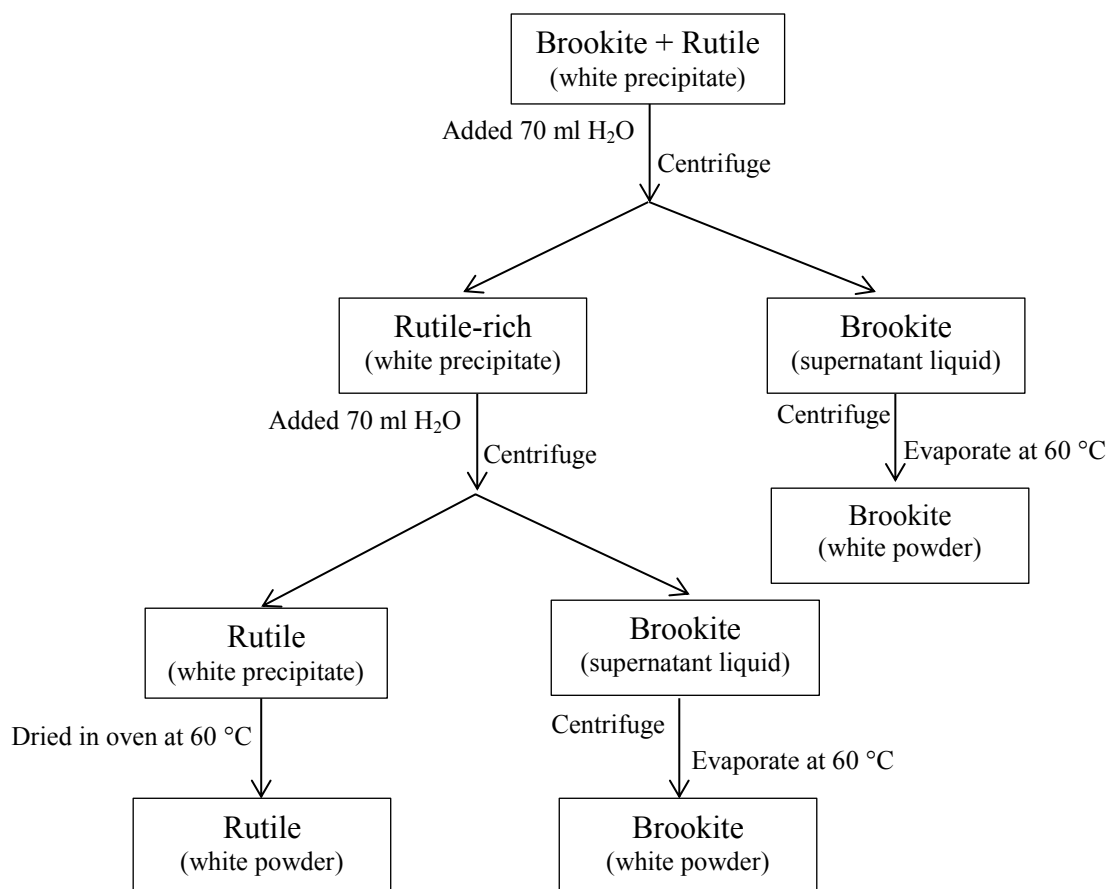
5.1.3 Separation of phase-pure Brookite particles by peptization

By hydrothermal treatment with HCl 3.0 M, the resulting powders consist of a mixture of Brookite and Rutile. Therefore, Brookite was separated from the mixture by two ways.

(1) Peptization with water as shown in Scheme 4.

- The first centrifugation (9000 rpm, 10 min): the product, white precipitate was decanted from the reaction solution to remove the excess HCl solution after hydrothermal treatment.
- The second centrifugation (7000 rpm, 10 min): the product was dispersed well in 70 ml H₂O. After centrifugation, an unclear and white supernatant liquid of Brookite particles formed while the Rutile remained as precipitate. The first supernatant liquid was centrifuged again one more time for surely getting pure Brookite before decantation and storing in 100 ml round-bottom flask.
- The third centrifugation (7000 rpm, 10 min): The white precipitate that obtained after the second centrifugation was dispersed in 70 ml H₂O. After centrifugation, the second supernatant liquid of Brookite particles was formed and the Rutile precipitate remained as precipitate. The supernatant liquid was centrifuged again one more time for surely getting phase-pure Brookite before decantation and storing in 100 ml round-bottom flask.

The Brookite supernatant liquids were dried in vacuum by evaporation process at 60 °C to get final powder. The precipitates of Rutile were completely dried at ambient temperature overnight, then further in oven at 60 °C.



Scheme 4. Separation of Brookite from the mixture by peptization with distilled water.

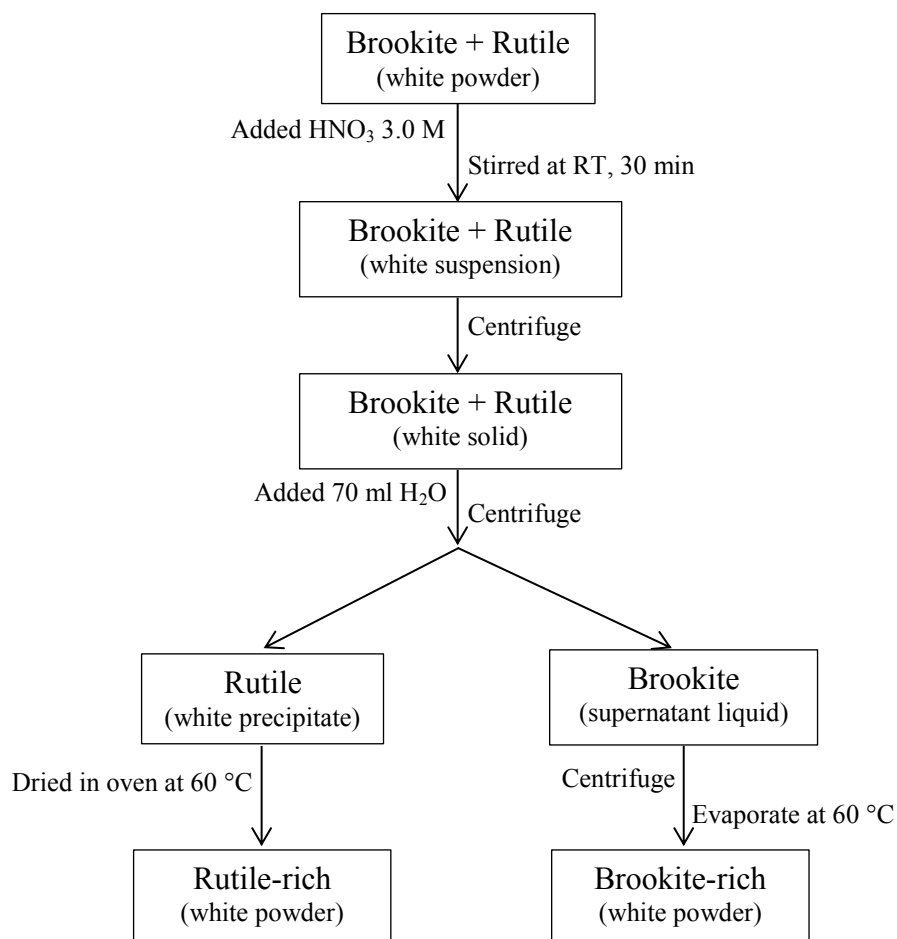
(2) Peptization with HNO₃ was followed by three steps as shown in Scheme 5.

- Firstly, 70 ml of 3.0 M HNO₃ solution was prepared by slowly adding 14.5 ml of pure HNO₃ solution to 17.5 ml of distilled water and adjustment the final volume of solution to 70 ml with distilled water.
- Secondly, 1 g of titania mixture of Brookite and Rutile powder (dried already at RT and in vacuum) was given into 100 ml glass beaker.
- Finally, 70 ml of 3.0 M HNO₃ solution was added, immediately a white suspension was formed. The suspension was magnetically stirred at RT for 30 min.

The suspension was centrifuged (4000 rpm, 5 min) to remove the clear, colourless HNO₃ solution and get the white solid. The recovered solid phase was dispersed in 70 ml of distilled water and centrifuged again (7000 rpm, 10 min). After the last centrifugation, the supernatant liquid contained mostly Brookite particles while the Rutile particles remained in the

precipitate. The Brookite and Rutile powders were collected by the same way as described in peptization with water.

All obtained products were grinded in a porcelain mortar by hand to get a fine white powder which consists of different crystalline phases (Anatase, Brookite or Rutile).



Scheme 5. Separation of Brookite from the mixture by peptization with HNO₃.

5.2 Characterization methods

5.2.1 Photocatalyst powder characterization

X-ray powder diffraction (XRD)

The X-ray diffraction (XRD) investigation was carried out on a STADI-P X-ray diffractometer (STOE) using monochromatic CuK_α radiation ($\lambda = 1.5406 \text{ \AA}$). The crystallite size of particles can be estimated from a XRD line broadening analysis by using the Scherrer equation:

$D = K\lambda / \beta \cos\theta$, where D is the average crystallite size, K is Scherrer constant (0.89 or 0.9), λ is X-ray wavelength, θ is diffraction angle of the studied phase, and β is peak width at half height.

Raman spectroscopy

The Raman spectra of the synthesized photocatalysts were recorded using the LabRAM HR 800 Raman microscope system (Horiba Jobin YVON) equipped with a high stability BX40 microscope (Focus 1 μm). A blue laser (473 nm, 20 mW air-cooled solid-state laser) was used for excitation.

Scanning electron microscope (SEM)

The morphology (size and shape) of the synthesized TiO_2 powders was studied by an S4800 field emission scanning electron microscope (FE-SEM, Hitachi, Japan) at an accelerating voltage of 5 kV.

Diffuse reflectance UV-vis spectroscopy

The UV-vis diffuse reflectance spectra were measured at RT using a Cary 5000 spectrometer (Varian) equipped with a diffuse reflectance accessory (praying mantis, Harrick). The spectra were collected in the range of 200-800 nm using BaSO_4 as reference material and converted into the Kubelka-Munk function $F(R)$ to determine band gap energy.

N_2 adsorption measurement

The N_2 sorption analysis was performed on Thermo Sorptomatic 1990 instrument. Before measurement, the solvent in samples was removed by heating at 130 $^\circ\text{C}$ and pumping under the reduced pressure. Nitrogen adsorption measurements were carried out at 77 K (-196 $^\circ\text{C}$). The specific surface area (SSA) values were calculated by the BET (Brunauer-Emmett-Teller) equation in the interval $0.05 \leq p/p_0 \leq 0.4$. The pore size distributions were calculated by using the BJH (Barrett-Joyner-Halenda) model applied to the desorption branch from p/p_0 0.3 to 0.95.

Differential Scanning Calorimetry (DSC) and Thermogravimetric Analysis (TGA)

Thermal analysis was performed on a Setaram TGA Labsys 1600 DSC under Ar gas at a heating rate of 10 °C/min. The weight losses were evaluated on the derivation of the thermogravimetry (TG) curve. All data were obtained by using the 2000 Setsoft software. Sample (20-40 mg) was put in a 0.1 cm³ alumina (Al₂O₃) crucible.

5.2.2 Analysis of photocatalytic treated solution characterization

UV-vis spectroscopy

UV-vis spectrometer (Lambda 19) was used to measure the absorbance of the photocatalytic treated solutions with irradiation time followed by the disappearance of the maximum absorption band belonging to the aromatic ring and colour band as well. Eight numbers corresponding to the concentrations (0.1, 0.5, 1, 2.5, 5, 7.5, 10, and 20 ppm) of solutions (e.g. Ibuprofen, IBP) were prepared for construction of calibration curve. Aqueous IBP solution was scanned to give absorption band at (λ_{max}) 221.5 nm. The absorbance vs. concentration data was plotted. This curve was used to determine IBP concentration during the photocatalytic experiment runs.

ESI-TOF Mass Spectroscopy

The formation of intermediates (by-products) of the photocatalytic treated solutions was measured by ESI-TOF Mass spectrometers using an electrospray ionization mass spectrometer HPLC System 1200/ESI-TOF-MS 6210 (Agilent). The analysis was carried out in negative and positive electrospray ionization modes. An aqueous solution containing 10 vol.% of methanol (MeOH for HPLC, gradient grade, $\geq 99.8\%$) and 0.1 vol.% formic acid HCOOH was used as mobile phase. The flow rate was 1.0 mL/min. The mass-to-charge range was scanned from m/z 0 to m/z 1000.

Total organic carbon (TOC) analysis

In order to assess the extent of mineralization of organic compounds, the carbon content of the collected aqueous samples was measured by a TOC analyzer instrument (TOC-L CSH/CSN, Shimadzu) by TOC-NPOC method.

5.3 Photocatalytic activity test

In each experiment, 250 ml of aqueous solution containing organic compound (e.g. ibuprofen IBP 10 ppm) and photocatalyst (TiO₂ 10 mg) is magnetically stirred in dark during 30 min to reach adsorption-desorption equilibrium before the photocatalytic reaction starts, and then continuously stirred at RT under UV-vis irradiation. The reaction pH is natural. The four UV-vis solarium lamps (15 W, Philips) with a total power of 60 W are used as light source. These lamps simulate the UV-vis part of sunlight (also by intensity) and emit a continuous spectrum ranging from *ca.* 370-400 nm. The distance between the applied lamps and the surface of organic solution is 15 cm. Four reactors corresponding to four photocatalytic experiments are placed into a closer aluminium box which is arranged above four corresponding magnetic stirrers. After a certain time, 5 ml of aliquot is taken by a syringe and separates from the catalyst by a filter membrane (0.45 µm PTFE filter). The remaining IBP content in the photocatalytic treated solutions is determined by the change of the intensity of IBP absorption band located at 221.5 nm. The abatement efficiency of IBP after various intervals of UV-vis irradiation time is calculated using the following equation:^[177,178]

$$\text{Abatement (\%)} = (A_0 - A_t) / A_0 \times 100,$$

where A_0 and A_t are the initial absorbance and the absorbance after various intervals of UV-vis irradiation time (t), respectively. All data were obtained at RT.

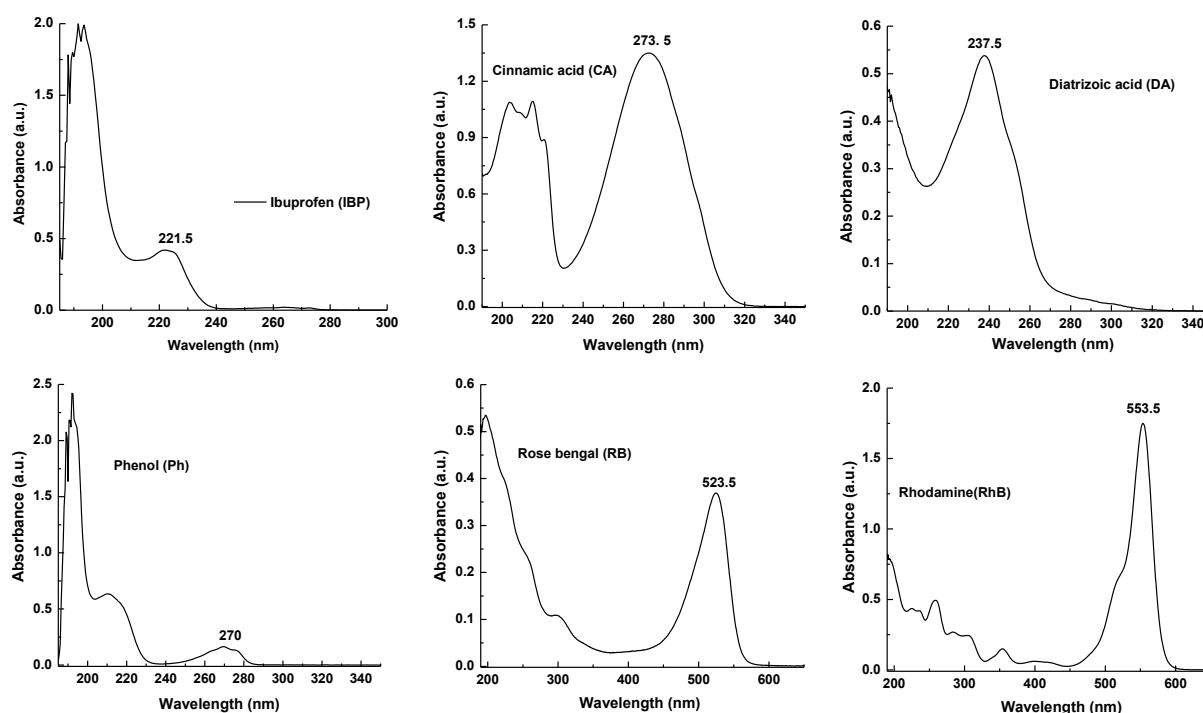


Figure 58. The absorbance spectra of the investigated organic solutions (conc.: 10 ppm).

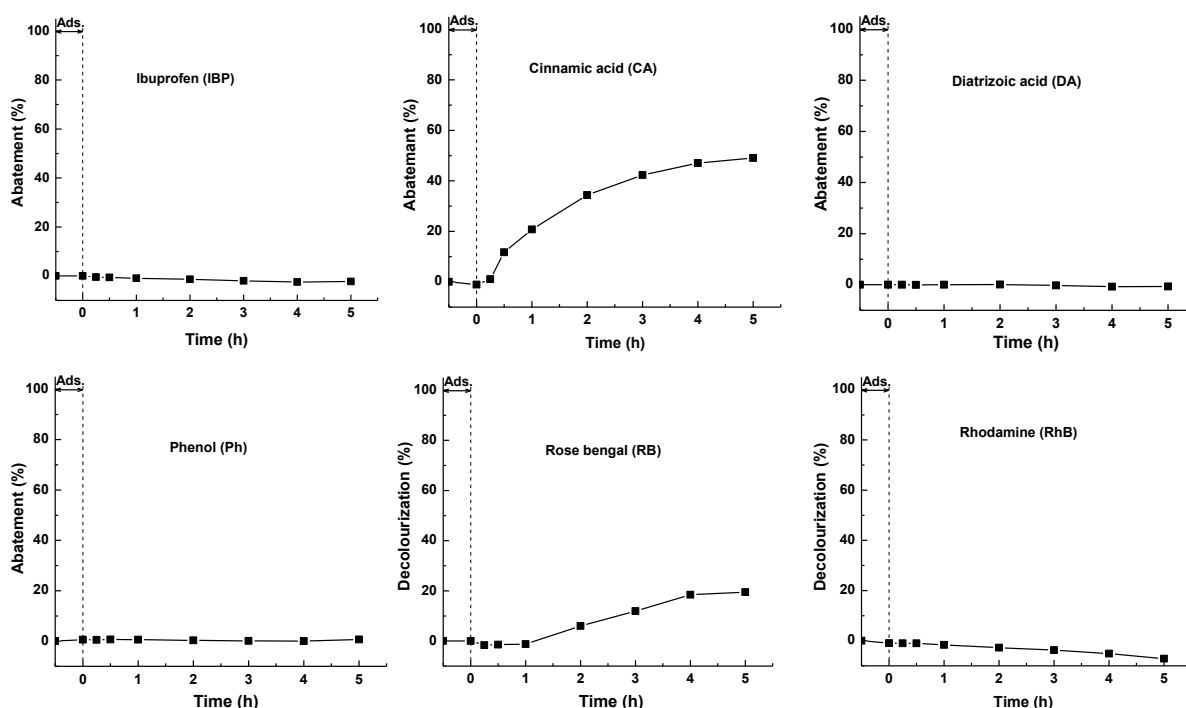


Figure 59. The UV-vis photolysis of IBP, CA, DA, Ph obtained by the abatement of aromatic ring and of RB, RhB obtained by the degradation of colour band.

In the present work, the organic compounds such as ibuprofen (IBP), cinnamic acid (CA), diatrizoic acid (DA), phenol (Ph) and dyes (RB_rose bengal and RhB_rhodamine B) were used to investigate the photocatalytic activities of the synthesized TiO_2 polymorphs. The absorption spectra of solutions (10 ppm) at the corresponding maximum wavelengths as well as the respective photolysis curves are shown in Figure 58 and 59, respectively.

A comparison with the activity of single-phase titania, the photocatalytic performance of mixtures obtained by physical mixing has been carried out. The mixtures with ratio of 80:20 were prepared by sonication the suspension containing certain catalyst powders (Table 24) and 0.5 ml H_2O for 10 min, then were dried in oven at 60°C , overnight.

Table 24: The mixed-phase titania samples obtained by physical mixing.

Sample	TiO ₂ content					
	Anatase		Brookite		Rutile	
A80B20	80%	100.21 mg	20%	25.17 mg		
A80R20	80%	100.53 mg			20%	25.58 mg
B80R20			80%	100.32 mg	20%	25.35 mg

The nature and role of active species formed in titania polymorphs Anatase, Brookite, and Rutile during the photocatalytic treatment were studied by a series of trapping experiments in which added different scavengers such as holes (h^+), hydroxyl radicals ($\cdot\text{OH}$), and superoxide

radicals ($O_2^{\bullet-}$). In the present work, EDTA (ethylenediaminetetraacetic acid) acts as a hole (h^+) scavenger, *t*-BuOH acts as a $\bullet OH$ radical scavenger and 1,4-BQ (1,4-Benzoquinone) acts as a $O_2^{\bullet-}$ radical scavenger. Namely, 1.46 mg of EDTA, 0.1 ml of *t*-BuOH, or 2.704 mg of 1,4-BQ, respectively were added into 250 ml of organic aqueous solution (10 ppm) containing catalyst (10 mg). Figure 60 presents the molecular structure of different scavengers.

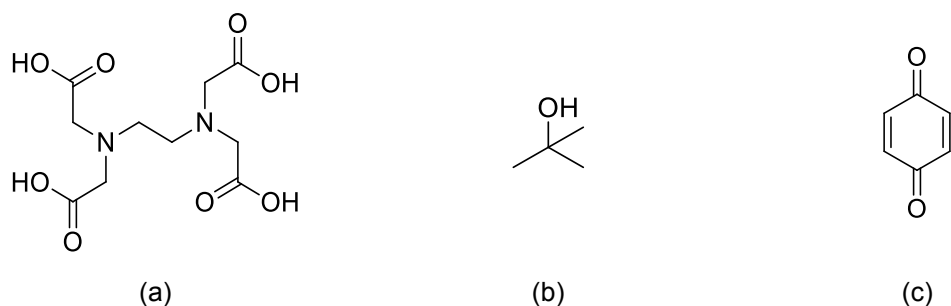


Figure 60. Molecular structure of (a) EDTA, (b) *t*-BuOH, and (c) 1,4-BQ.

5.4 List of chemicals used

Substance	Origin
Cinnamic acid ($C_9H_8O_2$)	Reachim, 99%
Diatrizoic acid ($C_{11}H_9I_3N_2O_4$)	Sigma-Aldrich, 98%
Ethylenediaminetetraacetic acid ($C_{10}H_{16}N_2O_8$)	Sigma-Aldrich, 99%
Glacial acetic acid (CH_3COOH)	Chemsolute, 99.7%
Hydrochloric acid (HCl)	Chemsolute, 35-38%
Ibuprofen sodium salt ($C_{13}H_{17}O_2Na$)	Sigma-Aldrich, 98%
Isopropanol (C_3H_8O)	
Nitric acid (HNO_3)	Chemsolute, 65%
RhodamineB ($C_{28}H_{31}ClN_2O_3$)	Polskie Odczynniki chemiczne gliwice
Rose bengal-natrium ($C_{20}H_2C_{14}I_4Na_2O_5$)	
tert-Butanol ($C_4H_{10}O$)	Sigma-Aldrich, 99%
Titanium dioxide P25 (TiO_2)	Evonik/Degussa, 99.5%
Titanium(IV) <i>i</i> -propoxide ($C_{12}H_{28}O_4Ti$)	Merck, 98%

6 References

- [1] C. Gadipelly, A. Pérez-González, G. D. Yadav, I. Ortiz, R. Ibáñez, V. K. Rathod, K. V. Marathe, *Ind. Eng. Chem. Res.* **2014**, *53*, 11571–11592.
- [2] H. Zangeneh, A. Zinatizadeh, M. Habibi, M. Akia, M. Hasnain Isa, *J. Ind. Eng. Chem.* **2015**, *26*, 1–36.
- [3] F. Akbal, *Environ. Prog.* **2005**, *24*, 317–322.
- [4] C. M. Teh, A. R. Mohamed, *J. Alloy. Compd.* **2011**, *509*, 1648–1660.
- [5] W. Peysson, E. Vulliet, *J. Chromatogr. A* **2013**, *1290*, 46–61.
- [6] M. Carballa, F. Omil, J. M. Lema, M. Llompарт, C. García-Jares, I. Rodríguez, M. Gómez, T. Ternes, *Water research* **2004**, *38*, 2918–2926.
- [7] F. S. Braz, M. R. A. Silva, F. S. Silva, S. J. Andrade, A. L. Fonseca, M. M. Kondo, *JEP* **2014**, *05*, 620–626.
- [8] J. Choina, C. Fischer, G.-U. Flechsig, H. Kosslick, V. A. Tuan, N. D. Tuyen, N. A. Tuyen, A. Schulz, *J. Photochem. Photobiol. A: Chem.* **2014**, *274*, 108–116.
- [9] J. Choina, H. Kosslick, C. Fischer, G.-U. Flechsig, L. Frunza, A. Schulz, *Appl. Catal. B: Environ.* **2013**, *129*, 589–598.
- [10] I. Georgaki, E. Vasilaki, N. Katsarakis, *AJAC* **2014**, *05*, 518–534.
- [11] Da Silva, J.C.C., Teodoro, J.A.R., Afonso, R.J.C.F., Aquino, S.F., Augusti, R., *J. Mass Spectrom.* **2014**, *49*, 145–153.
- [12] F. H. Li, K. Yao, W. Y. Lv, G. G. Liu, P. Chen, H. P. Huang, Y. P. Kang, *Bull. Environ. Contam. Tox.* **2015**, *94*, 479–483.
- [13] J. Madhavan, F. Grieser, M. Ashokkumar, *J. Hazard. Mater.* **2010**, *178*, 202–208.
- [14] M. Lezere, *IARC Monographs* **2010**, *99*.
- [15] R. J. Tayade, P. K. Surolia, R. G. Kulkarni, R. V. Jasra, *Sci. Technol. Adv. Mater.* **2007**, *8*, 455–462.
- [16] M. Choquette-Labbé, W. Shewa, J. Lalman, S. Shanmugam, *Water* **2014**, *6*, 1785–1806.
- [17] M. G. Alalm, A. Tawfik, *Int. J. Chem. Mol. Nucl. Mater. Metall. Eng.* **2014**, *8*, 144–147.
- [18] N. A. Laoufi, D. Tassalit, F. Bentahar, *Global NEST J.* **2008**, *10*, 404–418.
- [19] M. Lazar, S. Varghese, S. Nair, *Catalysts* **2012**, *2*, 572–601.
- [20] R. A. Kraemer, K. Choudhury, E. Kampa, *Protecting Water Resources: Pollution Prevention - Thematic Background Paper for the International Conference on Freshwater - Bonn, 3-7 December 2001. Ecologic, Institute for International and European Environmental Policy, Berlin.*

- [21] Z. Guo, R. Ma, G. Li, *Chem. Eng. J.* **2006**, *119*, 55–59.
- [22] E. Grabowska, J. Reszczyńska, A. Zaleska, *Water Res.* **2012**, *46*, 5453–5471.
- [23] F. S. Murakami, L. S. Bernardi, R. N. Pereira, B. R. Valente, *Pharma. Chem. J.* **2009**, *43*, 716–720.
- [24] E. Ugazio, M. E. Carlotti, S. Sapino, M. Trotta, D. Vione, C. Minero, *J. Dispers. Sci. Technol.* **2008**, *29*, 641–652.
- [25] T. Rastogi, C. Leder, K. Kümmerer, *Sci. Total Environ.* **2014**, *482-483*, 378–388.
- [26] A. Haiss, K. Kümmerer, *Chemosphere* **2006**, *62*, 294–302.
- [27] K. Fucke, J. A. K. Howard, J. W. Steed, *Chem. Commun.* **2012**, *48*, 12065–12067.
- [28] J. Jeong, J. Jung, W. J. Cooper, W. Song, *Water research* **2010**, *44*, 4391–4398.
- [29] C. Hessel, C. Allegre, M. Maisseu, F. Charbit, P. Moulin, *J. Environ. Manage.* **2007**, *83*, 171–180.
- [30] M. Cotto-Maldonado, *ACSJ* **2013**, *3*, 178–202.
- [31] N. Barka, S. Qourzal, A. Assabbane, A. Nounah, Y. Ait-Ichou, *J. Photochem. Photobiol. A: Chem.* **2008**, *195*, 346–351.
- [32] J. Kaur, S. Singhal, *Physica B: Condensed Matter* **2014**, *450*, 49–53.
- [33] Y. Wang, M. F. Ibad, H. Kosslick, J. Harloff, T. Beweries, J. Radnik, A. Schulz, S. Tschierlei, S. Lochbrunner, X. Guo, *Micropor. Mesopor. Mater.* **2015**, *211*, 182–191.
- [34] A. R. Ribeiro, O. C. Nunes, M. F. R. Pereira, A. M. T. Silva, *Environ. Int.* **2015**, *75*, 33–51.
- [35] T. S. Natarajan, M. Thomas, K. Natarajan, H. C. Bajaj, R. J. Tayade, *Chem. Eng. J.* **2011**, *169*, 126–134.
- [36] C. Wang, H. Liu, Y. Qu, *J. Nanomater.* **2013**, *2013*, 1–14.
- [37] J. O. Tijani, O. O. Fatoba, G. Madzivire, L. F. Petrik, *Water Air Soil Pollut.* **2014**, *225*, 2102.
- [38] V. Augugliaro, M. Litter, L. Palmisano, J. Soria, *J. Photochem. Photobiol. C: Photochem. Rev.* **2006**, *7*, 127–144.
- [39] A. S. Stasinakis, *Global NEST J.* **2008**, *10*, 376–385.
- [40] R. Andreozzi, *Catal. Today* **1999**, *53*, 51–59.
- [41] J. Herrmann, *Catal. Today* **1999**, *53*, 115–129.
- [42] M. Litter, *Appl. Catal. B: Environ.* **1999**, *23*, 89–114.
- [43] P. Pichat in *Photocatalysis and Water Purification: From Fundamentals to Recent Applications, Vol. 1* (Eds.: Y. Nosaka, A. Y. Nosaka), Wiley-VCH, Weinheim, 2013, pp. 3-23.

- [44] M. R. Hoffmann, S. T. Martin, W. Choi, D. W. Bahnemann, *Chem. Rev.* **1995**, *95*, 69–96.
- [45] T. Hirakawa, K. Yawata, Y. Nosaka, *Appl. Catal. A: Gen.* **2007**, *325*, 105–111.
- [46] H. Xu, S. Ouyang, L. Liu, P. Reunchan, N. Umezawa, J. Ye, *J. Mater. Chem. A* **2014**, *2*, 12642–12661.
- [47] S. Bai, J. Jiang, Q. Zhang, Y. Xiong, *Chem. Soc. Rev.* **2015**, *44*, 2893–2939.
- [48] J. Pan, G. Liu, G. Q. M. Lu, H.-M. Cheng, *Angew. Chem.* **2011**, *50*, 2133–2137.
- [49] W. Wu, C. Jiang, V. A. L. Roy, *Nanoscale* **2015**, *7*, 38–58.
- [50] C. A. Martínez-Huitle, L. S. Andrade, *Quim. Nova* **2011**, *34*, 850–858.
- [51] A. Ibhaddon, P. Fitzpatrick, *Catalysts* **2013**, *3*, 189–218.
- [52] M. Muruganandham, R. P. S. Suri, S. Jafari, M. Sillanpää, G.-J. Lee, J. J. Wu, M. Swaminathan, *Int. J. Photoenergy* **2014**, *2014*, 1–21.
- [53] W. Ashcroft, N. D. Mermin **1976**.
- [54] C. Kittel, *Copyright John Wiley & Sons, Inc.* **2005**.
- [55] W. S. Tung, W. A. Daoud, *J. Mater. Chem.* **2011**, *21*, 7858–7869.
- [56] W. H. Strehlow, E. L. Cook, *J. Phys. Chem. Ref. Data* **1973**, *2*, 163–199.
- [57] D. Friedmann, C. Mendive, D. Bahnemann, *Appl. Catal. B: Environ.* **2010**, *99*, 398–406.
- [58] J. Schneider, M. Matsuoka, M. Takeuchi, J. Zhang, Y. Horiuchi, M. Anpo, D. W. Bahnemann, *Chem. Rev.* **2014**, *114*, 9919–9986.
- [59] H. H. Mohamed, D. W. Bahnemann, *Appl. Catal. B: Environ.* **2012**, *128*, 91–104.
- [60] L. Zhang, H. H. Mohamed, R. Dillert, D. Bahnemann, *J. Photochem. Photobiol. C: Photochem. Rev.* **2012**, *13*, 263–276.
- [61] Y. Tamaki, A. Furube, M. Murai, K. Hara, R. Katoh, M. Tachiya, *Phys. Chem. Chem. Phys.* **2007**, *9*, 1453–1460.
- [62] A. Fujishima, X. Zhang, D. A. Tryk, *Surf. Sci. Rep.* **2008**, *63*, 515–582.
- [63] D. Zhang, R. Qiu, L. Song, B. Eric, Y. Mo, X. Huang, *J. Hazard. Mater.* **2009**, *163*, 843–847.
- [64] Z. Zhang, C. Wang, R. Zakaria, J. Y. Ying, *J. Phys. Chem. B* **1998**, *102*, 10871–10878.
- [65] G. M. R. Vinu, *J. Indian Inst. Sci.* **2010**, *90*, 189–230.
- [66] M. Murai, Y. Tamaki, A. Furube, K. Hara, R. Katoh, *Catal. Today* **2007**, *120*, 214–219.
- [67] B. Ohtani, *Catalysts* **2013**, *3*, 942–953.
- [68] S. Banerjee, D. D. Dionysiou, S. C. Pillai, *Appl. Catal. B: Environ.* **2015**, *176–177*, 396–428.

- [69] M. A. Henderson, *Surf. Sci. Rep.* **2011**, *66*, 185–297.
- [70] J. C. Colmenares, R. Luque, *Chem. Soc. Rev.* **2014**, *43*, 765–778.
- [71] A. N. Ökte, M. S. Resat, Y. Inel, *Tox. Environ. Chem.* **2001**, *79*, 171–178.
- [72] M. Buchalska, M. Kobielski, A. Matuszek, M. Pacia, S. Wojtyła, W. Macyk, *ACS Catal.* **2015**, *5*, 7424–7431.
- [73] J. Mo, Y. Zhang, Q. Xu, J. J. Lamson, R. Zhao, *Atmos. Environ.* **2009**, *43*, 2229–2246.
- [74] C. Minero, G. Mariella, V. Maurino, D. Vione, E. Pelizzetti, *Langmuir* **2000**, *16*, 8964–8972.
- [75] T. Tachikawa, M. Fujitsuka, T. Majima, *J. Phys. Chem. C* **2007**, *111*, 5259–5275.
- [76] R. Nakamura, Y. Nakato, *J. Am. Chem. Soc.* **2004**, *126*, 1290–1298.
- [77] R. Nakamura, T. Okamura, N. Ohashi, A. Imanishi, Y. Nakato, *J. Am. Chem. Soc.* **2005**, *127*, 12975–12983.
- [78] T. Tan, D. Beydoun, R. Amal, *J. Photochem. Photobiol. A: Chem.* **2003**, *159*, 273–280.
- [79] H. Wang, X. Yuan, Y. Wu, G. Zeng, X. Chen, L. Leng, Z. Wu, L. Jiang, H. Li, *J. Hazard. Mater.* **2015**, *286*, 187–194.
- [80] R. R. Marques, M. J. Sampaio, P. M. Carrapiço, C. G. Silva, S. Morales-Torres, G. Dražić, J. L. Faria, A. M. Silva, *Catal. Today* **2013**, *209*, 108–115.
- [81] N. Serpone, I. Texier, A. V. Emeline, P. Pichat, H. Hidaka, J. Zhao, *J. Photochem. Photobiol. A: Chem.* **2000**, *136*, 145–155.
- [82] M. Ibadurrohman, K. Hellgardt, *Int. J. Hydrogen Energy* **2014**, *39*, 18204–18215.
- [83] J. Qi, K. Zhao, G. Li, Y. Gao, H. Zhao, R. Yu, Z. Tang, *Nanoscale* **2014**, *6*, 4072–4077.
- [84] Y. Wang, R. Shi, J. Lin, Y. Zhu, *Appl. Catal. B: Environ.* **2010**, *100*, 179–183.
- [85] J. Liu, R. Liu, H. Li, W. Kong, H. Huang, Y. Liu, Z. Kang, *Dalton Trans.* **2014**, *43*, 12982–12988.
- [86] M.-Q. Yang, Y. Zhang, N. Zhang, Z.-R. Tang, Y.-J. Xu, *Sci. Rep.* **2013**, *3*, 3314.
- [87] J. Zhang, Y. Nosaka, *J. Phys. Chem. C* **2014**, *118*, 10824–10832.
- [88] Z. Wang, W. Ma, C. Chen, H. Ji, J. Zhao, *Chem. Eng. J.* **2011**, *170*, 353–362.
- [89] M. Marković, M. Jović, D. Stanković, V. Kovačević, G. Roglić, G. Gojgić-Cvijović, D. Manojlović, *Sci. Total Environ.* **2015**, *505*, 1148–1155.
- [90] L. G. Devi, K. E. Rajashekar, *J. Mol. Catal. A: Chem.* **2011**, *334*, 65–76.
- [91] E. Grabowska, J. Reszczyńska, A. Zaleska, *Water Res.* **2012**, *46*, 5453–5471.
- [92] X. Pang, C. Chen, H. Ji, Y. Che, W. Ma, J. Zhao, *Molecules* **2014**, *19*, 16291–16311.
- [93] S. Leong, A. Razmjou, K. Wang, K. Hapgood, X. Zhang, H. Wang, *J. Membr. Sci.* **2014**, *472*, 167–184.

- [94] V. Augugliaro, M. Bellardita, V. Loddo, G. Palmisano, L. Palmisano, S. Yurdakal, *J. Photochem. Photobiol. C: Photochem. Rev.* **2012**, *13*, 224–245.
- [95] T. K. Tseng, Y. S. Lin, Y. J. Chen, H. Chu, *Int. J. Mol. Sci.* **2010**, *11*, 2336–2361.
- [96] K. Hashimoto, H. Irie, A. Fujishima, *Jpn. J. Appl. Phys.* **2005**, *44*, 8269–8285.
- [97] A. Fujishima, K. Honda, *Nature* **1972**, *238*, 37–38.
- [98] A. Di Paola, M. Bellardita, L. Palmisano, *Catalysts* **2013**, *3*, 36–73.
- [99] M. Mohamad, B. U. Haq, R. Ahmed, A. Shaari, N. Ali, R. Hussain, *Mater. Sci. Semicon. Proc.* **2015**, *31*, 405–414.
- [100] D. A. H. Hanaor, C. C. Sorrell, *J. Mater. Sci.* **2011**, *46*, 855–874.
- [101] D. Reyes-Coronado, G. Rodríguez-Gattorno, M. E. Espinosa-Pesqueira, C. Cab, R. de Coss, G. Oskam, *Nanotechnology* **2008**, *19*, 145605–145615.
- [102] Y. Ma, X. Wang, Y. Jia, X. Chen, H. Han, C. Li, *Chem. Rev.* **2014**, *114*, 9987–10043.
- [103] V. N. Koparde, P. T. Cummings, *ACS nano* **2008**, *2*, 1620–1624.
- [104] W.-K. Jo, T. S. Natarajan, *Chem. Eng. J.* **2015**, *281*, 549–565.
- [105] T. Ohno, T. Higo, H. Saito, S. Yuajn, Z. Jin, Y. Yang, T. Tsubota, *J. Mol. Catal. A: Chem.* **2015**, *396*, 261–267.
- [106] R. Kaplan, B. Erjavec, A. Pintar, *Appl. Catal. A: Gen.* **2015**, *489*, 51–60.
- [107] H. Zhang, J. F. Banfield, *Chem. Rev.* **2014**, *114*, 9613–9644.
- [108] J. Zhang, P. Zhou, J. Liu, J. Yu, *Phys. Chem. Chem. Phys.* **2014**, *16*, 20382–20386.
- [109] D. Beydoun, R. Amal, G. Low, S. McEvoy, *J. Nanopart. Res.* **1999**, *1*, 439–458.
- [110] Y. Kakuma, A. Y. Nosaka, Y. Nosaka, *Phys. Chem. Chem. Phys.* **2015**, *17*, 18691–18698.
- [111] W. Li, T. Zeng, *PloS one*, **2011**, *6*, e21082.
- [112] P. Bouras, E. Stathatos, P. Lianos, *Appl. Catal. B: Environ.* **2007**, *73*, 51–59.
- [113] T. Ohno, K. Sarukawa, K. Tokieda, M. Matsumura, *J. Catal.* **2001**, *203*, 82–86.
- [114] B. K. Mutuma, G. N. Shao, W. D. Kim, H. T. Kim, *J. Colloid Interface Sci.* **2015**, *442*, 1–7.
- [115] V. Etacheri, C. Di Valentin, J. Schneider, D. Bahnemann, S. C. Pillai, *J. Photochem. Photobiol. C: Photochem. Rev.* **2015**, *25*, 1–29.
- [116] Y. Liao, W. Que, Q. Jia, Y. He, J. Zhang, P. Zhong, *J. Mater. Chem.* **2012**, *22*, 7937.
- [117] M. Landmann, E. Rauls, W. G. Schmidt, *J. Phys.: Condens. Matter* **2012**, *24*, 195503.
- [118] A. Beltrán, L. Gracia, J. Andrés, *J. Phys. Chem. B* **2006**, *110*, 23417–23423.

- [119] T. Luttrell, S. Halpegamage, J. Tao, A. Kramer, E. Sutter, M. Batzill, *Sci. Rep.* **2014**, *4*, 4043-4051.
- [120] J. Zhang, P. Zhou, J. Liu, J. Yu, *Phys. Chem. Chem. Phys.* **2014**, *16*, 20382–20386.
- [121] M. Xu, Y. Gao, E. M. Moreno, M. Kunst, M. Muhler, Y. Wang, H. Idriss, C. Wöll, *PRL* **2011**, *106*, 138302-138306.
- [122] A. Li, *ASP Conference Series* **2003**, *000*, 1–36.
- [123] W. Hu, L. Li, G. Li, C. Tang, L. Sun, *Cryst. Growth Des.* **2009**, *9*, 3676–3682.
- [124] Y. Wang, L. Li, X. Huang, Q. Li, G. Li, *RSC Adv.* **2015**, *5*, 34302–34313.
- [125] L. Andronic, D. Perniu, A. Duta, *J. Sol-Gel Sci. Technol.* **2013**, *66*, 472–480.
- [126] M. E. Simonsen, E. G. Søgaaard, *J. Sol-Gel Sci. Technol.* **2010**, *53*, 485–497.
- [127] C. S. Lim, J. H. Ryu, D. H. Kim, S. Y. Cho, W. C. Oh, *J. Ceram. Proc. Res.* **2010**, *11*, 736–741.
- [128] M. Altomare, M. V. Dozzi, G. L. Chiarello, A. Di Paola, L. Palmisano, E. Selli, *Catal. Today* **2015**, *252*, 184–189.
- [129] H. Cheng, J. Ma, Z. Zhao, L. Qi, *Chem. Mater.* **1995**, *7*, 663–671.
- [130] M. J. López-Muñoz, A. Revilla, G. Alcalde, *Catal. Today* **2015**, *240*, 138–145.
- [131] S. Cassaignon, M. Koelsch, J.-P. Jolivet, *J. Mater. Sci.* **2007**, *42*, 6689–6695.
- [132] A. V. Vinogradov, V. V. Vinogradov, P. Gouma, *J. Am. Ceram. Soc.* **2014**, *97*, 290–294.
- [133] S. Mahshid, M. Askari, M. S. Ghamsari, *J. Mater. Process. Tech.* **2007**, *189*, 296–300.
- [134] Y. Wang, Y. He, Q. Lai, M. Fan, *J. Environ. Sci. China* **2014**, *26*, 2139–2177.
- [135] J.-G. Li, T. Ishigaki, X. Sun, *J. Phys. Chem. C* **2007**, *111*, 4969–4976.
- [136] J. Yang, S. Mei, J. M. F. Ferreira, *J. Am. Ceram. Soc.* **2001**, *84*, 1696–1702.
- [137] K. Chen, L. Zhu, K. Yang, *J. Environ. Sci. China* **2015**, *27*, 232–240.
- [138] W. W. So, S. B. Park, K. J. Kim, C. H. Shin, S. J. Moon, *J. Mater. Sci.* **2001**, *36*, 4299–4305.
- [139] J. Sun, L. Gao, Q. Zhang, *J. Am. Ceram. Soc.* **2003**, *86*, 1677–1682.
- [140] Y. Zou, X. Tan, T. Yu, Y. Li, Q. Shang, W. Wang, *Mater. Lett.* **2014**, *132*, 182–185.
- [141] N. Tomić, M. Grujić-Brojčin, N. Finčur, B. Abramović, B. Simović, J. Krstić, B. Matović, M. Šćepanović, *Mater. Chem. Phys.* **2015**, *163*, 518–528.
- [142] A. Di Paola, G. Cufalo, M. Addamo, M. Bellardita, R. Campostrini, M. Ischia, R. Ceccato, L. Palmisano, *Colloids. Surf. A Physicochem. Eng. Asp.* **2008**, *317*, 366–376.
- [143] H. Lin, L. Li, M. Zhao, X. Huang, X. Chen, G. Li, R. Yu, *J. Am. Chem. Soc.* **2012**, *134*, 8328–8331.
- [144] V. Štengl, D. Králová, *Mater. Chem. Phys.* **2011**, *129*, 794–801.

- [145] M. Inada, K. Iwamoto, N. Enomoto, J. Hojo, *J. Ceram. Soc. Japan* **2011**, *119*, 451–455.
- [146] J. Zhang, S. Yan, L. Fu, F. Wang, M. Yuan, G. Luo, Q. Xu, X. Wang, C. Li, *Chinese J. Catal.* **2011**, *32*, 983–991.
- [147] X. Shen, B. Tian, J. Zhang, *Catal. Today* **2013**, *201*, 151–158.
- [148] P. E. Hockberger, *Photochem. Photobiol.* **2002**, *76*, 561–579.
- [149] J. Xie, X. Lü, J. Liu, H. Shu, *Pure Appl. Chem.* **2009**, *81*.
- [150] T.-D. Nguyen-Phan, E. J. Kim, S. H. Hahn, W.-J. Kim, E. W. Shin, *J. Colloid Interface Sci.* **2011**, *356*, 138–144.
- [151] B. Zhao, F. Chen, Y. Jiao, J. Zhang, *J. Mater. Chem.* **2010**, *20*, 7990.
- [152] H. Zhang, J. F. Banfield, *J. Phys. Chem. B* **2000**, *104*, 3481–3487.
- [153] M.-H. Yang, P.-C. Chen, M.-C. Tsai, T.-T. Chen, I.-C. Chang, H.-T. Chiu, C.-Y. Lee, *CrystEngComm* **2014**, *16*, 441–447.
- [154] G. A. Tompsett, G. A. Bowmaker, R. P. Cooney, J. B. Metson, K. A. Rodgers, J. M. Seakins, *J. Raman Spectrosc.* **1995**, *26*, 57–62.
- [155] Y. Hu, H.-L. Tsai, C.-L. Huang, *J. Eur. Ceram. Soc.* **2003**, *23*, 691–696.
- [156] M. Zhao, H. Xu, H. Chen, S. Ouyang, N. Umezawa, D. Wang, J. Ye, *J. Mater. Chem. A* **2015**, *3*, 2331–2337.
- [157] Z. Li, S. Cong, Y. Xu, *ACS Catal.* **2014**, *4*, 3273–3280.
- [158] F. Tian, Y. Zhang, J. Zhang, C. Pan, *J. Phys. Chem. C* **2012**, *116*, 7515–7519.
- [159] W. F. Zhang, Y. L. He, M. S. Zhang, Z. Yin, Q. Chen, *J. Phys. D: Appl. Phys.* **2000**, *33*, 912–916.
- [160] S. Kohtani, E. Yoshioka, H. Miyabe in *InTech*.
- [161] M. Koelsch, S. Cassaignon, J. Guillemoles, J. Jolivet, *Thin Solid Films* **2002**, *403-404*, 312–319.
- [162] N. Boonprakob, J. Tapad, P. Jansanthea, B. Inceesungvorn, *International Conference on Chemical, Metallurgy and Material Science Engineering (CMMSE-2015) August 10-11, 2015 Pattaya, Thailand*.
- [163] K. J. A. Raj, B. Viswanathan, *Indian J. Chem.* **2009**, *48A*, 1378–1382.
- [164] L. Jiqiao, H. Baiyun, *Int. J. Refract. Metals Hard Mater.* **2001**, *19*, 89–99.
- [165] J. Choina, A. Bagabas, C. Fischer, G.-U. Flechsig, H. Kosslick, A. Alshammari, A. Schulz, *Catal. Today* **2015**, *241*, 47–54.
- [166] T. Tachikawa, T. Majima, *Chem. Soc. Rev.* **2010**, *39*, 4802–4819.
- [167] J. C. Colmenares, R. Luque, *Chem. Soc. Rev.* **2014**, *43*, 765–778.
- [168] S. K. Wallace, K. P. McKenna, *J. Phys. Chem. C* **2015**, *119*, 1913–1920.

- [169] T. Ohno, K. Sarukawa, M. Matsumura, *New J. Chem.* **2002**, 26, 1167–1170.
- [170] P. M. Kowalski, M. F. Camellone, N. N. Nair, B. Meyer, D. Marx, *PRL* **2010**, 105, 146405-146415.
- [171] R. Kaplan, B. Erjavec, G. Dražić, J. Grdadolnik, A. Pintar, *Appl. Catal. B: Environ.* **2016**, 181, 465–474.
- [172] D. Wang, P. Kanhere, M. Li, Q. Tay, Y. Tang, Y. Huang, T. C. Sum, N. Mathews, T. Sritharan, Z. Chen, *J. Phys. Chem. C* **2013**, 117, 22894–22902.
- [173] B. Ohtani, O. O. Prieto-Mahaney, D. Li, R. Abe, *J. Photochem. Photobiol. A: Chem.* **2010**, 216, 179–182.
- [174] G. Li, K. A. Gray, *Chem. Phys.* **2007**, 339, 173–187.
- [175] R. Quesada-Cabrera, C. Sotelo-Vazquez, J. C. Bear, J. A. Darr, I. P. Parkin, *Adv. Mater. Interfaces* **2014**, 1, 1400069-1400076.
- [176] D. O. Scanlon, W. C. Dunnill, J. Buckeridge, A. S. Shevlin, J. A. Logsdail, M. S. Woodley, A. R. C Catlow, J. M. Powell, G. R. Palgrave, P. I. Parkin, W. G. Watson, W. T Keal, P. Sherwood, A. Walsh, A. A. Sokol, *Nat. Mater.* **2013**, 12, 798–801.
- [177] X. Wei, G. Zhu, J. Fang, J. Chen, *Int. J. Photoenergy* **2013**, 2013, 1–6.
- [178] X. Wang, W. W. Li, Y. F. Xiao, L. Zhu, X. Y. Liu, *AMM* **2013**, 361-363, 736–739.

List of Figures

Figure 1.	The ratio of treated to untreated wastewater reaching water bodies from 10 regions across the globe.....	2
Figure 2.	Band gaps and band edge positions of some semiconductor photocatalysts on a potential scale (V) versus the normal hydrogen electrode (NHE) at pH 0	7
Figure 3.	Band gap diagram of (a) an insulator, (b) a semiconductor, and (c) a conductor	8
Figure 4.	Mechanism of TiO ₂ semiconductor photocatalysis	10
Figure 5.	Photo-induced reactions on TiO ₂ photocatalyst and the corresponding time scales.....	10
Figure 6.	Formation of (1) side chain products and (2) deep oxidation products, (3) aromatic ring opening of phenol as intermediate during the photocatalytic degradation of ibuprofen...	14
Figure 7.	TiO ₆ polyhedra for the TiO ₂ phases (a) Anatase, (b) Brookite and (c) Rutile (Ti ⁴⁺ (white), O ²⁻ (red), and gray lines represent the unit cell).....	16
Figure 8.	The difference in recombination pathways of photogenerated electron-hole pairs in (left) direct and (right) indirect band gap semiconductors.....	17
Figure 9.	Relative numbers of research articles focused on photocatalysis per year: search results in the period of 1995–2016 with the “Web of ScienceDirect” by the keyword “TiO ₂ and photocatalytic activity” (blue bars) and by the keyword “Brookite and photocatalytic activity” (red bars)	18
Figure 10.	XRD patterns of titania materials obtained by peptization of Brookite/Rutile mixture with HNO ₃ : (a) Brookite/Rutile mixture, (b) Brookite-rich phase, (c) Rutile-rich phase, and theoretical diffraction patterns with corresponding lines of Brookite and Rutile.....	23
Figure 11.	XRD patterns of titania materials obtained by peptization of Brookite/Rutile mixture with water: (a) Rutile, Brookite after the (b) first and (c) second peptization. Pattern (a) and (b) include the calculated diffraction lines from the corresponding JCPDS database (a) 96-900-9084 and (b) 96-900-9088	23
Figure 12.	XRD patterns of (a) amorphous titania, (b) Anatase, (c) Brookite, (d) Rutile, and (e) titania P25 for comparison. Pattern (b), (c) and (d) include the calculated diffraction lines from the corresponding JCPDS database (b) 96-900-9087, (c) 96-900-9088 and (d) 96-900-9084. A, B, and R represent Anatase, Brookite, and Rutile phase, respectively	25
Figure 13.	Raman spectra of (a) amorphous titania, (b) titania P25, and the synthesized titania polymorphs (c) Anatase, (d) Brookite, (e) Rutile, respectively	27
Figure 14.	TG-DSC curves of (left) amorphous titania and (right) Brookite/Rutile mixture	28
Figure 15.	TG-DSC curves of (a) Anatase, (b) Brookite, (c) Rutile, and (d) titania P25.....	29
Figure 16.	SEM images of (a) amorphous titania, (b) Anatase, (c) Brookite, and (d) Rutile	31
Figure 17.	SEM images of Brookite samples obtained after (left) the first and (right) the second peptization with H ₂ O. Images (a, c) represent precipitates and (b, d) represent corresponding liquids obtained after centrifugation of the Brookite supernatant liquids	31
Figure 18.	SEM images of the (a) synthesized Brookite/Rutile mixture, (b) titania P25, (c) Brookite-rich, and (d) Rutile-rich recovered by peptization with HNO ₃	32
Figure 19.	UV-vis diffuse reflectance spectra of the amorphous titania, the as-prepared titania polymorphs, and titania P25 (top). Tauc plots for the determination of the band gap	

	energy E_g for direct and indirect transitions (bottom). A_m , A, B, and R represent amorphous titania, Anatase, Brookite, and Rutile, respectively	33
Figure 20.	(Left) N_2 sorption isotherms and (right) corresponding pore size distribution curves of Anatase, Brookite, Rutile, and titania P25 (from top to bottom)	35
Figure 21.	The UV-vis absorption spectra of the IBP solutions photocatalytically treated with Brookite. Reaction conditions: RT, IBP conc.: 10 ppm, aqueous reaction solution: 250 ml, catalyst loading: 10 mg.....	38
Figure 22.	(Left) Photocatalytic abatement and (right) mineralization of IBP over (▲) Brookite and (■) titania P25. (□) Photolysis of IBP. Formation and decomposition of IBP intermediates (inset). Reaction conditions: RT, IBP conc.: 10 ppm, aqueous reaction solution: 250 ml, catalyst loading: 10 mg	39
Figure 23.	Negative ESI-TOF-MS spectra of the aqueous IBP solutions after photocatalytic treatment with Brookite: (a) starting solution, the photocatalytically treated solutions after (b) 0 min, (c) 1 h and (d) 5 h. Reaction conditions: RT, IBP conc.: 10 ppm, aqueous reaction solution: 250 ml, catalyst loading: 10 mg	41
Figure 24.	Photocatalytic abatement of different organic compounds cinnamic acid (CA), phenol (Ph), diatrizoic acid (DA) and the dyes rose bengal (RB) and rhodamine B (RhB) over Brookite. RhB and RB curves represent decolourization. Reaction conditions: RT, organic conc.: 10 ppm, aqueous reaction solution: 250 ml, catalyst loading: 10 mg	42
Figure 25.	Negative ESI-TOF-MS spectra of the aqueous CA solutions after photocatalytic treatment with Brookite: (a) starting solution, the photocatalytically treated solutions after (b) 0 min, (c) 1 h and (d) 5 h. Reaction conditions: RT, CA conc.: 10 ppm, aqueous reaction solution: 250 ml, catalyst loading: 10 mg	43
Figure 26.	Negative ESI-TOF-MS spectra of the aqueous DA solutions after photocatalytic treatment with Brookite: (a) starting solution, the photocatalytically treated solutions after (b) 0 min, (c) 1 h and (d) 5 h. Reaction conditions: RT, DA conc.: 10 ppm, aqueous reaction solution: 250 ml, catalyst loading: 10 mg	44
Figure 27.	Positive ESI-TOF-MS spectra of the aqueous DA solutions after photocatalytic treatment with Brookite: (a) starting solution, the photocatalytically treated solutions after (b) 0 min, (c) 1 h and (d) 5 h. Reaction conditions: RT, DA conc.: 10 ppm, aqueous reaction solution: 250 ml, catalyst loading: 10 mg	45
Figure 28.	Impact of different scavengers on the photocatalytic abatement of IBP over Brookite. Reaction conditions: RT, IBP conc.: 10 ppm, aqueous reaction solution: 250 ml, catalyst loading: 10 mg. (■) No scavenger. Scavengers: (●) 1.46 mg EDTA, (▼) 0.1 ml t-BuOH, and (▲) 2.704 mg 1,4-BQ	46
Figure 29.	The effect of thermal pre-treatment on photocatalytic activity of Brookite: (a) as-prepared and calcined at (b) 100 °C, (c) 200 °C, (d) 300 °C, (e) 400 °C, (f) 500 °C, (g) 700 °C for 2 h in air. Reaction conditions: RT, IBP conc.: 10 ppm, aqueous reaction solution: 250 ml, catalyst loading: 10 mg.....	47
Figure 30.	The effect of thermal pre-treatment on (left) Raman spectra and (right) XRD patterns of Brookite samples: (a) as-prepared and calcined at (b) 100 °C, (c) 200 °C, (d) 300 °C, (e) 400 °C, (f) 500 °C, (g) 700 °C for 2 h in air. B and R represent Brookite and Rutile, respectively	48

- Figure 31. The UV-vis absorption spectra of the IBP solutions photocatalytically treated with Anatase. Reaction conditions: RT, IBP conc.: 10 ppm, aqueous reaction solution: 250 ml, catalyst loading: 10 mg..... 49
- Figure 32. (Left) Photocatalytic abatement and (right) mineralization of IBP over (●) Anatase and (■) titania P25. (□) Photolysis of IBP. Formation and decomposition of IBP intermediates (inset). Reaction conditions: RT, IBP conc.: 10 ppm, aqueous reaction solution: 250 ml, catalyst loading: 10 mg 50
- Figure 33. Negative ESI-TOF-MS spectra of the aqueous IBP solutions after photocatalytic treatment with Anatase: (a) starting solution, the photocatalytically treated solutions after (b) 0 min, (c) 1 h and (d) 5 h. Reaction conditions: RT, IBP conc.: 10 ppm, aqueous reaction solution: 250 ml, catalyst loading: 10 mg 51
- Figure 34. Positive ESI-TOF-MS spectra of the aqueous IBP solutions after photocatalytic treatment with Anatase: (a) starting solution, the photocatalytically treated solutions after (b) 0 min, (c) 1 h and (d) 5 h. Reaction conditions: RT, IBP conc.: 10 ppm, aqueous reaction solution: 250 ml, catalyst loading: 10 mg 52
- Figure 35. Photocatalytic abatement of different organic compounds cinnamic acid (CA), phenol (Ph), diatrizoic acid (DA) and the dyes rose bengal (RB) and rhodamine B (RhB) over Anatase. RhB and RB curves represent decolourization. Reaction conditions: RT, organic conc.: 10 ppm, aqueous reaction solution: 250 ml, catalyst loading: 10 mg 53
- Figure 36. Impact of different scavengers on the photocatalytic abatement of IBP over Anatase. Reaction conditions: RT, IBP conc.: 10 ppm, aqueous reaction solution: 250 ml, catalyst loading: 10 mg. (■) No scavenger. Scavengers: (●) 1.46 mg EDTA, (▼) 0.1 ml *t*-BuOH, and (▲) 2.704 mg 1,4-BQ 54
- Figure 37. The UV-vis absorption spectra of the IBP solutions photocatalytically treated with Rutile. Reaction conditions: RT, IBP conc.: 10 ppm, aqueous reaction solution: 250 ml, catalyst loading: 10 mg..... 55
- Figure 38. (Left) Photocatalytic abatement and (right) mineralization of IBP over (►) Rutile and (■) titania P25. (□) Photolysis of IBP. Formation and decomposition of IBP intermediates (inset). Reaction conditions: RT, IBP conc.: 10 ppm, aqueous reaction solution: 250 ml, catalyst loading: 10 mg 55
- Figure 39. Negative ESI-TOF-MS spectra of the aqueous IBP solutions after photocatalytic treatment with Rutile: (a) starting solution, the photocatalytically treated solutions after (b) 0 min, (c) 1 h and (d) 5 h. Reaction conditions: RT, IBP conc.: 10 ppm, aqueous reaction solution: 250 ml, catalyst loading: 10 mg..... 57
- Figure 40. Photocatalytic abatement of different organic compounds cinnamic acid (CA), phenol (Ph), diatrizoic acid (DA) and the dyes rose bengal (RB) and rhodamine B (RhB) over Rutile. RhB and RB curves represent decolourization. Reaction conditions: RT, organic conc.: 10 ppm, aqueous reaction solution: 250 ml, catalyst loading: 10 mg 58
- Figure 41. Impact of different scavengers on the photocatalytic abatement of IBP over Rutile. Reaction conditions: RT, IBP conc.: 10 ppm, aqueous reaction solution: 250 ml, catalyst loading: 10 mg. (■) No scavenger. Scavengers: (●) 1.46 mg EDTA, (▼) 0.1 ml *t*-BuOH, and (▲) 2.704 mg 1,4-BQ 59
- Figure 42. (Left) Abatement of CA and (right) mineralization during the course of photocatalytic performance of (■) titania P25, (●) Anatase, (▲) Brookite and (►) Rutile. Reaction

	conditions: RT, CA conc.: 10 ppm, aqueous reaction solution: 250 ml, catalyst loading: 10 mg	60
Figure 43.	(Left) Abatement of IBP and (right) mineralization during the course of photocatalytic performance of (■) titania P25, (●) Anatase, (▲) Brookite and (▶) Rutile. Reaction conditions: RT, IBP conc.: 10 ppm, aqueous reaction solution: 250 ml, catalyst loading: 10 mg	61
Figure 44.	(Left) Abatement of Ph and (right) mineralization during the course of photocatalytic performance of (■) titania P25, (●) Anatase, (▲) Brookite and (▶) Rutile. Reaction conditions: RT, Ph conc.: 10 ppm, aqueous reaction solution: 250 ml, catalyst loading: 10 mg	63
Figure 45.	(Left) Abatement of DA and (right) mineralization during the course of photocatalytic performance of (■) titania P25, (●) Anatase, (▲) Brookite and (▶) Rutile. Reaction conditions: RT, DA conc.: 10 ppm, aqueous reaction solution: 250 ml, catalyst loading: 10 mg	64
Figure 46.	(Left) Decolourization of RB and (right) abatement of aromatic ring during the course of photocatalytic performance of (■) titania P25, (●) Anatase, (▲) Brookite, and (▶) Rutile. Reaction conditions: RT, RB conc.: 10 ppm, aqueous reaction solution: 250 ml, catalyst loading: 10 mg.....	65
Figure 47.	(Left) Decolourization of RhB and (right) abatement of aromatic ring during the course of photocatalytic performance of (■) titania P25, (●) Anatase, (▲) Brookite, and (▶) Rutile. Reaction conditions: RT, RhB conc.: 10 ppm, aqueous reaction solution: 250 ml, catalyst loading: 10 mg.....	66
Figure 48.	Photocatalytic abatement of IBP over (a) Rutile and (b) titania P25 by changing amount of the addition of EDTA: (▲) 0.73 mg, (●) 1.46 mg, (▼) 2.92 mg, (◀) 5.72 mg. No scavenger with (▶) Rutile and (■) titania P25. Reaction conditions: RT, IBP conc.: 10 ppm, aqueous reaction solution: 250 ml, catalyst loading: 10 mg	70
Figure 49.	Photocatalytic abatement of IBP over titania P25 by increasing addition of <i>t</i> -BuOH: (●) 0.1 ml, (▲) 0.2 ml, (▼) 0.3 ml, (▶) 0.4 ml. (■) No scavenger. Reaction conditions: RT, IBP conc.: 10 ppm, aqueous reaction solution: 250 ml, catalyst loading: 10 mg	71
Figure 50.	Summary of the photocatalytic abatement of IBP over (▨) titania P25, (▩) Anatase, (▧) Brookite, (▦) Rutile, respectively, and hole/radical trapping experiments with three different scavengers (under UV-vis irradiation for 2 h)	73
Figure 51.	Recalcitrance of organic compounds against photocatalytic degradation. Photocatalytic abatement of Cinnamic acid (CA), Ibuprofen (IBP), Phenol (Ph), and Diatrizoic acid (DA) over (■) titania P25, (●) Anatase, (▲) Brookite, and (▶) Rutile.....	74
Figure 52.	Photocatalytic abatement of IBP over (▶) synthesized Rutile R1, (▼) Rutile R2 obtained by peptization with water, (▲) Rutile R3 obtained by grinding, and (◀) Rutile R4 obtained by calcination of synthesized Brookite at 700 °C. Reaction conditions: RT, IBP conc.: 10 ppm, aqueous reaction solution: 250 ml, catalyst loading: 10 mg.....	75
Figure 53.	SEM images of (a) synthesized Rutile R1 and (b) Rutile R2 obtained by peptization with water. Raman microscopic images of (c) Rutile R3 obtained by grinding and (d) Rutile R4 obtained by calcination of synthesized Brookite at 700 °C.....	76
Figure 54.	(Left) Predicted equilibrium shape of a Rutile TiO ₂ nanocrystal obtained using the DFT calculated surface energies and the Wulff construction and (right) SEM image of Rutile..	76

Figure 55.	(Left) Abatement and (right) mineralization in the photocatalytic degradation of IBP over (top) A80B20, (middle) A80R20, and (bottom) B80R20 composites, respectively. Reaction conditions: RT, IBP conc.: 10 ppm, aqueous reaction solution: 250 ml, catalyst loading: 10 mg. Single components (●) Anatase, (▲) Brookite, (▶) Rutile, and (■) composite.....	79
Figure 56.	Photocatalytic abatement of IBP over (▲) Brookite, (▼) Rutile obtained from synthesized Brookite/Rutile mixture after peptization with water, and (▶) synthesized Brookite/Rutile mixture. Reaction conditions: RT, IBP conc.: 10 ppm, aqueous reaction solution: 250 ml, catalyst loading: 10 mg.....	81
Figure 57.	Impact of different scavengers on the photocatalytic abatement of IBP over (a) A80B20, (b) A80R20, and (c) B80R20 composites. Reaction conditions: RT, IBP conc.: 10 ppm, aqueous reaction solution: 250 ml, catalyst loading: 10 mg. (■) No scavenger. Scavengers: (●) 1.46 mg EDTA, (▼) 0.1 ml <i>t</i> -BuOH, and (▲) 2.704 mg 1,4-BQ.....	82
Figure 58.	The absorbance spectra of the investigated organic solutions (conc.: 10 ppm).....	92
Figure 59.	The UV-vis photolysis of IBP, CA, DA, Ph obtained by the abatement of aromatic ring and of RB, RhB obtained by the degradation of colour band.....	93
Figure 60.	Molecular structure of (a) EDTA, (b) <i>t</i> -BuOH, and (c) 1,4-BQ.....	94

List of Schemes

Scheme 1.	Synthesis of phase-pure titania	22
Scheme 2.	Separation of Brookite from the mixture by peptization	22
Scheme 3.	Steps in the synthetic pathway affording amorphous titania	86
Scheme 4.	Separation of Brookite from the mixture by peptization with distilled water.....	88
Scheme 5.	Separation of Brookite from the mixture by peptization with HNO ₃	89

List of Tables

Table 1:	Main contaminants affecting water quality and their main sources	3
Table 2:	Molecular formula, chemical structure, and molecular weight of studied organic compounds	4
Table 3:	Oxidation potential (E_{ox}) of various oxidizing agents at pH 0	8
Table 4:	Summary of studies of preparation and photocatalytic degradation of pollutants in water using phase-pure Brookite as photocatalyst.....	19
Table 5:	Compositions and weight fraction of the as-prepared titania powders	24
Table 6:	The crystallite size of the as-prepared Anatase, Brookite, Rutile, and titania P25	26
Table 7:	The densities of the physisorbed water and chemisorbed OH^- groups calculated based on the weight loss and S_{BET} for Anatase, Brookite, Rutile, Brookite/Rutile mixture, and titania P25	30
Table 8:	The band gap energies of the amorphous titania, the as-prepared titania polymorphs, and titania P25 calculated by the Kubelka–Munk absorption function	34
Table 9:	The specific surface area, pore diameter, pore volume and average particle size of Anatase, Brookite, Rutile, and titania P25	36
Table 10:	The characteristics of the as-prepared titania powders and titania P25	37
Table 11:	Degree of mineralization of RB after photocatalytic treatment over titania photocatalysts	65
Table 12:	Degree of mineralization of RhB after photocatalytic treatment over titania photocatalysts	66
Table 13:	Summary of the obtained abatement and mineralization of different pollutants after photocatalytic treatment (2 h) over titania photocatalysts	67
Table 14:	Summary of the obtained abatement and mineralization of different pollutants after photocatalytic treatment (5 h) over titania photocatalysts	67
Table 15:	Relative decrease of the photocatalytic abatement of IBP (%) over titania polymorphs and titania P25 after addition of the hole (h^+) scavenger EDTA	69
Table 16:	Relative decrease of the photocatalytic abatement of IBP (%) over titania polymorphs and titania P25 after addition of the $\bullet OH$ radical scavenger <i>t</i> -BuOH	71
Table 17:	Relative decrease of the photocatalytic abatement of IBP (%) over titania polymorphs and titania P25 after addition of the $O_2^{\bullet -}$ radical scavenger 1,4-BQ.....	72
Table 18:	The order of relative contribution of different active species in the IBP abatement over the synthesized titania polymorphs and titania P25 obtained after 2 h of the photocatalytic treatment	73
Table 19:	Crystal and crystallite size of different Rutile crystals determined by SEM and XRD	75
Table 20:	Calculated and experimental abatement and mineralization of IBP over the titania polymorphs and composites after 2 h of the photocatalytic treatment.....	80
Table 21:	Relative decrease of the IBP abatement (%) after addition of various scavengers obtained after 2 h of the photocatalytic treatment	82
Table 22:	Yield of the obtained amorphous TiO_2 powders.....	86
Table 23:	Hydrothermal conditions to form different crystalline titania	87
Table 24:	The mixed-phase titania samples obtained by physical mixing.....	93

Personal data

Name / Address: Huyen Thuong Thi Tran

263 Ngoc Hoi, Van Dien, Thanh Tri, Ha Noi

Phone: (+84) 906 072 519

Date of Birth: April 19, 1983

Place of birth: Bacninh

Marital status: Married

Nationality: Vietnamese



Education

- 09/1989 - 06/1994: Thong Nhat Elementary School, Thainguyen, Vietnam
- 09/1994 - 06/1998: Chu Van An Secondary School, Thainguyen, Vietnam
- 09/1998 - 06/2001: Thai Nguyen High School, Thainguyen, Vietnam
- 08/2001 - 06/2005: Thai Nguyen University of Education, Thainguyen, Vietnam.
(BS degree in Physics)
- 07/2005 - 11/2007: Institute of Physics (IOP), Vietnam Academy of Science and Technology (VAST), Hanoi, Vietnam
(MS degree in Solid Physics)
- 10/2013 - present: Institute of Materials Science (IMS), Vietnam Academy of Science and Technology (VAST), Hanoi, Vietnam and Department of Inorganic Chemistry, Institute of Chemistry, University of Rostock, Germany
(The Sandwich PhD programme in Chemistry)

Employment and Academic Responsibility

- 09/2005 - 10/2011: Lecturer in Faculty of Physics, Thai Nguyen University of Education
- 10/2011 - Present: Researcher in Laboratory of Optoelectronic Materials, Institute of Materials Science (IMS), Vietnam Academy of Science and Technology (VAST), Hanoi, Vietnam

Referees:

1. Prof. Dr. Axel Schulz (University of Rostock, Institute of Chemistry)
2. Prof. Dr. Nguyen Quang Liem (University of Science and Technology of Hanoi,
Institute of Materials Science, Vietnam Academy of Science and Technology)
3. Prof. Dr. Wolfram Seidel (University of Rostock, Institute of Chemistry)

Date of delivery: 28.01.2016

Date of defense: 07.06.2016